Fabrication of Intensity-based Long-Period-Grating Fiber Sensor with CO_2 Laser for Refractive Index Sensing

Ziwei Zuo

Thesis submitted to the Faculty of the
Virginia Polytechnic Institute and State University
in partial fulfillment of the requirements for the degree of

Master of Science
in
Electrical Engineering

Anbo Wang, Chair
James R. Heflin, Co-Chair
Ting-Chung Poon

April 27, 2015
Blacksburg, Virginia

Keywords: Long-period-gratings (LPGs), CO_2 laser, fiber modulation, fiber sensing, ionic-self-assembling-multilayers (ISAMs) thin film

Fabrication of Intensity-based Long-Period-Grating Fiber Sensor with CO_2 Laser for Refractive Index Sensing

Ziwei Zuo

(ABSTRACT)

This thesis investigates the fabrication technique and procedures for producing long period grating (LPG) fiber sensors with point-by-point irradiation under a CO_2 laser beam. The type of fiber sensor under examination is desirable to be highly sensitive to the variation of the thickness and refractive index of a thin film deposited on the LPGs, making it a promising candidate as a core sensor component in a biosensor system developed for detection and verification of pathogenic bacteria, such as Methicillin-resistant Staphylococcus aureus (MRSA), *Francisella tularensis*, and so on.

We have previously demonstrated [1] that a UV-induced long-period-grating (LPG) based fiber sensor is extremely sensitive to small variation of refractive index (RI) and thickness of the surrounding medium. In this thesis, we will present a CO_2 laser and step-stage system that operate automatically under control of a Matlab program to inscribe LPGs with desired grating period and fabrication conditions.

Examples of CO_2 laser induced LPGs have been found to exhibit high sensitivity, with transmissive power attenuation of more than 15 dB at the resonant peak of 1402 nm under deposition of Ionic Self-Assembled Monolayer (ISAM) thin film that is around 50 nm in thickness. When tuned to its maximum sensitivity region, this LPG has shown a transmission

power reduction of 79% with the deposition of only 1 bilayer of ISAM thin film at the monitored wavelength. This result is comparable in sensitivity with the UV-induced LPGs, yet with the advantage of lower fabrication cost and simplified fabrication procedure.

Acknowledgments

Finishing this thesis can not be the work of my sole effort. There are so many people that stood besides me, encourages me and work with me through all the challenges in this project, or in life. I would like to dedicate this thesis to all of them.

Among them all, I would like to thank my project advisor Dr. Heflin, without his inspiring guidance and continuous support, I won't be able to finish this work even though I should be able to do even a better job. I also want to thank the Dr. Anbo Wang, who has provided all the assistance and guidance on assembling the experiment establishment. I work most of my time in Dr. Wang's lab and have received valuable advices on making this project advance. I wish to express my thanks to Dr. Poon as well, his class have been a great supplementary for me to finish the theoretical studies of this thesis.

In addition, I wish to thank Dr. Haifeng Xu, the discussion with whom have pointed me to the right direction of this research. Mr. Bo Liu, Mr. Zhipeng Tian and Mr. Di Hu have been great help in discussion problems I encountered during the research. They are great lab-mates.

And I can't forget the support from my fiance, Ms. Qing Li, who has always been supportive, understanding and encouraging to me. Without her I doubt I can continue this work a year back. She is wonderful and a blessing to me. I also want to thank my other friends from Chinese Bible study and Chinese Church, the great fellowship with them have erased the dullness from the repeating work I have to live with in this research project. Among them I would like to especially thank Dr. Y-A Liu, Dr. H-H Liu, Dr. Johnny Yu, Dr. Jessie Yu-Chen, Dr. Chao Shang, Dr. Qiang Li, Dr. Fei Zhang, and so many others that I can't list all here, otherwise they could exceed the length of the rest of this thesis.

I want to say to you, I appreciate all your help and I'm in debts of all your great support to me. Even though I'm not a Lannister, I 'always pay my debts'.

Contents

List of Figures

List of Tables

Chapter 1

Introduction

Conventional optical fibers can be fabricated with different dopants and cross-sectional structures for various applications and research purposes. The effective refractive index (RI) of the inner and outer cross-section structure are slightly different from each other to facilitate the process of total internal reflection and form the waveguide for the propagation of optical waves along the axis of the fiber. The most common and widely used optic fiber is known as the single mode fiber (SMF), whose cross-sectional structure consists of the fiber core, the cladding ring wrapping the core and the buffer/jacket area as the outer region of the fiber, as shown in Fig. 1.1. The SMF is named after its trait to accommodate only one spatial guided mode but it can accommodate with a broad band of frequencies in the fiber core. The spatial propagation pattern of optical waves at different frequencies is unique within a SMF, which eliminates the mode dispersion associated with multi-mode fiber (MMF) and reduces the power attenuation rate over long distance.

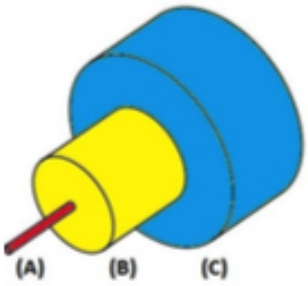

Figure 1.1: An illustration of the cross-section structure of a typical SMF: (A) Fiber's core, where the optical signals are carried and confined within; (B) Cladding layer, which will possess a smaller refractive index than that of the core. Total reflection takes place at the boundary between core and cladding; (C) Buffer/jacket layer, which is used to protect the inner structure of the fiber as well as enhance fiber's durability.

Researchers discovered that in order to make SMF truly useful for telecommunication, the RI distribution of each structure region along fiber's longitudinal axis needs to be homogeneous and void of any defect. Transmission of the guided mode can sense even small material cracks or RI perturbation of the fiber core, which will lead to massively magnified attenuation of transmission power as a ramification. Modern fiber technology has successfully developed highly symmetrical and homogeneous optical fiber that has an absence of structural defects or inhomogeneous regions over long lengths, such that the propagation of the optical signal will retain the information it carries for a longer distance without significant distortion or attenuation.

Nevertheless, introduction of controlled defect at specific locations along the fiber can be beneficial in certain scenarios, and it has inspired a broad range of research themes. Application of Fresnel's law in fiber optics reveals that an incident ray will reflect as well as refract at the interface of materials with different RI. RI contrast at the interface, optical parameters of the material and the nature of the incident optical wave will all affect the power distri-

bution and the phases of the split waves. This has inspired studies and demonstrations in various research themes, such as dielectric mirror and distributed Bragg reflector, [4, 5] band rejection filter, [6] fiber Fabry-Perot interferometer (FPI), [7] multiplexer and demultiplexers, [8, 9] fiber lasers system, [10, 11] fiber Bragg grating (FBG) and Long-period-gratings (LPG) sensors. [1, 12, 13, 14]

Among these well established fiber optic structures, fiber long-period-gratings (LPGs) have drawn wide attention. The idea of periodic fiber structures has first introduced and demonstrated by Hill *et al.* [15] in 1978, with the help of swift development of both lasers and optical fiber technologies during the 1960s. In 1996, Vengsarkar *et al.* [16] reported the first LPG written in a SMF, which prompted further development of the LPG inscription technology. Since then, numerous of LPG inscription methods have been explored and developed, including ultra-violet (UV) laser irradiation, [16, 17, 18, 19] CO_2 laser exposure, [20, 21, 22, 23, 24, 25, 26] electric arc discharge, [27, 28, 29] femtosecond laser irradiation, [30, 31, 32] mechanical bending, [33, 34] ion beam exposure, [35, 36] *etc.*.

LPGs are known for their ability to couple the guided core mode with the co-propagating cladding modes that travel in the same direction in the optical fiber. The establishment of the mode coupling at the resonant wavelength will disperse a notable portion of the power into the coupled high-order cladding mode, whose transmission power will be attenuated significantly within a range of a few centimetres due to dispersion and absorption. The power conversion between the core and coupled cladding mode is proportional to the degree of the mode coupling. Theoretical study by Vengsarkar *et al.* [16] found that LPG's mode

coupling behaviour is controlled by the phase matching condition. That is to say, once the propagation constant of the core mode matches that of a cladding mode, a resonance will form between the two modes and power transition from the guided core mode to cladding mode at the resonant wavelength will be established. Under such circumstance, we say the phase matching condition is met between the core and the cladding mode. The phase matching condition can be written as:

$$\beta_{0,1}{}^{core} - \beta_{0,n}{}^{clad} = \frac{2\pi}{\Lambda} \tag{1.1}$$

where $\beta_{0,1}{}^{core}$, $\beta_{0,n}{}^{clad}$ are the propagation constant of the core and coupled cladding mode, respectively; and Λ is the grating period.

Given the fact that a few dozens of cladding modes are allowed in the cladding of a conventional SMF, a set of loss peaks are expected to be observed at corresponding wavelengths in the transmission spectrum. The phase matching curve (PMC) has been widely used for description of the relationship between the core and cladding modes, as well as for understanding the grating behaviour of a LPG. The PMC is derived from the phase matching condition and it usually consists of curves for each cladding mode that indicate the location of the resonant wavelength at the underlying grating period. Fig. 1.2 displays a PMC of a turnaround-point (TAP) LPG and the theoretical prediction of its transmission spectrum under 6 different grating periods, work conducted by Wang *et al.*. [37] The PMC and mode-coupling in LPGs will be discussed in detail in Chapter 2.

The location and shape of an LPG's PMC is determined by a few factors, such as the cladding mode number (*ie.*, $LP_{0,3}$, $LP_{0,7}$, $LP_{0,12}$), the RI variation of the grating (namely Δn),

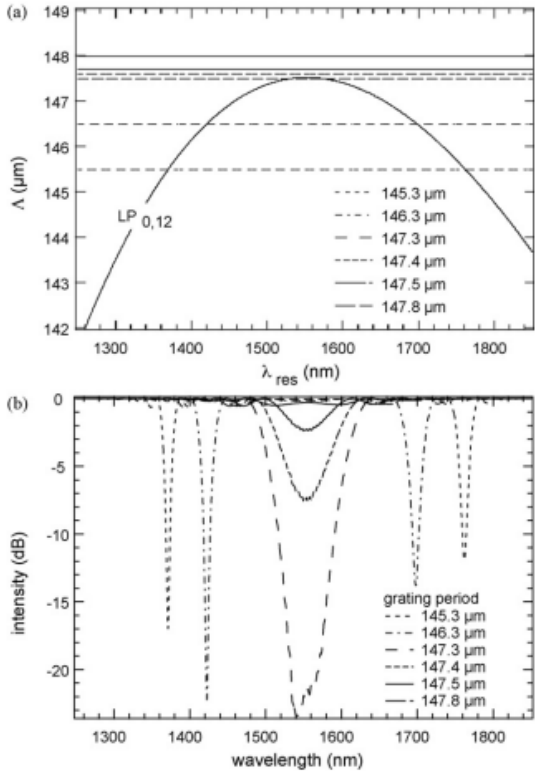

Figure 1.2: (a) Theoretical calculation of the phase matching curve (PMC) between $LP_{0,1}$ core mode and $LP_{0,12}$ cladding mode. Cross points between PMC and specific grating periods (145.3 μm, 146.3 μm, 147.3 μm, 147.4 μm, 147.5 μm and 147.8 μm from bottom to top, respectively). (b) Simulated transmission spectrum for each of the 6 grating periods, respectively.

the modification of the fiber structure due to inscription of the grating and underlying fiber's characteristic parameters (*ie.*, radius of core and cladding, fiber's aperture). Once written, the LPG's grating period becomes a constant if not placed under harsh environment. The location of such LPG's resonant wavelength is thus determined.

Nevertheless, when experience temperature change, variation of cladding's effective refraction index, external stress or curvature of the LPG, the relative or absolute location of the effective grating period and/or PMC of the LPG will shift, ending up with a modifica-

tion to the transmission spectrum. As a result, one will observe a wavelength shift of the transmission loss peak and/or variation of the peak's depth, depending on the type of LPG under investigation. Since the discussion of the phase matching condition falls in the range of optical wavelength, or nanometre scale, LPG tends to be extremely responsive to variation of ambient conditions, making it a viable candidate for optical sensor.

Guided by the phase matching theory, various LPG based fiber sensor platforms have been developed and demonstrated in sensing and/or monitoring of stress, temperature, humidity, gas leakage, RI variation of the ambient environment, thickness of the deposition film, *etc.*. With deposition of a proper biological transducer film with affinity to an analyte that identifies the species of micro-organisms, an LPG can be made into a biological sensor.

We have previously demonstrated [38] the TAP LPG based biosensor system is capable of detecting and diagnosing sparse existence of pathogenic bacteria, such as MRSA, *F. tularensis*, Brucella, *etc.* from sample suspensions. Early diagnosis of such bacteria is critical to constrain potential infection to healthy people, reduce fatality rate of the infected patients and help reduce the cost of treatment. Compared with existing early diagnosis methods, the LPG based fiber optical biosensor system has shown the advantage of quick feedback of the testing results (around 1 hour, compared to 24 to 48 hours of conventional microbiology detection methods), compact and uncomplicated system design, cheap and easy maintenance process, and lower training requirement for operating technicians. Therefore, developing LPG fiber sensors that can help facilitate and establish evidence for early diagnoses of epidemic diseases has become an interesting and important research subject. This is the major

motive behind the studies of this thesis.

Producing an LPG with a CO_2 laser is beneficial for its low cost (compared with UV laser writing methods), high reproducibility and predictability in manufacturing quality LPG sensors (compared with arc-discharge methods). The carbon dioxide laser (CO_2 laser) has been widely used in industrial applications for engraving, welding and cutting. [39] SMF under direct exposure of focused CO_2 laser beam will cause heating of the fiber and a thermal process that leads to the transformation of the affected silica glass.[40] Consequently, the refractive index of the irradiated fiber region will be altered and creat a grating along the longitudinal axis of the fiber. The power requirement for writing LPG on a SMF is relatively low comparing to other industrial tasks, thus the cost for assembling and maintaining the LPG writing facility remains low.

In this thesis, we have successfully demonstrated that LPGs made by irradiation of a CO_2 laser are sensitive to the thickness variation of the coated organic thin film, which simulates the biological transducer's response to the targeted micro-organisms. With deposition of 7 bilayers of ISAMs thin film that is equivalent to 10 nm in increment of the average cladding radius, the LPG's attenuation peak at 1400 nm shifted from -10 dB to -25 dB. Deposition of each additional ISAMs bilayer leads to a signal reduction between 21% and 78%, depending on the number of underneath bilayers. This result is consistent with the analysis prediction that the LPG tends to lose more transmissive power at the resonant wavelength as it is tuned to reach the phase matching condition.

A variety of LPG inscription parameters have been explored here. We have determined

a series of grating parameters that will produce quality LPG with resonant wavelength available from 1400 nm till 1570 nm under the current experimental settings. The flexible choice of resonant wavelength opens the door for usage of commercially available laser sources in the near-infrared range for the biosensor system. As a conclusion, with designated inscription parameters, the proposed LPG fabrication procedure and technique can fully satisfy the sensitivity requirement for biosensor system while the manufacturing cost per LPG is considerably low.

More detailed discussion of realizing LPG in a single mode fiber will be presented in chapter 2. The underlying principle of writing LPG with CO_2 laser will be discussed in chapter 2 as well.

Experimental procedure and techniques for producing quality LPG sensor that is specifically customized for biosensor application will be discussed in chapter 3.

Chapter 4 will focus on the LPG and TAP-LPG that are made from the current fabrication settings. Such fiber sensor's capability of detecting the thickness variation of the deposited film, which is the main effect expected from the positive interaction between the biological transducer film and targeted micro-organisms, will be examined in chapter 4 as well.

Chapter 5 will focus on discussion of future work and summarizing the results obtained during the study of this thesis.

Chapter 2

Theory of Long-period-gratings and Their Fabrication

2.1 Fiber optics

2.1.1 Optical waveguide

The fundamental principle that underlies and controls the behaviour of fiber optics is Snell's law: $n_1 \sin(\theta_1) = n_2 \sin(\theta_2)$, where an incident ray hits the interface between media of refractive index n_1 and n_2, respectively, with incident angle of θ_1 and refractive angle of θ_2 with respect to the normal to the interface.

Snell's law predicts that the propagation pattern of an optic ray will alter at the interface of media with different RI. The refractive angle will be smaller than that of the incident angle, if $n_1 < n_2$, and the other way around, with the expression of the refractive angle deduced

from Snell's law: $\theta_2 = \arcsin(\frac{n_1}{n_2}\sin(\theta_1))$. Since the upper boundary of the sine function is 1, it is possible to create situations where a real number solution is not't be allowed with the condition $n_1 > n_2$. The incident angle where the Snell's law cease to apply, under the condition $n_1 > n_2$, is called the critical angle, where $\theta_{crit} = \theta_{incid} = \arcsin(\frac{n_2}{n_1})$. For an optical ray whose incident angle is greater than the critical angle, the ray will not pass through the interface and all its transmission power and information will be retained and reflected back into the incident medium. Such optical phenomenon is called total internal reflection.

Total internal reflection guarantees the phase and wave amplitude integrity of the incident wave, which will maintain its propagation in the incident media without power or information leaking through the media interface. Application of total reflection inspired the invention of fiber optics, where silica or plastic fiber serves as the dielectric waveguide and confines the transmission of the optical wave along the longitudinal axis of the fiber. In opposition to metal waveguides, optical fiber has a more pliable and deformable structure. Optical waves that are travelling along optical fibers tend to experience low attenuation loss over long distances and are immune to electromagnetic interference, making it perfect for telecommunication, power transmission, imaging and spectroscopy, fiber optic sensors and so on.

An optical fiber is a cylindrical transverse structure that consists of two general layers: the fiber core and the cladding. Total reflection of the transmissive optical wave occurs at the boundary between core and cladding, with the RI of fiber core slightly higher than that of the cladding. In specific for a step index optical fiber whose RI are homogeneous within

the core or cladding, the core is usually made of SiO_2 doped with Ge and/or B, while the cladding is of pure fused silica. Dopant inside the fiber core and residual stress accumulated along the fiber fabrication process are the main cause of the RI discrepancy between fiber core and cladding. Such discrepancy can be as small as 0.005 to 0.01, or 0.35% to 0.7% of the core RI. [41] According to the waveguide analysis and deduction from Maxwell's equations, only discrete and limited number of spatial modes of optical waves are allowed to propagate along the fiber. Consequently, optical fibers are generally categorized into three types: multimode fiber (MMF), graded-index fiber, and single mode fiber (SMF). They are illustrated in Fig. 2.1

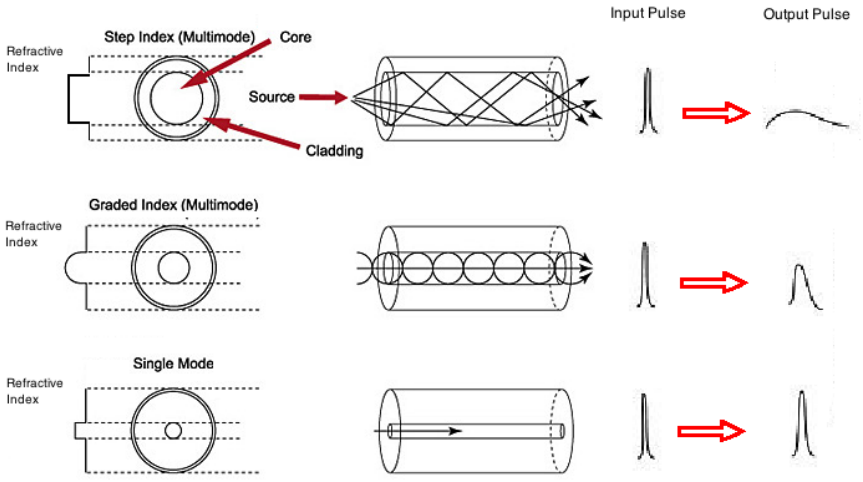

Figure 2.1: Three general types of fibers. Top: multimode fiber, whose core radius is large enough to accommodate multiple modes of optcial waves. Middle: graded-index fiber, whose RI of core varies along the radius. Bottom: single mode fiber, whose radius is much smaller than that of its core, resulting in only one mode allowed in transmission.

MMF along with the graded-index fiber are able to support the propagation of multiple modes within the core. However, different modes can interfere with the transmission of each

other and generate mode dispersion. Waveguide analysis of the MMF reveals unbearable pulse dispersion and signal distortion. To the contrary, SMF has shown the merit of low dispersion to light with near infrared wavelength (below 0.4 dB/km for 1310 nm and 1550 nm) and ability to sustain high signal rates for transmission (up to 40 Gbits/s in deployed systems). [42] For step index fiber designs, the requirement for single mode guidance is given by V ¡ 2.405, where V is defined as:

$$V = \frac{2\pi}{\lambda} a \sqrt{n_{core}^2 - n_{clad}^2} \tag{2.1}$$

By observing Eq. 2.1, it is easy to notice that the V-number is a function of the wavelength λ, meaning the single mode guidance can only be maintained within a limited wavelength range. For a ray of smaller wavelength beyond the cut-off wavelength, there will exist multiple modes within the fiber core. Most SMF are manufactured for usage in near-infrared wavelength range, with minimum dispersion bandwidth found around 1310 nm and 1550 nm.

2.1.2 Single mode fiber

The core diameter of a typical SMF is between 8 and 10 μm with a cladding of 125 μm. Though SMF only supports one single mode within the fiber core, there still are a large number of cladding modes that exist in the cladding, since the fiber's cladding-jacket boundary also forms a waveguide and it will accommodate transmission of the cladding modes unintentionally fed into the source end of the fiber. Much like the core modes in MMF, the cladding modes of a typical SMF are often short lived, where mode dispersion and leakage

into the buffer coatings will strongly attenuate the transmissive power and eliminate most of the cladding modes within a few centimetre along the fiber's longitudinal axis. Due to differences in waveguide geometry, the propagation constants of core and cladding modes are distinct from each other, which guarantees the integrity of the core mode in its propagation without noticeable interference from the co-propagating cladding modes.

Nevertheless, Vengsarkar *et. al.* discovered that by introducing gratings with periodicities in the hundreds of microns to the fiber core, a practical method can be established to disrupt the original propagation mode of the core mode, phase matching and coupling it with one or more cladding modes at a corresponding wavelength. An illustration of LPG's disruption to the propagation of original core mode can be found in Fig. 2.2. As a result, power conversion will be established between the core and cladding modes, which would otherwise propagate independently and disperse under different patterns. [16, 43, 44] Due to the strong attenuation of the cladding modes, the core mode will lose a majority of its transmission power at the wavelength where mode-coupling is formed, and hence display a series of attenuation peaks in the transmission spectrum.

The coupling between core and cladding modes is useful in carrying the information of ambient conditions and its variation at the grating's location by the transmission light, which can be read and analysed at a distant location. Furthermore, the phase matching condition is very sensitive to the small variation of the grating period as well as the physical condition of the cladding layer, making fiber grating devices promising candidates for many fiber sensor applications.

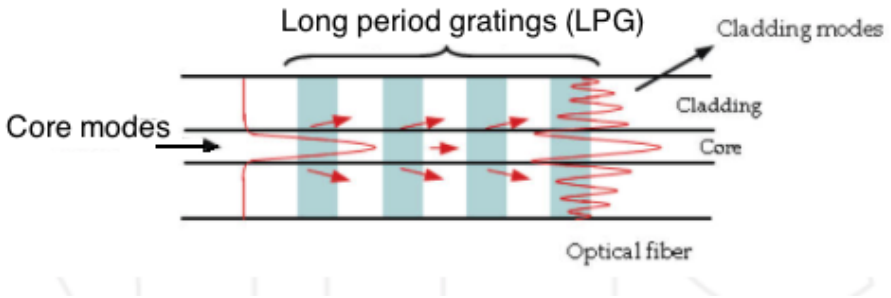

Figure 2.2: Illustration of LPG's disruption to core mode's propagation. The disturbed core mode can then be phase matches with one or more cladding modes and experiencing spiky loss to the transmission power at the resonant wavelength. Figure is modified from Coelho *et al.*. [40] J. M. P. Coelho, M. Nespereira, C. Silva, D. Pereira, and J. Rebordo, Current Develop- ments in Optical Fiber Technology, ch. Advances in Optical Fiber Laser Micromachining for Sensors Development. InTech, 2013. (Used under fair use, 2015.)

2.2 Long period gratings

2.2.1 Fiber Bragg conditions

Fiber Bragg gratings, or FBG, is the direct application of Bragg conditions in fiber optics. A simple example of FBG comprises a uniform series of fiber gratings in the fiber core where the gratings' RI have been modulated and the gratings are of constant distance from each other. At the boundary front between gratings and fiber core, the transmission ray will be scattered into co-propagation modes and counterpropagation modes. Once the grating period is in right position for the Bragg condition between counterpropagating modes to be satisfied, a constructive superposition between such modes will form a reflection peak at resonant wavelength. [45, 46] With the reservation of wave vectors in mind, the expression for the fiber Bragg condition can be expressed as:

$$2(\frac{2\pi n_{eff}}{\lambda_B}) = \frac{2\pi}{\Lambda}, \tag{2.2}$$

which can be simplified to the general form:

$$\lambda_B = 2n_{eff}\Lambda, \tag{2.3}$$

where λ_B indicates the location of the expected peak on the reflection spectrum, Λ refers to the grating period and n_{eff} denotes the effective refractive index of the fiber core after inscription of fiber Bragg gratings.

A conventional FBG couples the counterpropagation core or cladding modes, which requires a large grating wave vector, the K-vector, and hence the grating periods have to be small – usually at the scale of a few hundred nanometres. FBG sensor systems generally demand the deployment of an optical multiplexer and optical switch to properly extract and monitor the reflection spectrum, where reflection peaks would shift and/or deform in response to the variations of environmental parameters that the FBG is designed to detect.

In contrast, in a typical LPG the Bragg condition is satisfied between the scattered core mode and the cladding modes that are copropagating along the same direction. In particular, the difference between the wave vector of the core mode, $\mathbf{k}_{core}$, and the wave vector of the coupled cladding mode, $\mathbf{k}_{clad}$, shall equal the grating wave vector, $\mathbf{K}$, or: $\mathbf{k}_{core}$ - $\mathbf{k}_{clad} = \mathbf{K}$. Since such wave vectors are all along the longitudinal direction of the fiber, it is plausible to write down the scalar formation as:

$$n_{eff}^{core}\frac{2\pi}{\lambda_{res}} - n_{eff}^{clad}\frac{2\pi}{\lambda_{res}} = \frac{2\pi}{\Lambda} \tag{2.4}$$

where n_{eff}^{core} and n_{eff}^{clad} are the refractive indices of the fiber's core and cladding, respectively. λ_{res} denotes the resonant wavelength where the mode coupling is expected. Λ refers to the

grating period.

Reducing Eq. 2.4 will generate the phase matching condition for LPG, known as the fiber Bragg condition:

$$\Lambda = \frac{\lambda_{res}}{n_{eff}^{core} - n_{eff}^{clad}} \tag{2.5}$$

2.2.2 Evaluation of LPG's phase matching curve

For silica fiber, the refractive index of fiber core (n_{core}) and cladding (n_{clad}) are wavelength dependent, as approximated in the Sellmeier equation: $n(\lambda) = \left[1 + \frac{A_1\lambda^2}{\lambda^2-\lambda_1^2} + \frac{A_2\lambda^2}{\lambda^2-\lambda_2^2} + \frac{A_3\lambda^2}{\lambda^2-\lambda_3^2}\right]^{1/2}$. Table. 2.1 contains the Sellmeier coefficients for a standard SMF, whose core is made of germanium-doped glass (7 m/o GeO_2, 93 m/o SiO_2) well cladding is made of pure fused silica (100 m/o SiO_2). These listed Sellmeier coefficients are also used for simulation of the phase matching curve and transmission spectrum in the later part of this thesis.

Table 2.1: Sellmeier coefficients of a SMF doped with 7 w/m in its core

	A_1	A_2	A_3	$\lambda_1(\mu m^2)$	$\lambda_2(\mu m^2)$	$\lambda_3(\mu m^2)$
n_{core}	0.6869829	0.4447950	0.7907351	0.0780875	0.1155184	10.436628
n_{clad}	0.6961663	0.4079426	0.8974794	0.0684043	0.1162414	9.896161

With knowledge of n_{core} and n_{clad} for the designated resonant wavelength, one can solve for the effective refractive index of the corresponding linear polarization modes (LP modes) from the eigenvalue equation enforced by the boundary condition of Maxwell's equations in

a SMF:

$$\frac{J_l(u)}{uJ_{l-1}(u)} + \frac{K_l(w)}{wK_{l-1}(w)} = 0. \tag{2.6}$$

For solving the core's effective index, $u_{core} = k_0 a\sqrt{n_{core}^2 - n_{eff}^2}$, $w_{core} = k_0 a\sqrt{n_{eff}^2 - n_{clad}^2}$, $k_0 = 2\pi/\lambda_{res}$ and is the wave vector of the resonant wavelength, a is the radius of the fiber core; for solving cladding's effective index, $u_{clad} = k_0 b\sqrt{n_{clad}^2 - n_{eff}^2}$, $w_{clad} = k_0 b\sqrt{n_{eff}^2 - n_{air}^2}$, b is the radius of the cladding, assuming fiber's jacket is stripped off for the denoted region of the LPG. Given solution of u_{core} and u_{clad}, it is trivial to prove that:

$$n_{eff}^{core} = \sqrt{n_{core}^2 - \left(\frac{u_{core}}{ak_0}\right)^2}, \tag{2.7}$$

and:

$$n_{eff}^{clad} = \sqrt{n_{clad}^2 - \left(\frac{u_{clad}}{bk_0}\right)^2}. \tag{2.8}$$

It can also be proven mathematically that an LPG only couples core modes with spatially symmetrical cladding modes, which are $LP_{0,m}$ modes, where $l = 0$ and m refers to the mth solution to Eq. 2.6.

Supposing the given germanium-doped SMF has a core radius of $a = 3.5\mu m$, cladding radius of $b = 62.5\mu m$ and average RI change of $\delta n = 1.4 \times 10^{-3}$ due to inscription of gratings, we can calculate the phase matching curve (PMC) as shown in Fig. 2.3. [47, 48, 49]

2.2.3 Turnaround points and TAP-LPGs

It is worth noting that for high order cladding modes, say $LP_{0,11}$ to $LP_{0,18}$, the phase matching curves exhibits a concave down shape in the considered wavelength range (1.0 μm

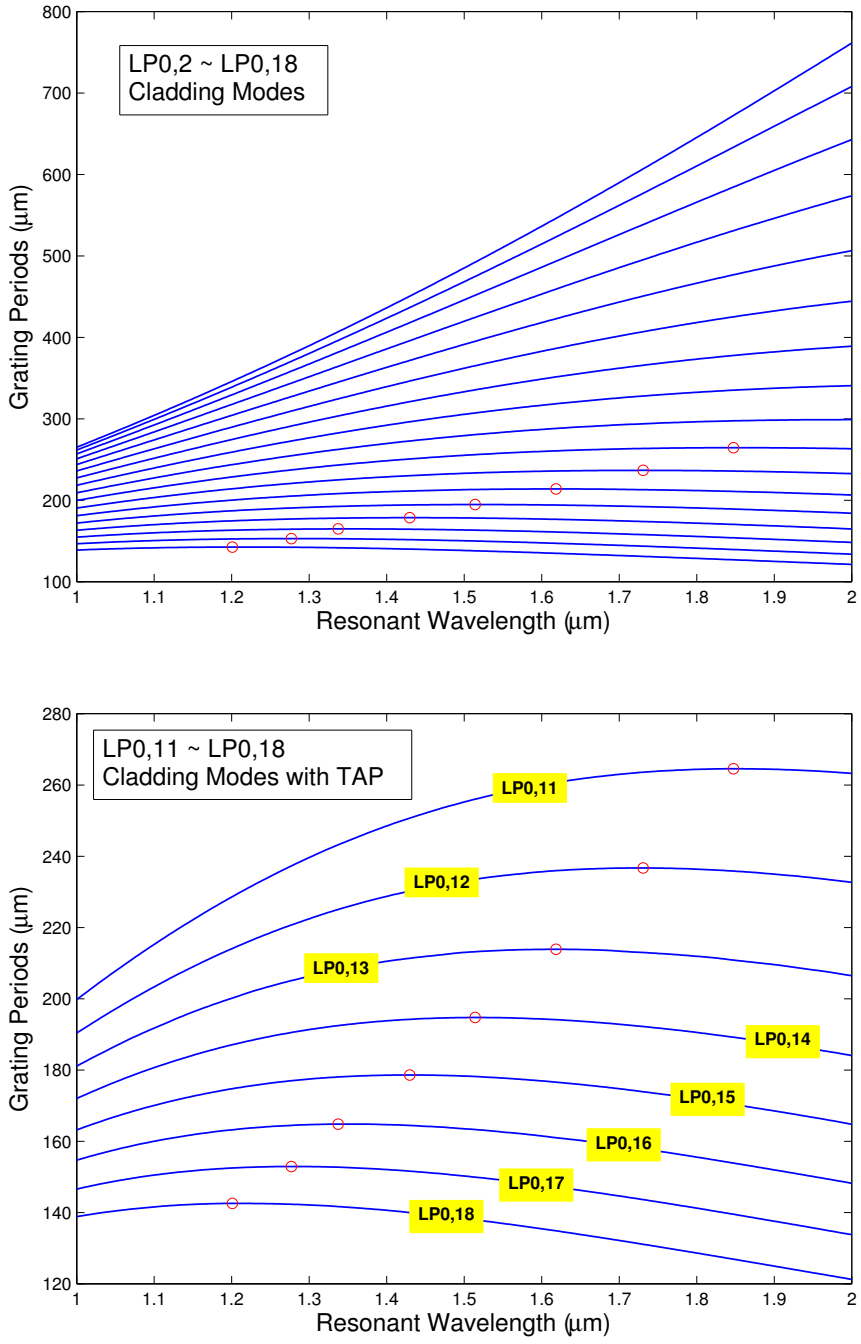

Figure 2.3: Phase matching curves (PMC) calculated for an SMF with core diameter of $7\mu m$, cladding diameter of $125\mu m$, average RI change due to inscription of gratings is $\delta n = 1.4 \times 10^{-3}$. Top: The PMC of coupling $LP_{0,1}$ core mode to $LP_{0,2}$ $LP_{0,18}$ cladding modes. Bottom: Selected phase matching curves from $LP_{0,11}$ $LP_{0,18}$ modes, where turnaround points (TAP) begin to become available in the 1.0 μm 2.0 μm bandwidth. The red circles indicates the location of the TAP on the phase matching curves.

to 2.0 μm). The turning points on such curves are called turnaround points (TAP). [1, 37, 2] For mode coupling between core and lower order cladding modes in LPG, variation of the sensing elements are reflected and measured via the shift of the resonant wavelength in the transmission spectrum, which is the direct consequence of the monotonically increasing phase matching curve in the examined bandwidth, as shown in the top chart of Fig. 2.4.

In contrast, for phase matching curves that possess a TAP, each grating period will make two crossings with the phase matching curve of the coupled cladding mode that correspond to dual-peaks in the transmission spectrum. The variation of the sensing element will lead to the shift of dual-peaks toward or away from each other. In the extreme circumstance, the dual-peaks merges into a single peak as TAP moves near the grating period. Such situation is known as the 'before-TAP' region. Heflin *et al.* have demonstrated that for LPG fiber sensor tuned to operate in the 'before-TAP' region, the variation of the sensing elements will correspond to the magnitude change of the attenuation peak at a fixed wavelength. [1, 37, 38] This can be very convenient for building a simplified LPG sensor system, where the broadband light source can be replaced by a smaller, less complex and much cheaper laser source that's operating at telecommunication wavelength, while the optical spectrum analyzer can be replaced by a more compact and transportation-friendly transmission power detector. An example of the TAP-LPG is shown in the bottom chart of Fig. 2.4.

More specifically, Grubsky *et al.* have shown that the Talyor expansion of the dispersion function of a LPG can be written as: [3]

$$\Phi(\lambda) - \Phi(\lambda_{res}) = a_1(\lambda - \lambda_{res}) + a_2(\lambda - \lambda_{res})^2 + ..., \tag{2.9}$$

where $\Phi(\lambda)$ is the phase matching function under wavelength λ, a_i is the ith order coefficient of the expansion, and $i = 1, 2, 3, ...$, λ_{res} refers to the resonant wavelength of the considered cladding mode.

For the case of low order cladding mode coupling, it can be shown that the shift of the resonant wavelength is in proportion to the variation of the grating period:

$$\delta\lambda = -\delta\Lambda \cdot \frac{2\pi}{a_1\Lambda^2}. \tag{2.10}$$

Eq. 2.10 explains the monotonic characteristic of the phase matching curves for the low order cladding modes.

Nevertheless, for the case of higher order cladding mode coupling, the first order expansion coefficient is negligible ($a_1 = 0$) while the second order expansion coefficient becomes the leading term in deciding the relationship between $\delta\lambda$ and $\delta\Lambda$:

$$\delta\lambda = \pm\left(-\delta\Lambda \cdot \frac{2\pi}{a_2\Lambda^2}\right)^{\frac{1}{2}}. \tag{2.11}$$

In Eq. 2.11, the minus sign inside the square root implies the value of a_2 is negative, which explains that the phase matching curves for such cladding modes need to be concave down. Since the leading coefficient a_2 is associated with the quadratic term in the expansion of the dispersion function, the phase matching curves will exhibit a parabolic shape with the TAP at the concave tip.

Vengsarkar *et al.* [16] have also shown that the full width at half maximum (FWHM) $\Delta\lambda$ of the loss peak can be approximated by:

$$\Delta\lambda = \frac{0.8\lambda^2}{L\left(n_{eff}^{core} - n_{eff}^{clad}\right)}. \tag{2.12}$$

For example, for a LPG whose resonant wavelength locates at 1550 nm, with length of 10 mm, n_{eff}^{core} 1.45 and n_{eff}^{clad} 1.44 at the resonant wavelength, the estimated FWHM bandwidth is 19.2 nm. As will be seen in the simulated transmission spectrum, the attenuation peak of a quality LPG is sharp and narrow, which is especially desired for a performance-demanding sensor system.

Whereas guidance is provided from the plots of PMC for the given LPG, a few experimental factors would also play an important role in the evaluation of n_{eff}^{core} and n_{eff}^{clad}, such as the variation of the geometry and optical properties of the underlying SMF due to laser exposure, inhomogeneous RI variation induced at the gratings, the inconsistent grating period due to instrumental accuracy limit, *etc.*. Therefore the dependence of the resonant wavelength to the grating periods rarely follow closely with the prediction of the PMC. Some LPG characteristics can still be shown in general. However, to determine the ideal grating period for the coupling between core and a particular cladding mode in LPG, one may need to explore a variety of grating parameter settings.

In addition, Eq. 2.5 also reveals an important fact that though the grating period of a LPG remains constant after inscription of gratings and putting in a normal laboratory environment, one can still expect to observe a shift of the resonant wavelength when the LPG experiences a variation to the effective RI of fiber's cladding and/or core, though the latter case is rather rare. The shift can take place either along the magnitude of the transmission loss peak for merged dual-peak case, or along the wavelength of the peak otherwise. Such characteristic of the LPG is the driving cause for its application in sensing surrounding

media's RI or deposited film's thickness.

2.2.4 Study of LPG spectra

Following the LPG theory and analysis proposed by Erdogan *et al.*, [50] we can define the detuning parameter δ, which is used to describe the coupling efficiency between the core and cladding mode in a LPG, as:

$$\delta(\lambda) = \frac{1}{2}\{\beta_{0,1} - \beta_{0,n} - \frac{2\pi}{\Lambda}\} = \pi(n_{eff}^{core} - n_{eff}^{clad})(\frac{1}{\lambda} - \frac{1}{\lambda_{res}}) \tag{2.13}$$

where $\beta_{0,1}$ and $\beta_{0,n}$ are the propagation constants of fiber's core and cladding modes, respectively, and λ indicates the wavelength where the detuning parameter is studied.

Comparing Eq. 2.13 with Eq. 2.4, the meaning of the detuning parameter becomes clear: as a function of the underlying wavelength, the detuning parameter δ measures how far has the coupling been detuned away. $\delta = 0$ occurs at the resonant wavelength corresponding to the coupled modes, where the fiber Bragg condition is fully met and one shall expect zero detuning. The degree of detuning can also be estimated from the PMC. The distance between the actual grating period of the LPG and the calculated grating period corresponding to the complete phase matching at the wavelength measures how detuned the underlying cladding mode is from coupling with the core mode. The smaller this distance is, the more coupling will take place between the core and cladding modes with a larger attenuation peak observed from the transmission spectrum, and vice versa.

Calculations conducted by Hall *et al.* [51] for codirectional mode coupling revealed that

the power conversion from the guided $LP_{0,1}$ mode to the coupled cladding mode has the expression of:

$$P_{0,n}^{clad}(\lambda) = \frac{\sin^2\left(\kappa_g L\sqrt{1+(\delta(\lambda)/\kappa_g)^2}\right)}{1+\left(\delta(\lambda)/\kappa_g\right)^2} P_{0,1}^{core} \tag{2.14}$$

where $P_{0,n}^{clad}(\lambda)$ refers to the power conversion at the wavelength λ, $P_{0,1}^{core}$ refers to the transmission power of the core mode, L refers to the length of the gratings and κ_g is the coupling coefficient for the gratings. The coupling coefficient κ_g is proportional to the induced RI change Δn and has monotonically increasing impact over the power conversion rate. It is trivial to prove that for maximum power conversion from the core mode to the coupled cladding mode, condition $\kappa_g L = \frac{\pi}{2}$ has to be satisfied.

Eq. 2.14 provides the essential mathematical tool for determining the spectral dependence of the periodic gratings in a SMF. It can be used for simulation of the transmission spectrum. Simulations performed by Dr. Zhiyong Wang [52] have shown transmission spectrum of the LPG with fiber core radius of $a = 5\mu m$, cladding radius of $b = 62.5\mu m$, core and cladding RI of 1.455 and 1.45, respectively, grating length of 10 mm and grating period of 240 μm. The resonant wavelength is found at 1410 nm, and the spectra correspond to the mode coupling between core and $LP_{0,12}$ cladding mode. The simulated spectrum with different average RI changes to the core (namely, δn_{core}), due to inscription of gratings, have been depicted in Fig. 2.5.

Fig. 2.5 makes a clear indication that the attenuation peak is extremely sensitive to the value of the average RI change to the core, or δn. An increment of an additional 0.02% variation (or about 3×10^{-4}) to the core refractive index is able to bring the LPG close to a

complete Bragg condition with 99% of transmission power loss at the resonant wavelength (δn from 4×10^{-4} to 7×10^{-4}), or significantly enhance the detuning between the designated modes such that the attenuation peak is almost eliminated (δn from 1×10^{-3} to 1.5×10^{-3}).

This can be understood straightforwardly from Eq. 2.5. δn affects the value of n_{eff}^{core} that appears in the denominator of the equation, therefore, even a small variation will be considerably magnified and shift the corresponding PMC. For the case studied in Fig. 2.5 where PMC possess a TAP, shifting of PMC from $\delta n = 7 \times 10^{-4}$ to $\delta n = 1.5 \times 10^{-3}$ leads to the split into dual-peaks, where the transmission power loss of the single attenuation peak is redistributed symmetrically into dual peaks while the original modes resonance at 1410 nm is broken.

Fig. 2.6 depicts the impact of average core RI variation induced by gratings, whose core radius is 3.5 μm and cladding radius is 62.5 μm. In this figure, the increases of the δn value will shift the underlying PMC of $LP_{0,14}$ mode up, where the TAP moves up from 194.37 μm (with $\delta n = 7 \times 10^{-4}$) to 195.09 μm (with $\delta n = 2.1 \times 10^{-3}$), or 0.3% of the change. Using Eq. 2.14 one can also simulate the transmission spectrum that reflects the influence of δn.

Suppose there is a LPG with 300 gratings and grating period of $\Lambda = 194.74\mu$m, which is the TAP of the $LP_{0,14}$ mode with $\delta n = 1.4 \times 10^{-3}$, one can simulate the spectrum based on different δn values, as shown in the bottom chart of Fig. 2.6. Since this Λ is the TAP for LPG with $\delta n = 1.4 \times 10^{-3}$, its transmission spectrum show the single resonant attenuation peak at the resonant wavelength of 1510 nm, where 99% of the transmission intensity is lost. This grating period is also in the 'before-TAP' region for LPG with $\delta n = 7 \times 10^{-4}$, therefore,

it can be seen from the figure that the attenuation peak is much smaller than that of the 'at-the-TAP' spectrum and implying a much weaker coupling between the core and $LP_{0,14}$ cladding mode. For LPG with $\delta n = 2.1 \times 10^{-3}$, the grating period Λ has already passed the TAP, where dual-peaks are expected and they are observed in the spectrum. This example has provided a direct view of the LPG's sensitivity to the δn value, that a small variation can lead to a distinguishable change to the transmission spectrum.

Since we have shown in Fig. 2.6 that the transmission spectrum is sensitive to the value of δn, it is critical to retain the stability and consistency of the LPG grating system such that the average grating-induced RI variation to the fiber core will fall within the acceptant range and the attenuation peak be tuned to the designated operating wavelength.

2.2.5 Sensitivity study of the LPG as optical fiber sensor

Since its invention, the LPG has stirred broad research interests in turning the LPG into a fiber sensor. Numerous applications have been found and demonstrated in sensing temperature, strain, bend, torsion, pressure and biochemical targets. The measured parameters should affect one or more components that defines the shape and location of the phase matching curve in Eq. 2.5. For instance, higher ambient temperature will cause expension of the LPG fiber, leading to a lengthened grating period as well as initiating RI variation to the fiber core and cladding.

Shu *et al.* [2] have analysed three major effects that will be responsible for shifting the PMC as well as the transmission attenuation peak: temperature, strain and surrounding RI

variation. Analytic expressions have been devised to explain the impact of these external influences. For temperature, the LPG's sensitivity is denoted as $d\lambda_{res}/dT$, for strain the sensitivity is denoted as $d\lambda_{res}/d\epsilon$ and for surrounding RI variation, the sensitivity is denoted as $d\lambda_{res}/dn_{sur}$. More specifically, the sensitivity terms can be written as:

$$\frac{d\lambda_{res}}{dT} = \gamma\lambda_{res}\left(\alpha + \Gamma_{temp}\right), \tag{2.15}$$

$$\frac{d\lambda_{res}}{d\epsilon} = \gamma\lambda_{res}\left(1 + \Gamma_{strain}\right), \tag{2.16}$$

$$\frac{d\lambda_{res}}{dn_{sur}} = \gamma\lambda_{res}\Gamma_{sur} \tag{2.17}$$

where α in Eq. 2.15 refers to the thermal expansion coefficient of the underlying fiber, γ in all three expressions has the meaning of waveguide dispersion and is defined as: [48, 53]

$$\gamma = \frac{d\lambda_{res}/d\Lambda}{n_{eff}^{core} - n_{eff}^{clad}}, \tag{2.18}$$

Γ_{temp}, Γ_{strain} and Γ_{sur} are the LPG's response coefficient to the temperature, strain and surround RI variation, respectively. Since this thesis will focus on the detection of the ambient RI change, or more specifically the influence of the deposition thin film to the shifting of transmission attenuation peak, we are more interested in the details and the meaning of Γ_{sure}, which has the expression of: [2]

$$\Gamma_{sur} = -\frac{u_m^2\lambda_{res}^3 n_{sur}}{8\pi r_{clad}^3 n_{clad}(n_{eff}^{core} - n_{eff}^{clad})(n_{clad}^2 - n_{sur}^2)^{3/2}}. \tag{2.19}$$

where r_{clad} refers to the cladding radius, n_{clad} refers to the refractive index of the cladding, and u_m is the mth root to the Bessel function of the first kind while $l = 0$. Replacing γ and

Γ_{sur} in Eq. 2.17 with expressions from Eq. 2.18 and Eq. 2.19, one can make the sensitivity chart under coupling the core mode to various cladding modes.

Suppose an LPG has core and cladding radius of 4.9 μm and 62.5 μm, respectively, the average RI variation to fiber core $\delta n = 7 \times 10^{-4}$ and the ambient material has a RI of 1.4. The sensitivity charts can then be plotted via Matlab programs (as attached in appendix A), as shown in Fig. 2.7. In the context of this thesis, an LPG's sensitivity refers to the wavelength shifting per change of refractive index, or the value of $\frac{d\lambda}{dn_{sur}}$ as defined in Eq. 2.17. The unit of the sensitivity defined above is nanometer per 10^3 RI change, or nm/10^3. In each of the subplot, the y-axis represents the scale of the calculated sensitivity, which represents how much transmission attenuation peak would shift in response to the ambient RI variation. The larger sensitivity value indicates LPG is more sensitive to the change of the sensing parameter. The x-axis of each subplot represents the resonant wavelength, at which the LPG is fabricated to and operated.

There are a few interesting characteristics that are worth noting from Fig. 2.7. For plot (a) and (b) the coupled cladding modes are $LP_{0,2}$ and $LP_{0,7}$, respectively, the sensitivity curves are monotonically increasing with increment of the resonant wavelength. This is in accordance with the fact that the phase matching curve are monotonically increasing with larger $d\lambda_{res}/d\Lambda$ at higher resonant wavelength. In addition, the range of the sensitivity of the LPG coupled to $LP_{0,7}$ mode is much larger than that of the LPG coupled to $LP_{0,2}$ mode. One can conclude that coupling to higher cladding modes will lead to higher LPG sensitivity. This judgement is true for all cladding modes whose PMC is monotonically increasing in the

considered resonant wavelength band and will be shown in later discussion.

For plots (c) through (f) the coupled cladding modes are $LP_{0,10}$, $LP_{0,12}$, $LP_{0,14}$ and $LP_{0,20}$, respectively. The maximum sensitivity is obtained at the TAP wavelength for each coupled mode, where the TAP begins to appear on the PMC within the discussed wavelength range and one can observe drastic change of sensitivity values. The explanation can be straightforward: the TAP represents the tip of a concave down and parabolic-like PMC, where the gradient $d\lambda_{res}/d\Lambda$ changes sign. Recall the expression of γ in Eq. 2.18, the value of γ will flip the sign as well and consequently, the sensitivity value will be associate with opposite signs on both sides of the TAP wavelength.

Another interesting point worth mentioning is that the maximum sensitivity obtained around the TAP in $LP_{0,12}$ is over 10^3 nm/10^3 and is much larger than the maximum sensitivity obtained from the 'wavelength-shifting' LPG coupled to lower order of cladding modes. This phenomenon renders the direct evidence that the LPG operated around the TAP can exhibit outstanding sensitivity, which one would not expect from a 'wavelength-shifting' LPG.

Though calculation of sensitivity-resonant wavelength relationship from the $LP_{0,2}$ mode till the $LP_{0,20}$ mode and extraction of the maximum sensitivity for the coupled cladding mode, one can plot the sensitivity map containing the information regarding to which cladding mode would the LPG reach the highest possible sensitivity and at what resonant wavelength. This information can then be translated into choosing a grating period for constructing the designated LPG and with how much RI variation one would need for the core gratings, with the assistance of the PMC. Fig.2.8 depicts a sensitivity map of an evaluated LPG with core

and cladding radius of 4.9 μm and 62.5 μm, respectively, while the average RI variation brought to fiber core due to periodic gratings is set at 7×10^{-4}. The y-axis represents the sensitivity value of the mode, in log-scale; and the x-axis represents the resonant wavelength in μm.

It is instructive to note that the maximum possible sensitivity of the LPG example is obtained from coupling the guided core mode to the $LP_{0,11}$ cladding mode, whose resonant wavelength is 1.823 μm (TAP of this mode) with a sensitivity of 1.92×10^4 nm/10^3 at the resonant wavelength. Furthermore, the 'wavelength-shifting' modes whose PMC exhibits monotonically increasing behaviour possess smaller sensitivity than all 'TAP' modes, except the $LP_{0,19}$ mode. This conclusion reinforces the previous statement that the TAP-LPGs are more sensitive than the conventional 'wavelength-shifting' LPG. Another notable characteristic is that the TAP shifts to smaller resonant wavelength with the increment of the coupled cladding mode order, which has also been observed in the PMC in Fig. 2.3. As a matter of fact, for much higher cladding modes, the TAP will move out of the considered wavelength range and the PMC will exhibit the monotonically decreasing behaviour.

Pursuing the maximum possible sensitivity can be done in the laboratory, however, it may not be practical and economical for realistic LPG sensor design. Most widely deployed laser sources are tuned to operate at a single wavelength, *i.e.* 1310 nm or 1550 nm for telecommunication applications, which may not cover the LPG's most sensitive resonant wavelength. Tuning the LPG such that the highest sensitivity can be obtained at an 'economical' resonant wavelength should be the criteria of choosing the LPG fabrication

parameters. The 'economical' resonant wavelength refers to the one at which cost-efficient and compact laser sources operate. In the scope of this thesis, we choose 1550 nm as the 'economical' resonant wavelength.

The LPG tuning can be performed through varying the average induced RI (δn) of the gratings. Increasing δn from 7×10^{-4} to 1.1×10^{-3} will enhance the sensitivity of the $LP_{0,13}$ mode from 432 nm/10^3 to 3065 nm/10^3, respectively. The reason of choosing the $LP_{0,13}$ for study is because for the LPG fiber studied for Fig.2.9, this mode is the only one rendering TAP close to the 'economical' resonant wavelength of 1550 nm. One can also search around the alternative δn values to find the most sensitive LPG fabrication parameter. The calculation results are summarized in the sensitivity searching map in Fig. 2.11.

Based on the calculation for the $LP_{0,13}$ TAP mode, the highest sensitivity can be found at $\delta n = 1.418 \times 10^{-3}$ where the resonant wavelength locates at 1534 nm. The grating period for these LPG parameters lies at 198.12 μm. If the goal is to set the resonant wavelength as close to 1550 nm as possible while achieving a high sensitivity, the next best recommendation for the value of δn is 1.173×10^{-3}, where the resonant wavelength is 1554.2 nm with the sensitivity equals 996.9 nm/10^3. The grating period found from the PMC lies at 195.28 μm. The Matlab code written for the calculations discussed above is attached in the appendix.

Another factor that can sometimes be overlooked though critical in determining the highest possible sensitivity is the length of the LPG, or the number of gratings. Eq. 2.14 shows that the maximum power conversion between the coupled modes occurs at the condition that the fiber Bragg condition is fully met (where $\delta(\lambda) = 0$) and that $\kappa_g L = \frac{\pi}{2}$. At the

resonant wavelength, the fiber Bragg condition is automatically satisfied as definition, then Eq. 2.14 is reduced to the following form:

$$P_{0,n}^{clad}(\lambda) = P_{0,1}^{core} \cdot \sin^2(\kappa_g L). \tag{2.20}$$

This means that the LPG sensor will not make its maximum sensitivity at the resonant wavelength unless the total length of the gratings satisfy the condition: $L = \dfrac{(2m+1)\pi}{2\kappa_g}$, where $m = 0, 1, 2, 3, ...$ Or assuming the grating period of the LPG is Λ, then the required number of gratings to see the maximum power conversion at resonant wavelength is:

$$N = \frac{(2m+1)\pi}{2\kappa_g \Lambda} (m = 0, 1, 2, 3, ...) \tag{2.21}$$

Failure to fabricate the right number of gratings close to the ideal gratings number identified by Eq. 2.21 could possibly end up with total elimination of the attenuation peak at the resonant wavelength and create 'false' peaks at wavelengths where $\delta(\lambda) \neq 0$. This would significantly damage the sensitivity of the LPG sensor, even if it's fabricated at the right grating period and value of δn for the designated resonant wavelength.

Eq. 2.21 has also revealed the importance of the coupling coefficient κ_g, which become the main factor that vary the power loss at the resonant wavelength once the LPG was fabricated and the number of the gratings were set. The coupling coefficient is defined in the equation below:

$$\kappa_g = \frac{1}{4}\omega\epsilon_0 \cdot \int_s \Delta\epsilon \vec{e}_m^* \cdot \vec{e}_{core} ds, \tag{2.22}$$

where ω is the frequency of the light, ϵ_0 is the vacuum permittivity, $\Delta\epsilon$ refers to the perturbation to the permittivity, approximately $\Delta\epsilon = 2n\delta n$, where $\delta n << n$. $\vec{e}_m$ and $\vec{e}_{core}$ are

the spatial distribution of the electric field of the mth cladding mode and the guided mode, respectively. The integral region is the cross-section of the fiber.

It is known from Eq. 2.8 that the effective RI of the cladding mode is determined by the environmental RI as well, hence with change of fiber's immersing media the coupling coefficient would change accordingly and consequently affect the power conversion rate. This is the leading cause for the intensity-shift of an LPG's transmission spectra at the change of the immersing media (*i.e.*, from air to PBS solution). In addition, deposition of organic layer-by-layer thin film that has a higher average RI than the cladding, the radius of the LPG's cladding is effectively expanded with the spatial redistribution of the electric field of the cladding mode. Therefore, the evaluation of the integral will generate a different answer than the integral before thin-film deposition, which eventually vary the power conversion phase term of $\kappa_g L$ in the end. This is the direct cause for the change of attenuation intensity at the resonant wavelength of the LPG with deposition of thin film.

Fig. 2.12 displays the simulation from a LPG whose grating period locates at "before-TAP" region. The spectra correspond to LPG with increase of average cladding radius at the deposition of thin film to the surface. Before deposition of any thin film, the resonant wavelength locates at 1535 nm. Then with 25 nm of average thickness increment, the resonant wavelength is found to be at 1533 nm, a 2 nm shifting to the shorter wavelength. Then with an additional deposition of another 25 nm equivalent thin film, along with the growth of the intensity peak, the resonant wavelength also shifts with a new position of 1542 nm, a 7 nm shifting to the longer wavelength. This simulation reveals the fact that despite the

intensity shifting is the main phenomena one can expect from a TAP-LPG, it is inevitable that a slight resonant wavelength shifting can also be observed.

Once the sensitivity searching map is constructed, one can establish a more objective view of the relationship between the LPG's sensitivity and its fabrication parameters. The map can also facilitate the search for the optimized value of the average RI variation induced to the fiber core for the LPG to operate at the desired 'economical' resonant wavelength.

2.2.6 Intensity based LPG fiber sensor

The theoretical analysis has proven the extreme sensitivity of the TAP-LPG when operating close to the TAP wavelength. Fig. 1.2 has shown the evolution of the transmission spectra as the relative position between grating period and the PMC varies. When the grating period is getting closer to the TAP of the PMC, the resonant coupling would start to form and gain strength. In the transmission spectrum, one will observe an intensity loss at a fixed wavelength, the resonant wavelength where the mode coupling is carried out. Once the grating period reaches the TAP of the PMC, the fiber Bragg condition will be met and the maximum power conversion will be established, such that the a attenuation peak in the transmission spectrum would be expected at the resonant wavelength. As the grating period passes below the TAP, the sole attenuation peak begins to split into two that then move away from one another.

In order to build intensity based TAP-LPG fiber sensor where the transmission intensity at the resonant wavelength is monitored and measured for comparison, the LPG will be tuned

in the 'before-TAP' region. That is to say, the written grating period will be slightly higher than the grating period of the TAP such that the detuning will vanish swiftly upon small variation of the measuring element and be reflected as the loss of transmission intensity at the resonant wavelength.

A few pioneering research studies have been conducted in turning TAP-LPG into intensity based fiber sensor element. Shu *et al.* have demonstrated a temperature sensor and a ambient refractive index sensor in their paper. [2] The refractive index sensor is built with a TAP of 1410 nm, which also has a -6 dB attenuation peak at the resonant wavelength. As immersing into oil with RI of 1.3, the sole attenuation peak splits into two immediately, as predicted by TAP's characteristic. The dual-peaks keep shifting away from one another as the surrounding RI is increasing.

Another temperature sensor has also been demonstrated by Shu *et al.*. [2] The TAP-LPG is tuned to operate at 1465 nm, which exhibits a -9 dB transmission reduction at the resonant wavelength as the environment temperature raises from 12^oC to 26^oC. Transmission spectra were measured at 2^oC temperature increment step for examining the LPG's sensitivity to environmental temperature. As the temperature is increased, the attenuation peak also grows along the fixed resonant wavelength, as the LPG is manufactured just 'before-TAP'. The intensity loss are greater when approaching TAP, implying higher sensitivity when getting closer to the TAP.

Grubsky *et al.* have demonstrated a strain sensor, which operates at 1415 nm. [3] With reduction of the external strain exerted on the fiber axis direction from 9410 $\mu\epsilon$ to 1650

$\mu\epsilon$, an attenuation peak begins to show up at the resonant wavelength and keeps gaining depth. The attenuation peak begins to split at the final strain of 1650 $\mu\epsilon$, though the dual-peak separation is not obvious. Fig. 2.13 summarizes the transmission evolution plots under influence of the measuring element's variation from the mentioned TAP-LPG examples just discussed: the ambient RI sensor is shown in subplot (a), the temperature sensor is shown in subplot (b), and the strain sensor is shown in subplot (c).

This thesis will focus on fabrication of the intensity-based LPG and TAP-LPG that will operate close to the telecommunication wavelength range. The fiber sensor needs to be tuned to be most sensitive to the ambient RI variation. As a matter of fact, the LPG biosensor system previously demonstrated by Zuo *et al.* [38] measures the growth of the deposited biofilm's thickness, as well as the variation of the cladding's average refractive index. The goal in this research is to fabricate LPG and TAP-LPG with enhanced sensitivity to the thickness and RI variation of the deposited biofilm layer.

Suppose there is a TAP-LPG that has core and cladding radius of 3.5 μm and 62.5 μm, respectively, an average RI modulation of 1.4×10^{-3}, grating period of 188.46 μm that is around 0.18 μm larger than the TAP of $LP_{0,14}$ mode and locates within the 'before-TAP' region, and 300 periods with the total LPG length of 56.538 mm. With deposition of 50 nm of an ISAM thin film that has a larger RI than the fiber's cladding, it is possible to view the deposition as the expansion of fiber's cladding radius by 50 nm, which will shift the PMC up by a merely 0.2% and alleviate TAP to the exact location of the grating periods. However, if plotting the transmission spectra using Eq. 2.14, one can observe an additional

40% transmission power loss at the resonant wavelength of 1562 nm as the fiber Bragg condition is fully satisfied at this point.

Fig. 2.14 depicts the shift of the PMC and the consequent percentage change of intensity percentage loss on the transmission spectra. The imprinted grating period of the bare LPG is separated from the TAP by 0.18 μm, even though a partial coupling can already be observed from the transmission spectrum with a 60% of intensity loss at the resonant wavelength. With the deposition of a thin film at the thickness of 50 nm, a significant transmission intensity loss will take place due to complete phase matching and power conversion between the core and coupled cladding mode. This example has shown the potential and extreme sensitivity of the TAP-LPG, which is able to sense thickness variation of a thin film deposited on the LPG at the nanometer scale.

2.3 LPG fabrication with CO_2 laser

2.3.1 Cause of higher refractive index in fiber core

As has been discussed in the previous sections, without proper perturbation introduced to the core of a single-mode fiber, the propagation of the core mode will be spatially confined within the fiber core and thus is isolated from interference of the cladding modes. The transmitted ray will preserve its power and encoded information, however, it is not useful for sensor applications. On the contrary, random and/or irregular core perturbations are capable of disrupting the transmission pattern of the core mode and scatter the confined transmission

power into the cladding of the SMF, however, the scattering mode does not stably phase match a cladding mode to facilitate the power conversion through mode-coupling. Dispersion and power attenuation may be remarkably enhanced, though such scattering mode can barely carry any useful information for sensing applications. In summary, the goal of the grating writing method must be reliable in creating identical RI variations to each of the grating locations.

Before discussion of grating inscription in SMF, it would be helpful to review the fabrication procedure of SMF that can be essential to understand some LPG grating technique.

Apart from polymers or crystalline materials such as sapphire that are used for manufacturing optical fiber for specific purposes, ordinary SMF are mostly made of silica, as it exhibits well optical transmission over a wide bandwidth of wavelengths. The material absorption and dispersion in the telecommunication spectrum portion can be as low as 0.2 dB/km. Pure silica has a melting point of $1{,}600^oC$ and it has a rather broad range of glass-liquid transformation state. [54, 55] While heated to the glass-transition temperature, T_g, silica becomes partially molten and it can then be drawn into fibers of micrometer scale in radius. Fiber claddings are always made from pure silica, whereas the cores are doped with various materials to raise the refractive index and create RI difference to the cladding for total reflection and confinement of transmission power. Based on the dopant materials and doping ratio, various fiber types have been developed to meet optimized application in communications (except for very short distances with plastic optical fiber), fiber lasers, fiber amplifiers, and fiber-optic sensors.

Ultra pure materials for manufacture of the fiber core (*e.g.* $SiCl_4$, $GeCl_4$, $POCl_3$, oxygen and so on) are vaporized and mixed in gas form for proper chemical reactions to take place. The deposition of the reaction product to the tube chamber will create large oxide particle chains in the agglomeration form, which possess controlled refractive index profile and are called 'reform'. [56] The dopant materials such as germanium, erbium and ytterbium among other rare earth elements will be added to the gas composition when the deposition of the reform region designated as the fiber core is undergoing. The process is called the chemical vapor-deposition method. By controlling the supplied gas composition and the deposition process of the reform at each deposition stage, the optical profile at the cross-section of the reform should be identical in RI yet geometrically proportional to the final fiber product. The reform for manufacturing telecommunication fiber are usually cylindrically shaped.

The reform is then placed in a instrument known as the drawing tower, where the reform will be again heated and softened, then pulled out as a long string. The pulling speed and the tension exerted to the tip of the fiber are the main control of fiber's final geometry parameters. Fibers are usually coated with a buffer/jacket layer during the pulling process and coiled for future use.

During the reform drawing process, a thermoelastic stress will be engendered between the germonosilica fiber core and the cladding. This stress is the direct consequence of the fact that the doped fiber core carries a different thermal expansion property to that of the cladding, thereby as the reform is heated and cooled below the fictive temperature during the pulling the difference in thermal expansion rate will be transformed into built-in stress

at the core-cladding boundary.

Another source of the built-in stress can be traced to the mechanical stress, which is generated due to the fact that the core material and cladding material tend to exhibit different viscoelastic properties. The mismatch between the viscoelastic property will aggregate stress when the reform is pulled into long string. Depending on the pulling force, the mechanical stress can be high enough to dominate the rise of RI in the fiber core. Mechanical stress and thermal stress are the main contributors to the residual stress between fiber core and cladding after fabrication of SMF.

In summary, the rise of the refractive index in fiber core is governed by two essential factors: the dopant composition and molecule chain's formation in the fiber core, as well as the residual stress. Externally and permanently inducing changes to the mentioned factors of a fiber will lead to the RI variation to the fiber core, which is critical in creating gratings that have a different RI than the core and cladding, while retaining the fundamental function of the fiber as the waveguide. The methods and mechanisms of writing fiber gratings will be discussed in the following section.

2.3.2 Mechanisms of inducing RI modification

For the writing of gratings, a few mechanisms have been studied and are believed to be the causes attributed to the RI modification of fiber's core, such as photosensitive reactions, [57, 58, 59] stress-relief model, [60, 61, 62] glass densification, [63, 64, 65] to name a few. Such mechanisms can be generally described in two categories: the thermal effect and photonic

(non-thermal) effect. The former effect will induce heating and melting of the exposed fiber structure under high power intensity of the focused laser beam, while the latter would generally cause photochemical reactions that could produce defects in fiber structures. Some of the mechanisms are only associated with a specific RI modulation technique while others are universally applicable and hence essential to the RI modulation models.

Laser-matter interaction induced by laser pulses other than the thermal effects will excite ionization and dissociation of photosensitive molecules. The photon ionization process is led by the absorption of single or multiple photons from laser pulses, and consequently breaks down weaker molecule bonds (usually within the dopant related oxide) that will generate glass defects and variation to fiber core's refractive index. [61] Such process is highly wavelength dependent and would occur most actively in the ultra-violet (UV) range under low irradiation level, say below $10^7 W \cdot cm^{-2}$. [66] For Ge-doped SMF, the natural presence of Ge-O bond supplies suitable and sufficient ingredients for the photon effects, the photosensitive reaction would take place intrinsically and swiftly. This effect is the most essential cause of core RI modification for UV-laser irradiation methods.

However, in order to induce sufficient defects to the UV exposed region, the SMF undergoing writing needs to be prepared. For instance, the dopant composition should include the presence of photosensitive materials; the fiber will always be pre-loaded with hydrogen for better gratings quality. The hydrogen loading process can take up to 12 to 24 hours. In addition, after the inscription of the LPG it would take an equivalent amount of time for annealing and dehydration process. This can be inconvenient in producing LPGs at an

industrial level.

The thermal effect, as suggested in its name, primarily arises by material absorption of the irradiation power of the laser beam, where the absorbed energy is transformed into elevation of temperature from the exposed surface to the its bulk. For optically transparent materials (such as optical fiber, glass slides, etc.) the laser pulse is able to induce heating of the molecular lattice inside the bulk. Depending on the pulse power, the pulse length and repetition frequency, and the thermal diffusivity and conductivity of the material, the thermal effect can modify the exposed material quite differently. In general, three types of fiber modification can be attributed to the thermal effect: residual stress relief, glass densification, physical deformation. Each of them not only modifies the materials structure of the optical fiber in the exposure region, it may also induce high or low refractive index variation or engender propagation disruption to fiber modes.

As discussed in the previous section, the residual stress can be attributed to the built-in thermoelastic stress that is accumulated during the heating of the reform, and the mechanical stress that can be traced to the discrepancy of the viscoelastic properties between the core and cladding region. [67] Heating the fiber to the melting point will produce phase transformation of the core and cladding. When the exposure regions get cooled again following the removal of the laser beam, the residual stress will be partially, if not all, released. The relaxation of the residual stress generally reduces the refractive index in the fiber core of the affected region of the fiber. Since the mechanical stress is reduced the most during the laser heating-cooling process, the efficiency of refractive index modification under uniform laser exposure

is linear to the pulling force during the fiber fabrication process. A higher pulling force can lead to a larger RI variation in the fiber core, as shown in experiments conducted by Kim *et al.*. [61] Li *et al.* have shown that a large RI change of -7.2×10^{-4} can be generated to Corning SMF-28e fiber after exposure to a CO_2 laser beam. Relaxation of residual stress is the main RI modification effect for CO_2 laser induced LPG written technique. This effect can also be found in some UV laser inscription methods, though not as the driving factor in RI modification to the core.

The thermal effect will also soften the exposure area, which under the joint influence of gravity and pre-tension exerted along the axis direction of the fiber will be elongated or tapered. If the laser pulse power is strong and short enough to vaporize the cladding material of the fiber, it is possible to create surface grooves and create asymmetric LPGs. Fig. 2.15 presents such an example fabricated by Wang *et al.*.[24] The elongation or tapering of the fiber will stretch the cladding and core materials, ending up with a reduction in fiber diameter at the gratings. The geometry change modifies the effective refractive index and thereby create periodic gratings in the SMF. [68] Physical deformation can be critical in writing fiber gratings to air-hole photonic crystal fiber, where the fiber modes are disrupted due to partial or complete collapse of air holes under optical pressure and heating of the fiber structure.

Annealing the LPG is the leading reason for glass structure changes in a commercial boron-doped SMF. The RI will increase as the result of annealing under 380 ^oC or unannelaed along with the glass densification, while the RI will decrease if the annealing temperature

reaches 400 ^oC or higher, when the glass volume expands as the result of heat influx. [64] The annealing effect usually plays an essential role in LPG inscription in boron-doped SMF as its residual stress and the fictive temperature is much lower than a conventional Ge-doped or Ge-B-doped fiber.

Due to LPG's writing characteristic by CO_2 laser irradiation, in most occasions only one side of the fiber surface will be directly exposed to the focused laser beam and hence be facing high optical power influx. The asymmetry of laser exposure will generate heavier physical deformation and larger residual stress release on the beam-incident side of the fiber, than the other half of the fiber. The result is the so-called asymmetric gratings and mode coupling, which is in contrast to the homogeneous and symmetric gratings created by UV-laser irradiation. This unique optical property of CO_2 laser induced LPG have led to diverse sensing and communication applications. [22, 24] Fig. 2.16 depicts the cross-section of a fiber exposed to a laser beam from one-side of the fiber, which consequently induce nonuniform energy absorption on the beam-incident side of the fiber. The direct consequence of the asymmetric mode coupling is the observation of high polorization dependent loss. In addition, the asymmetric relaxation of residual stress and physical deformation also leads to asymmetric RI variation, which is the driving cause for showing distinct sensitivities to bending, twisting and transverse loading with strong dependence on the orientation of the LPG.

The orientation-dependent sensitivity induced by CO_2 laser irradiation can benefit certain applications, but should be avoided in other situations. Various methods have been

devised to limit the construction of asymmetrical gratings. Oh *et al.* have proposed to rotate the underlying fiber axially during exposure to write symmetrical gratings. They have also proposed an LPG fabrication method by focusing a ring-shaped laser beam to the fiber with help of a concave mirror, such that the laser power can be uniformly distributed in the cross-section plane. [70] Zhu *et al.* have conceived a multiedge exposure method that has shown promising results in reducing polarization dependent loss and fiber orientation-dependent sensitivity as well. [71]

Though some studies on making symmetrical gratings have also reported clear spectra, many other researchers following such approaches didn't observe considerable improvement to the transmission spectrum quality or increased sensitivity. Therefore, for the purpose of keeping our LPG fabrication system simple and easy to maintain, we won't adopt concave mirrors or spatially symmetric reflectors in the system design.

In the scope of this thesis, the LPG is fabricated using direct irradiation from one-side with a CO_2 laser beam. In addition, Corning SMF-28 fiber family is chosen as the underlying SMF, which is Ge-doped and operates with low dispersion and material absorption rate at telecommunication wavelengths (*e.g.* 1300 nm and 1550 nm). The grating writing process, as has been discussed in this chapter, will induce residual stress release and physical modification as well. As the consequence, refractive index variation will be introduced at the laser irradiation locations, which then serve as the fiber gratings for designated mode coupling.

2.3.3 Preceding work on fabricating LPG with CO_2 laser

Attempt to imprint LPG on a SMF with CO_2 laser irradiation can be traced back to 1998 when Davis *et al.* first reported their success. [27] Ever since many researchers have worked on optimizing the grating-writing technique using CO_2 laser system and correlation between fabrication parameters and the quality of the transmission spectrum.

Recent work performed by Li *et al.* [72] in 2008 have shown decent agreement in transmission spectra between theoretical simulation and experiments using CO_2 laser to induce LPG on a Corning SMF-28e fiber. They reported that with a grating period of 525 μm and 89 grating points, laser power of 8 W and 125 ms of total irradiation length at each grating point, the resonant wavelength located at 1561 nm with the peak strength of -22.3 dB.

Another work completed by Liu *et al.* in 2008 studied the impact of the attached weight to the quality of the spectrum. [73] They reported that with a grating period of 600 μm and 50 grating points, final laser irradiation at energy density of 6.0 J/mm^2 and an attached weight of 10 g generated a LPG whose resonant wavelength located at 1456 nm and spike loss of 19.5 dB at the resonant wavelength.

In 2014, Zhong *et al.* [74] have demonstrated that with increment of scanning/repetition cycles and precise control of the laser-stage system, the LPG with grating period of 320 μm and 30 gratings, a laser irradiation power of 5 W with 7 on-grating scanning cycles have shown -35.66 dB of transmission loss at resonant wavelength of 1547.8 nm, at which the core mode was coupled to $LP_{0,14}$ cladding modes.

The spectra of all three mentioned work are shown in Fig. 2.17.

Though there are many work regarding fabrication of LPG using CO_2 laser, due to different system settings and conditions of the laser systems used in each individual study, the fabrication parameters were distinct to each reported work. However, it can still be summarized that to fabricate conventional LPGs, it is advised to use a moderate attached weight (around 1 to 10 g), a few irradiation scanning cycles and a laser irradiation of energy density between 4.0 and 6.0 J/mm^2.

There has been a long history of fabricating TAP-LPG with UV-laser system ever since the invention of laser-induced fiber modulation technique. [2] However, it is only very recently that successful attempts to fabricate TAP-LPG with CO_2 laser system have been reported.

Chaubey *et al.* [75, 76, 77] have found that exposure of B-Ge codoped fiber (Fibercore, UK) to scanning CO_2 laser pulses with repetitive frequency 2 kHz, scanning line speed of 60 mm/s, average laser pulse power of 1 W and grating period of 208 μm would create resonant coupling between the core and 11th order cladding modes right on the TAP. The resonant wavelength of this TAP mode has been found to locate at around 1460 nm. With exposure of this TAP-LPG to Gamma radiation, which would further change the average cladding RI by inducing fiber defect within the LPG region, they have reported the split of the sole resonant peak into dual-peaks.

These reports state the scanning cycles were continued until a notable attenuation peak was observed without specifying the number of cycles for fabrication of quality TAP-LPG, thus they provided little useful guidance to the present work. In addition, as an improvement

to their work, this study will focus on fabricating LPGs on SMF without further doping or modulation, as well as using a single scanning process instead of repeating scanning cycles.

Another recent study conducted by Tian *et al.* also reported fabrication of TAP-LPG through CO_2 laser irradiation. [78] In this study, inscription of the LPG was performed on a conventional SMF. The grating period of the LPG was 238 μm and it coupled the core mode with $LP_{0,10}$ cladding mode. This LPG has shown enhanced sensitivity in detection of thin film deposited to the cladding. However, the study also used the resonant wavelength shifting as the measurement element upon deposition of organic thin film. This phenomenon is usually deemed as the main indication of the 'wavelength-shifting' LPG instead of the 'TAP-LPG'.

Transmission spectra of both work are presented in Fig. 2.18.

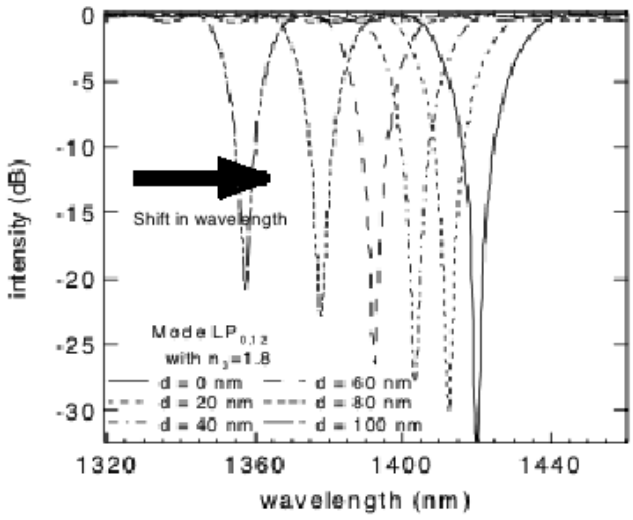

(a)

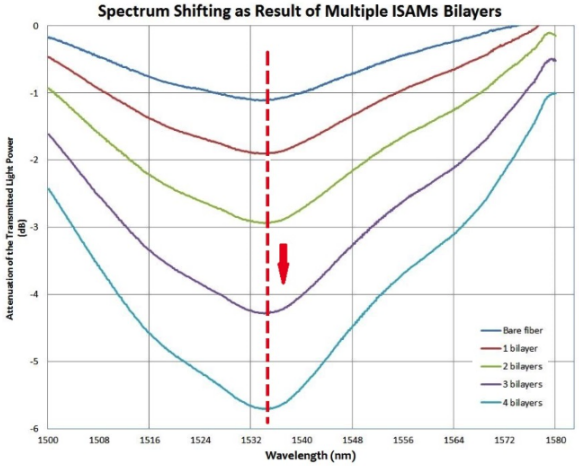

(b)

Figure 2.4: LPG operating on different measurement parameters: shift in wavelength vs. shift in attenuation magnitude. (a): Mode coupling between core and low order cladding mode. With addition of the thin film thickness the loss peak shifts to higher wavelength in the transmission spectrum. Transmission attenuation peaks from left to right: with addition of 0 nm, 20 nm, 40 nm, 60 nm, 80 nm and 100 nm of deposited thin film. Figure is modified from Wang *et al.* Z. Wang, J. Heflin, R. Stolen, and S. Ramachandran, Analysis of optical response of long period fiber gratings to nm-thick thin-film coating, Optics Express, vol. 13, no. 8, pp. 28082813, 2005. [1]. (b): Mode coupling between core and higher order cladding modes, or cladding modes operating in 'before-TAP' region. With addition of the thin film thickness the magnitude of the attenuation peak increases. Transmission attenuation peaks from top to bottom: bare LPG without thin film; 1 bilayer of ISAMs, 2 bilayers of ISAMs, 3 bilayers of ISAMs, 4 bilayers of ISAMs, respectively. Each bilayer of ISAMs thin film are consistent in thickness, which is around 5 nm per bilayer.

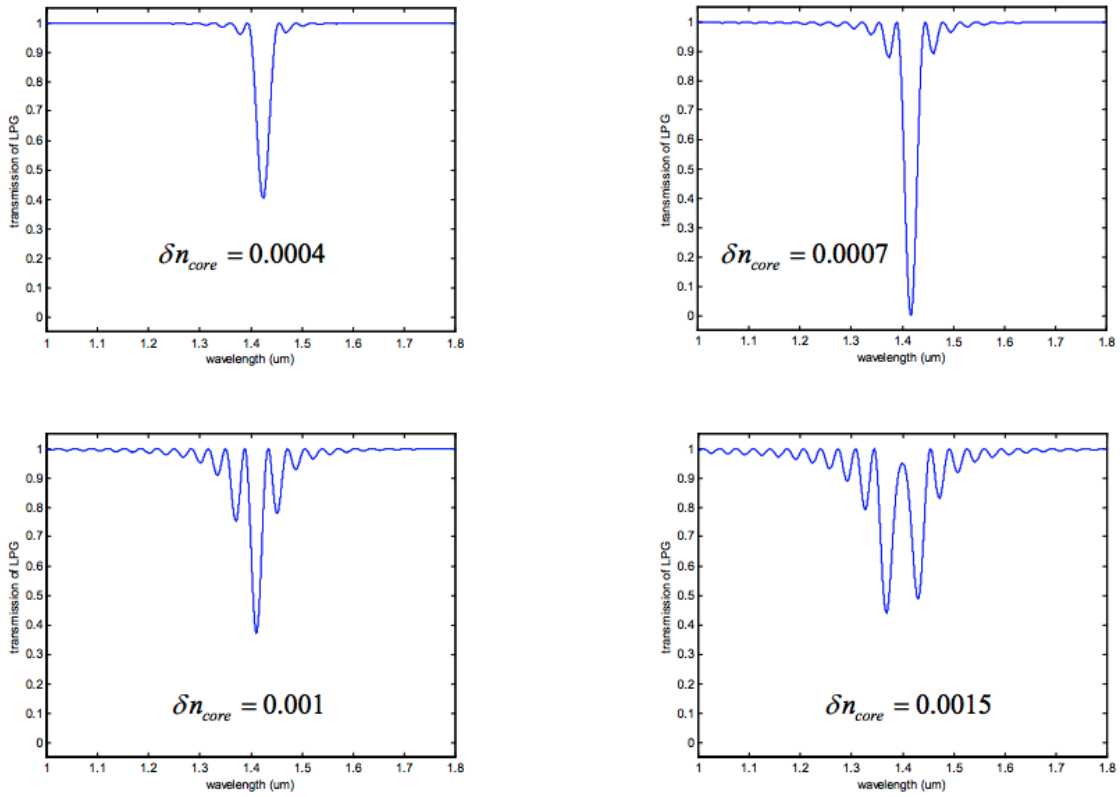

Figure 2.5: The simulated transmission spectrum of SMF with 5 μm radius core, 62.5 μm radius cladding, $n_{core} = 1.455$ and $n_{clad} = 1.45$, LPG's length is 10 mm with grating period of 240 μm, while the resonant wavelength is found at 1410 nm. Top left: average RI change to core (namely, δn_{core}) is 4×10^{-4}; top right: $\delta n_{core} = 7 \times 10^{-4}$; bottom left: $\delta n_{core} = 1 \times 10^{-3}$; bottom right: $\delta n_{core} = 1.5 \times 10^{-3}$. The spectrum simulations were conducted by Dr. Zhiyong Wang and presented in his dissertation. [52] Z. Wang, Ionic Self-Assembled Multilayers Adsorbed on Long Period Fiber Gratings for Use as Biosensors. PhD thesis.

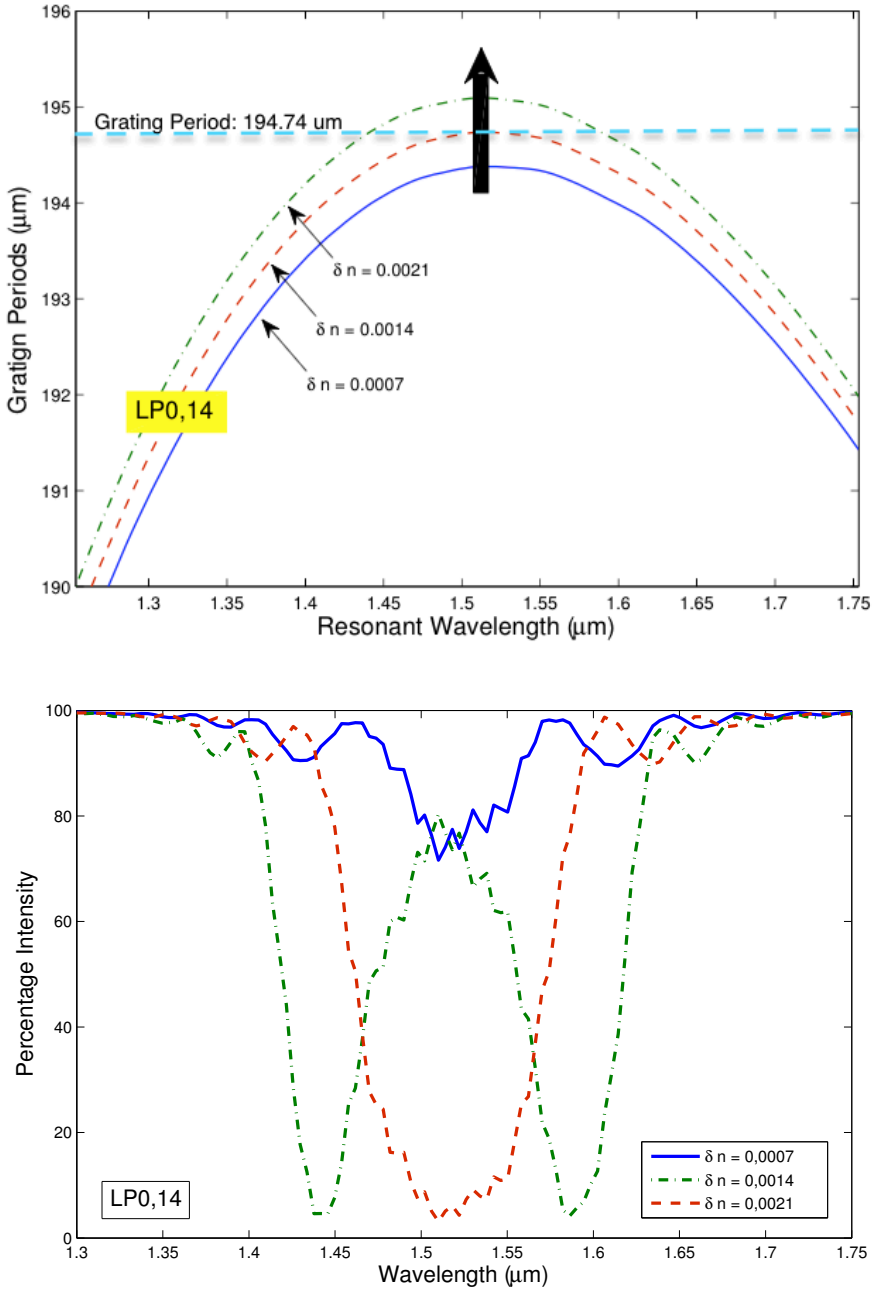

Figure 2.6: Value of the grating induced variation to the core RI has direct impact on the phase matching curve as well as the transmission spectrum. The increment of δn shifts the underlying PMC of $LP_{0,14}$ mode up. From the bottom curve to the top curve are: $\delta n = 7 \times 10^{-4}$, $\delta n = 1.4 \times 10^{-3}$ and $\delta n = 2.1 \times 10^{-3}$, respectively. Correspondingly, the TAP changes from 194.37 μm to 195.09 μm. The bottom plot shows the corresponding transmission spectrum simulation with LPG's grating period equals 194.74 μm, which is the TAP of LPG under $\delta n = 1.4 \times 10^{-3}$. This work was developed through the Matlab code written by the author.

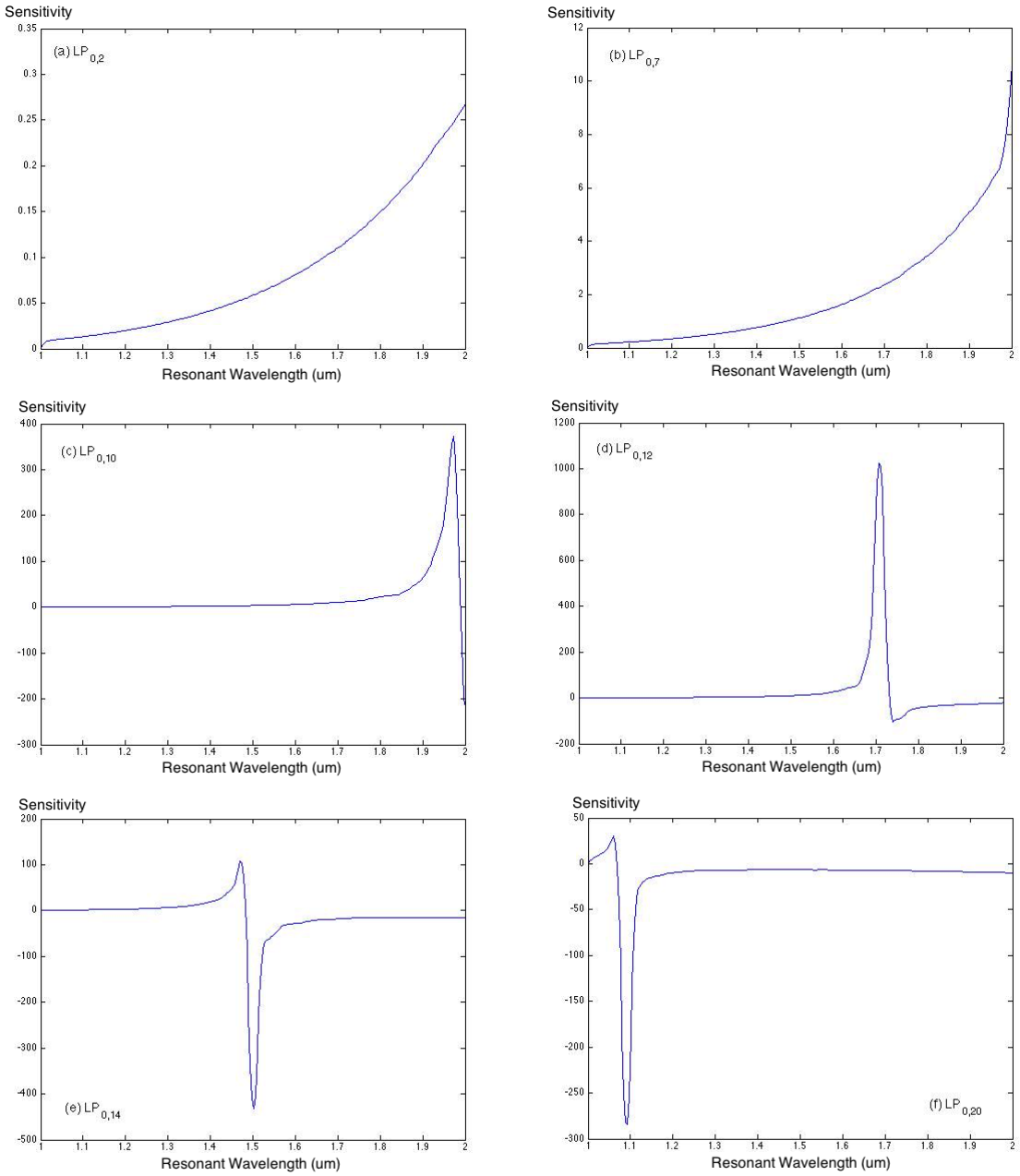

Figure 2.7: Plots of sensitivity-wavelength development of a LPG based on the coupled cladding modes. In each chart, the x-axis represents the wavelength of the transmission spectrum in μm, and the y-axis represents the scale of the sensitivity calculated from Eq. 2.17. (a) Coupled to $LP_{0,2}$; (b) Coupled to $LP_{0,7}$; (c) Coupled to $LP_{0,10}$; (d) Coupled to $LP_{0,12}$; (e) Coupled to $LP_{0,14}$; (f) Coupled to $LP_{0,20}$.

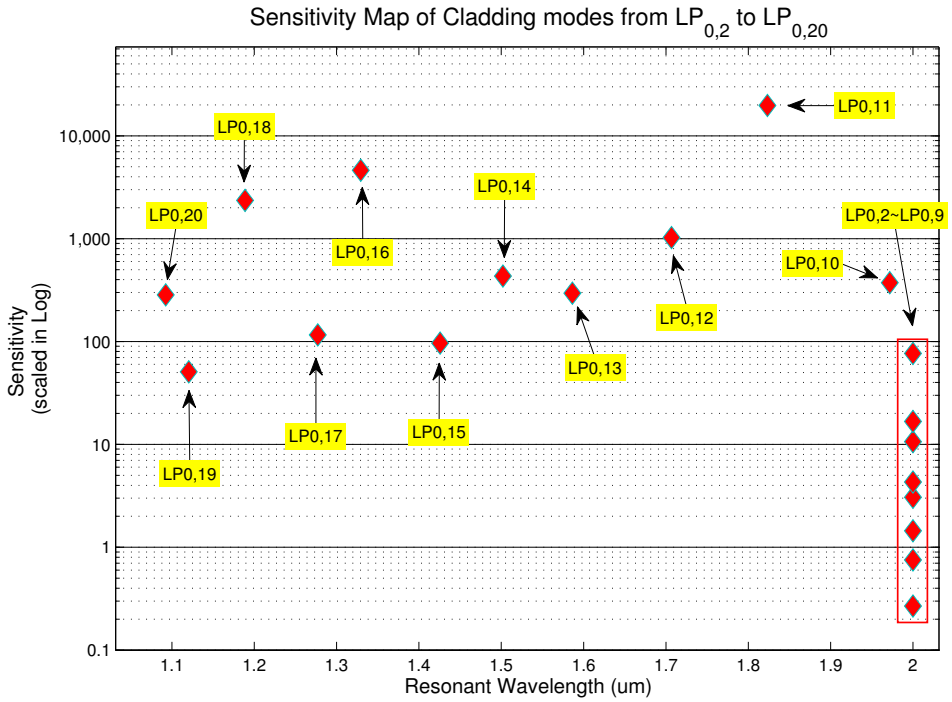

Figure 2.8: Sensitivity (value of $d\lambda/dn_{sur}$) map of the mentioned LPG, in regards of the maximum sensitivity value and the obtained wavelength. It is interesting to note that for cladding modes between $LP_{0,10}$ and $LP_{0,20}$, the maximum sensitivity is obtained at the locations of TAP, which falls within the 1.0 μm to 2.0 μm wavelength range in those cladding modes. This provides the proof that TAP-LPG has anomalously high sensitivity compared to conventional, 'wavelength-shifting' LPG.

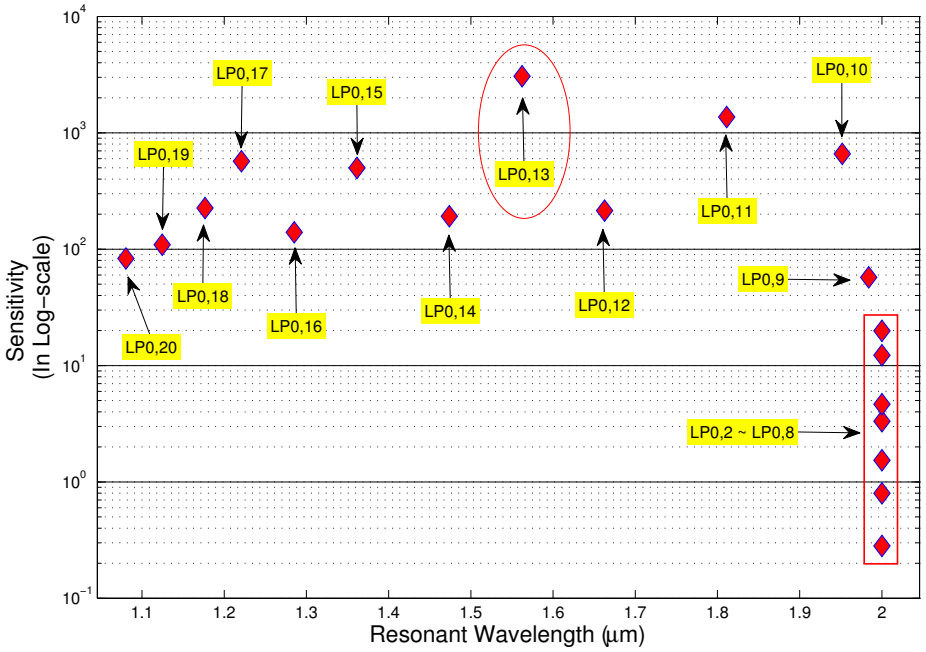

Figure 2.9: Finding the most sensitivity at the designated resonant wavelength by tuning LPG's δn. By increasing the average RI variation from $\delta n = 7 \times 10^{-4}$ in LPG discussed in Fig. 2.8 to $\delta n = 1.1 \times 10^{-3}$, the most sensitive cladding modes are found to locate at $LP_{0,13}$, whose resonant wavelength is 1.562 μm with the sensitivity of 3065 nm/10^3, up from 432 nm/10^3 in the previously mentioned LPG case with smaller δn.

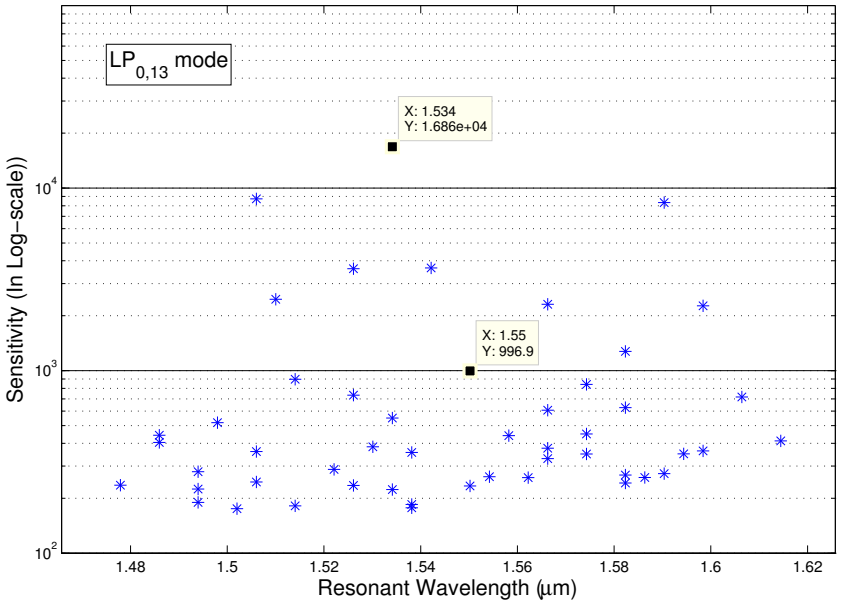

(a)

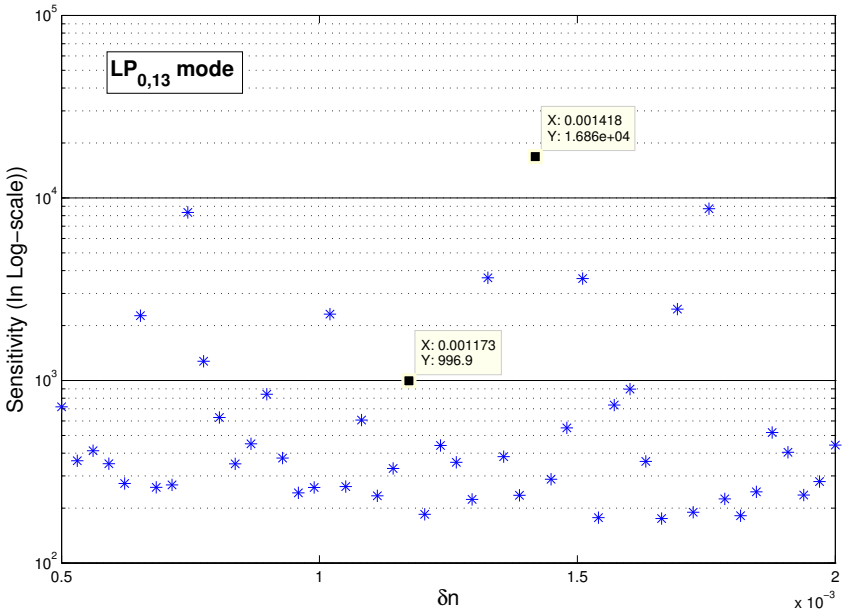

(b)

Figure 2.10: Sensitivity map for identifying the most sensitive LPG parameters such that its resonant wavelength falls close to 1550 nm. This requirement limits the LPG to couple to $LP_{0,13}$ mode. Top chart depicts the relationship between resonant wavelength and the sensitivity. The highest sensitivity is found with $\delta n = 1.418 \times 10^{-3}$ where the resonant wavelength locates at 1534 nm. Bottom chart depicts the relationship between the change of average RI with the sensitivity. It is obvious that choosing $\delta n = 1.173 \times 10^{-3}$ will give the resonant wavelength closest to the target, which is 1550 nm.

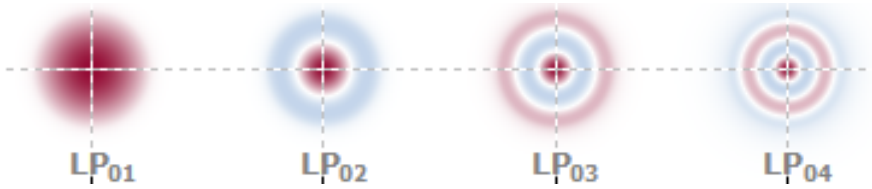

Figure 2.11: Spatial distribution of the first few $LP_{0,m}$ modes in a SMF. The value of the coupling coefficient κ_g is mainly determined by integral of the spatial overlapping between the core mode ($LP_{0,1}$) and cladding modes ($LP_{0,m}$). Figure is captured and modified from *http://www.rp-photonics.com/lpmodes.html*, the copyrights below to Dr. Rudiger Paschotta and RP Photonics Consulting GmbH. Used under fair use, 2015.

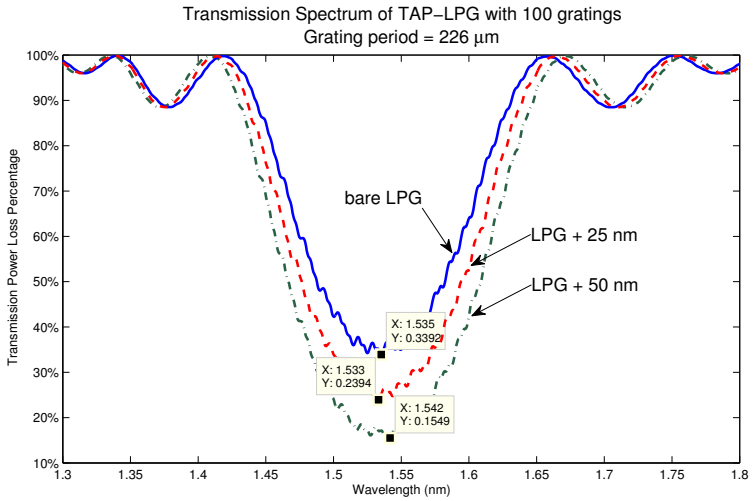

Figure 2.12: Spectrum simulation of a LPG fabricated at "before-TAP" region and showing slight wavelength shifting. This simulation explains the possibility that even to a TAP-LPG, there might be slight (around 2 to 5 nanometers) wavelength shifting due to thin film deposition.

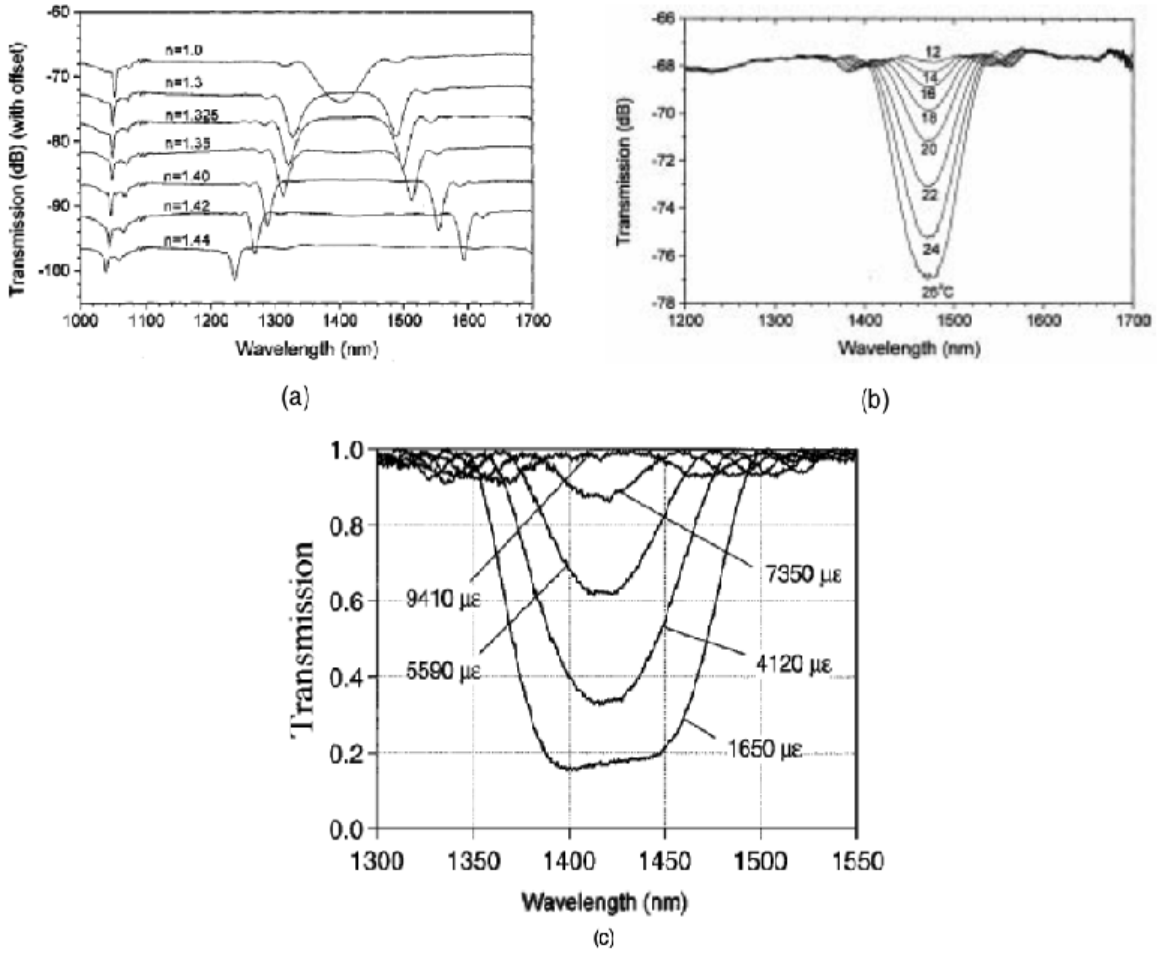

Figure 2.13: Examples of the intensity based TAP-LPG fiber sensors. Clockwise from top left: (a) temperature sensor, demonstrated by Shu *et al.* [2]; (b) temperature sensor, also demonstrated by Shu *et al.* [2] X. Shu, L. Zhang, and I. Bennion, Sensitivity characteristics of long-period fiber grat- ings, Journal of Lightwave Technology, vol. 20, no. 2, p. 255, 2002. Used under fair use, 2015; (c) strain sensor, demonstrated by Grubsky *et al.* [3] V. Grubsky and J. Feinberg, Long-period fiber gratings with variable coupling for real-time sensing applications, Optical Letters, vol. 25, p. 203205, 2000. Used under fair use, 2015.

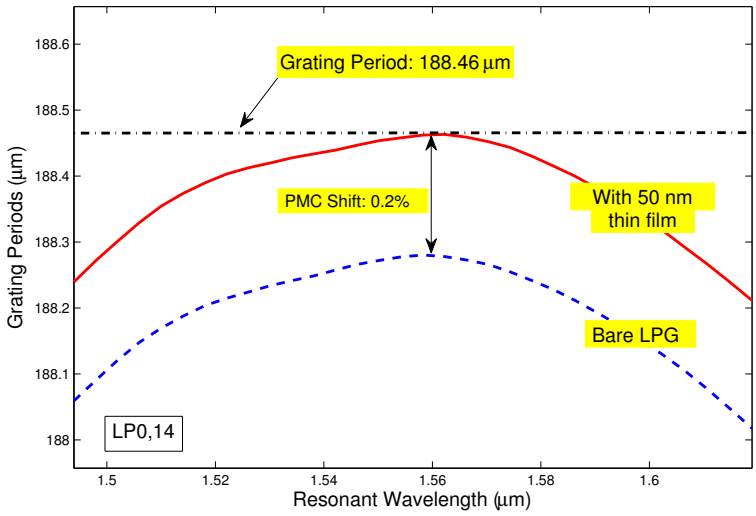

(a)

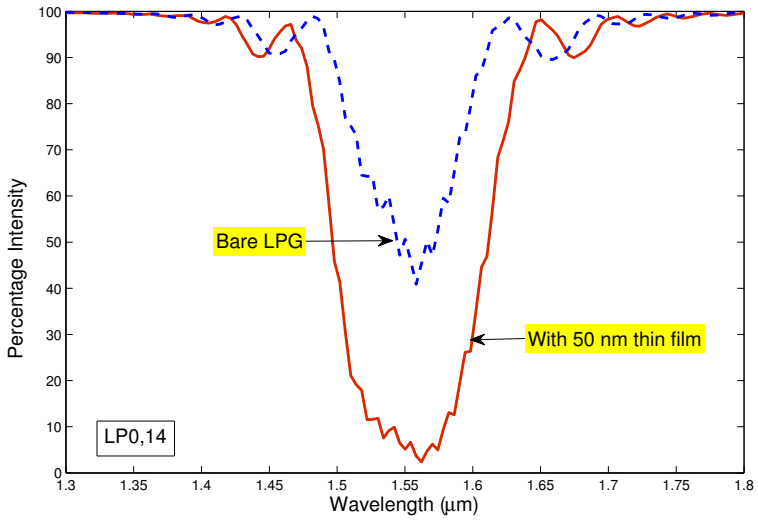

(b)

Figure 2.14: PMC shift due to deposition of 50 nm of ISMAs thin film, which results in an additional 40% loss of transmission power at the resonant wavelength. The TAP-LPG is able to sense the surface thin film's thickness variation of the nanometer-scale: (a) with deposition of ISAMs thin film at thickness of 50 nm, the PMC is shifted up by 0.2 μm, which is equivalent of 0.2% change. The bare LPG is tuned to the 'before-TAP' region for maximum sensitivity. (b) the resulting of transmission spectrum shifting due to deposition of ISAMs thin film. The transmission intensity undergoes an additional 40% loss at the resonant wavelength of 1562 nm.

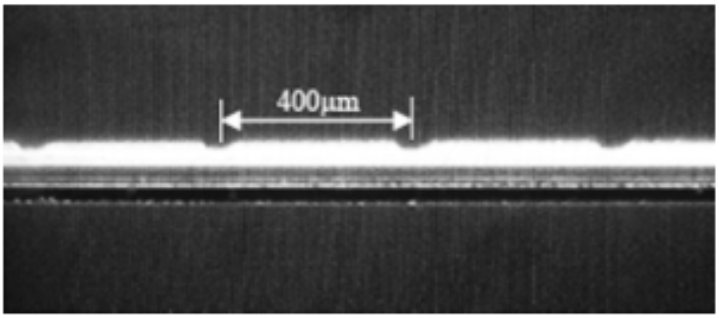

Figure 2.15: Exposure of SMF to high laser power can lead to carving grooves on the cladding of the fiber, due to surface vaporization and spallation. This will create an asymmetric LPG. Image is taken and modified from work conducted by Wang *et al.*. [24] Y.-P. Wang, D. N. Wang, W. Jin, Y.-J. Rao, and G.-D. Peng, Asymmetric long period fiber gratings fabricated by use of co2 laser to carve periodic grooves on the optial fiber, Appl. Phys. Lett., vol. 89, p. 151105, 2006. Used under fair use, 2015.

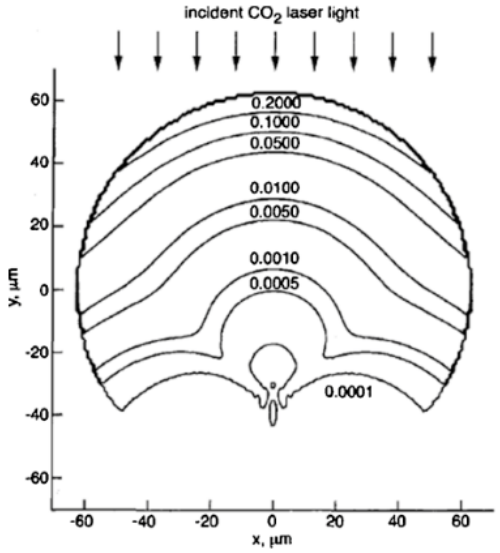

Figure 2.16: Exposure to an incident CO_2 laser beam will lead to asymmetric RI variation to the exposed side of the fiber. Figure shows the cross-section view of the fiber with optical laser power absorption at the laser beam incident side. Th figure is taken and modified from work done by VanWiggeren *et al.*. [69] G. D. VanWiggeren, T. K. Gaylord, D. D. Davis, M. I. Braiwish, E. N. Glytsis, and E. Anemogiannis, Tuning, attenuating, and switching by controlled flexure of long- period fiber gratings, Opt. Lett., vol. 26, no. 2, pp. 6163, 2001. Used under fair use.

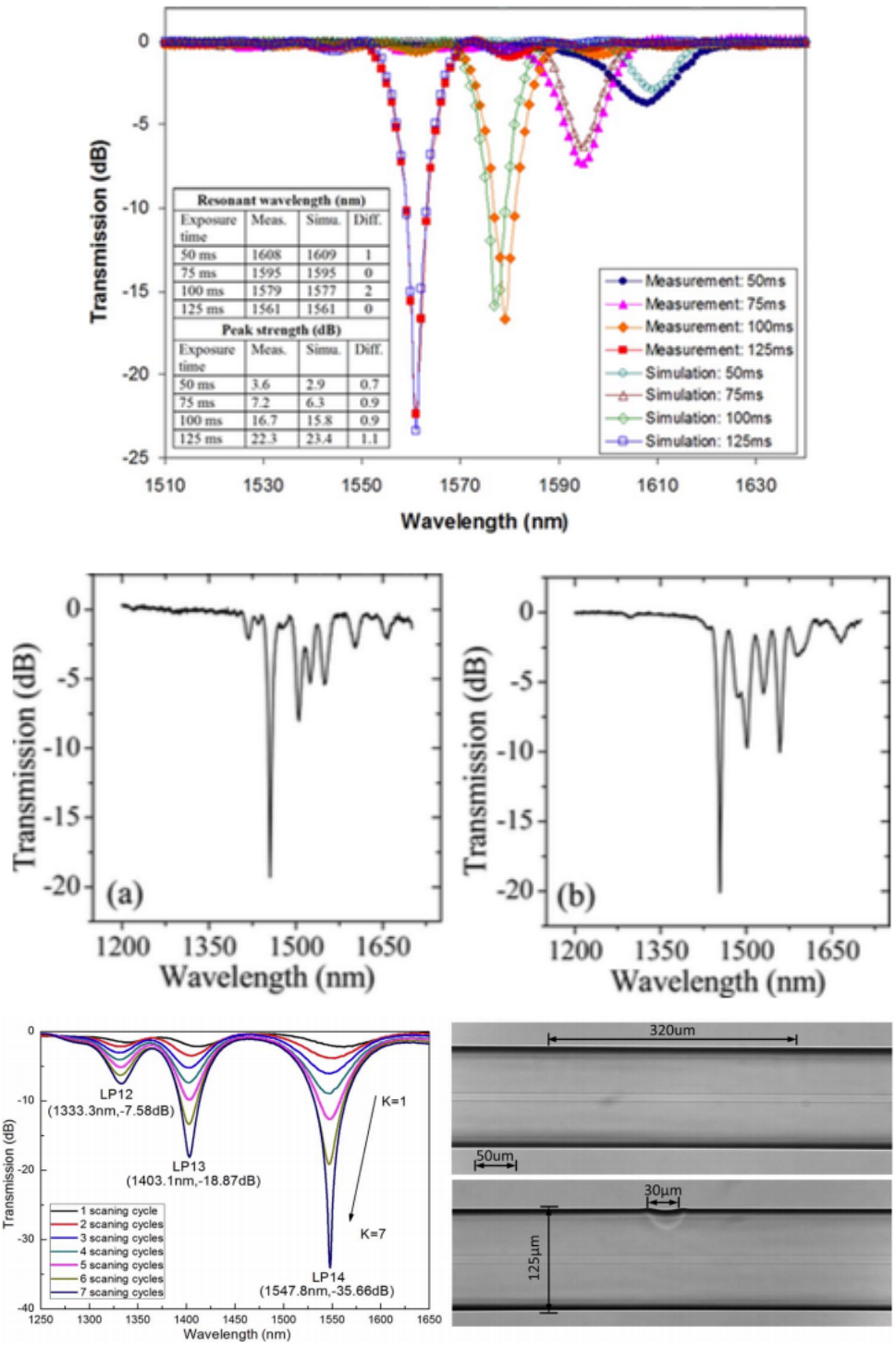

Figure 2.17: Spectrum examples of preceding work on fabrication of conventional LPG with CO_2 laser irradiation. Top: Work done by Li *et al.*, [72] (Y. Li, T. Wei, J. A. Montoya, S. V. Saini, X. Lan, X. Tang, J. Dong, and H. Xiao, Mea- surement of -laser-irradiation-induced refractive index modulation in single-mode fiber toward long-period fiber grating design and fabrication, Appl. Opt., vol. 47, p. 5296, 2008. Used under fair use.) the LPG has 89 points of gratings with period of 525 μm and resonant wavelength at 1561 nm. Middle: Work done by Liu *et al.*, [73] (Y. Liu and K. S. Chiang, Co2 laser writing of long-period fiber gratings in optical fibers under tension, Opt. Lett., vol. 33, p. 1933, 2008. Used under fair use,

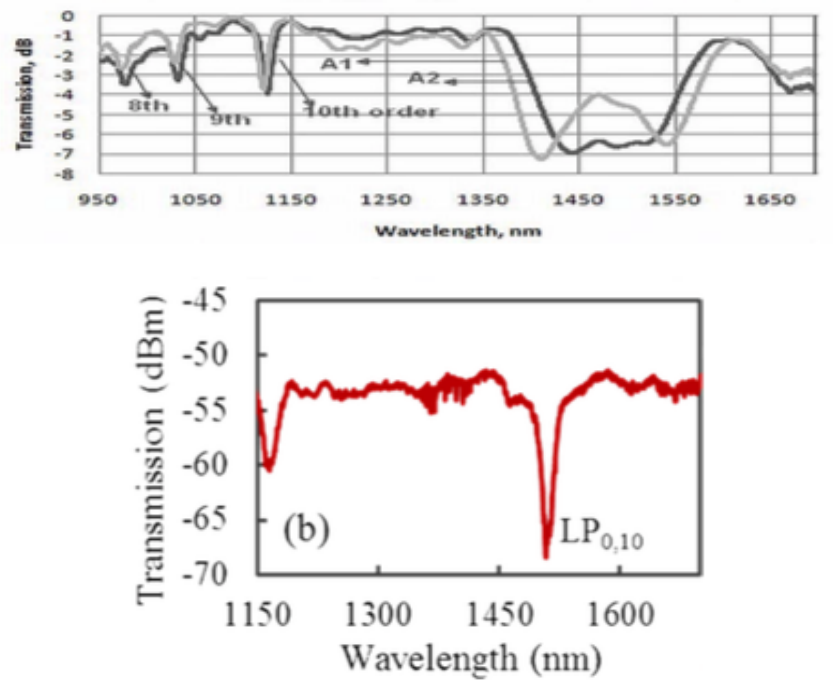

Figure 2.18: Spectrum examples of preceding work on fabrication of TAP-LPG with CO_2 laser irradiation. Top: Sole peak tuned right on the TAP, thus after exposure to Gamma radiation, the attenuation peak split to two. Figure was taken from work donw by Chaubey *et al.*. [75] (S. Chaubey, S. Kher, and S. M. Oak, Radiation and taper tuning of long period grating for high sensitivity strain measurement, Proc. IEEE 7th WFOPC, pp. 14, 2011. Used under fair use.) Bottom: Spectrum reported by Tian *et al.* [78] (F. Tian, J. Kanka, X. Li, and H. Du, Exploration of higher-order mode coupling in long- period gratings for sensitive monitoring of polyelectrolyte self-assembly at nanoscale, vol. 9098, pp. 90980R90980R8, 2014. Used under fair use.) for TAP-LPG that couples core mode with $LPG_{0,10}$ cladding modes.

Chapter 3

LPG Fabrication Setup and Procedure

3.1 Grating fabrication techniques

Despite a variety of techniques to induce RI variation in a fiber core, laser irradiation based LPG fabrication is the most popular and widely deployed method for LPG related research. Gratings can be induced by either UV-laser exposure or CO_2 laser irradiation technique. Compared to other gratings fabrication techniques, laser irradiation methods are more controllable and have demonstrated high reproducibility in producing quality LPGs. Therefore, this thesis will focus on discussion of laser induced grating-writing mechanisms and techniques.

Ultraviolet lasers, or UV lasers, are the laser systems that generate laser beams of continuous wave or pulses at a short wavelength in the ultraviolet spectrum, typically of a few hundred nanometers depending on the laser type. Excimer UV lasers have been the

most common laser systems for producing fiber gratings for their photon-material interaction characteristics. The excimer laser can disintegrate fine layers of materials through ablation rather than burning, promising exceptional precise removal of materials at the exposure region. Consequently excimer lasers have found wide applications in high-resolution photoligthography and micromachining. [79]

The first demonstration of writing LPG on fiber was demonstrated by Vengsarkar *et al.* through irradiating photosensitive optical fiber by a KrF laser. [16] UV-laser induced LPGs are often written using the phase-mask technique, where a piece of silica glass with a one dimensional slit array is set between UV laser and optical fiber to diffract the incident laser ray. The interference of the diffracted UV beam originates a fringe pattern, and with the help of a cylindrical lens, the pattern is focused along the fiber's core to induce photosensitive reactions that will modulate the refractive index at the intensity peaks of the fringe pattern. The profile of the phase mask is chosen in consideration of distributing the transmitted laser power properly for homogeneous RI modulation as well as setting the separations between intensity peaks , which spatially correspond to the fiber grating locations.

An alternative laser irradiation technique to inscribe a fiber grating is to use a CO_2 laser system. The CO_2 laser system was one of the earliest gas lasers, whose principal wavelength bands are centred around 9.4 μm and 10.6 μm. The CO_2 laser is known for its high output beam power and as been discussed in the previous chapter, the optical irradiation induced thermal effects will lead to the RI modulation of the underlying fiber and create fiber gratings.

Using a CO_2 laser for LPG production was first reported by Davis *et al.* [20] and

ever since have been popular in development of optical fiber sensors. [80] Due to the lack of available phase masks for CO_2 laser irradiation, fiber gratings are inscribed point by point. Unlike the phase mask technique where optical components are aligned before the irradiation and retain their positions during the gratings' fabrication, the point by point method requires the horizontal shift of either the irradiation beam or underlying fiber, or both, along the fiber direction during the fabrication of the LPG. In this process, the laser beam is focused directly on the surface of the fiber where a single grating is written and separated a grating period from the last one. The laser beam, though initially emitted as a Gaussian beam, can be focused to a circular spot or an elliptical spot, using a spherical lens or cylindrical lens, respectively. Focusing laser beam using cylindrical lens is favourable in creating small grating regions and LPGs with short grating periods, since the minor axis of the elliptical spot is always aligned with the fiber axis such that the affected fiber region can be much smaller than that of a circular spot with the same focal length.

Fig. 3.1 summarizes the discussed fabrication techniques: (a) compares different irradiation techniques – phase mask methods that are mainly used for UV-laser irradiation, and point by point methods that have been reported as used for both UV-laser and CO_2 laser irradiation. (b) compares different focused spots – circular spot is through spherical lens and elliptical spot through cylindrical lens, respectively. The affected longitudinal area of the elliptical spot is smaller than the area affected by circular spot, if the same Gaussian beam is focused through spherical or cylindrical lens with uniform focal length.

Compared with the UV-laser exposure technique, using a CO_2 laser as the laser irra-

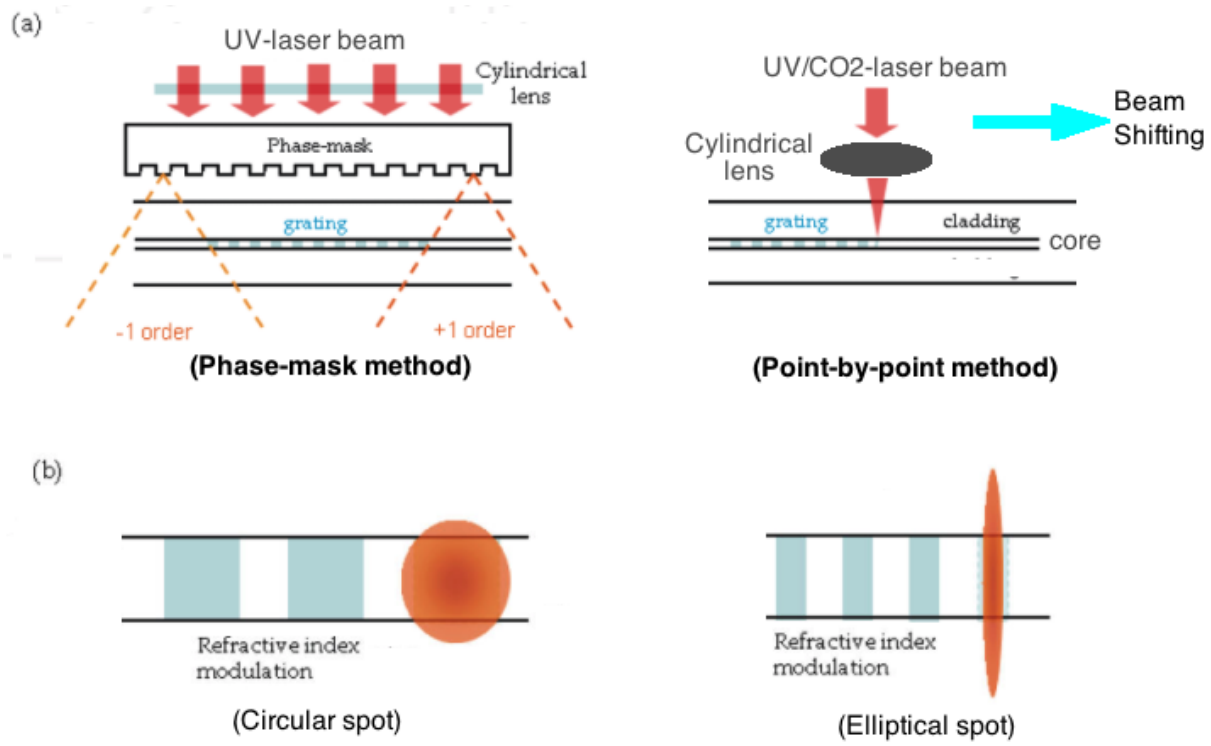

Figure 3.1: Comparison of various laser fabrication methods. (a) the phase mask method is shown on the left, and the point-by-point method is shown on the right. Phase mask method can only be used in UV-laser irradiations. (b) the circular spot is shown on the left, and the elliptical spot is shown on the right. The elliptical spot has shown a smaller affect fiber area and thereby is more ideal when writing LPG with short grating periods. Figure is taken and modified from Coelho *et al.*. [40] J. M. P. Coelho, M. Nespereira, C. Silva, D. Pereira, and J. Rebordo, Current Develop- ments in Optical Fiber Technology, ch. Advances in Optical Fiber Laser Micromachining for Sensors Development. InTech, 2013. Used under fair use, 2015.

diation source for inducing fiber gratings has many advantages. Since the thermal effect is the main cause of RI modulation instead of through photochemical processes required by UV-laser irradiation, fiber gratings can be written on most telecommunication fibers by CO_2 laser. Furthermore, CO_2 laser induced fiber gratings have a better temperature toleration range than the UV-laser induced gratings, making it capable in more applications. In addition, industrial applications of CO_2 laser systems have a long established history to reduce

the acquisition and maintenance cost, as well as boasting its availability and laser beam quality. The cost efficiency of deploying a CO_2 laser system is particularly an advantage over the UV-laser systems, which are expensive to operate and require a trained technician for regular maintenance. Therefore, in the scope of this thesis, the CO_2 laser system is the choice for fabricating LPG fiber sensors.

3.2 LPG fabrication system and conditions

The most important components of the LPG fabrication system are the CO_2 laser source system (Synrad UC-2000 controller + J48-2 CO_2 laser with maximum output power of 25W) and the translation stage system (Newport ESP300 Motion Controller/Driver + UTS100CC Linear Stage with on-axis accuracy of 100 nm). Both systems can be either operated separately in manual modes, or controlled and coordinated remotely through computer programs.

Fig. 3.2 depicts the design scheme of the LPG fabrication system. The CO_2 laser and the translation stage are connected to laser/stage controllers which can establish continuous communication with the commanding computer program once turned on. The computer will transmit controlling commands to the laser/stage controller first, where corresponding signals and operational pulses are translated and sent to the instrument to conduct particular tasks. The laser shutter is operated manually, which will only be opened right before the fabrication process. The CO_2 laser will remain 'ionized' while powered up and connected with the laser controller, which will keep sending so-called 'tickle' pulses at 5 kHz frequency

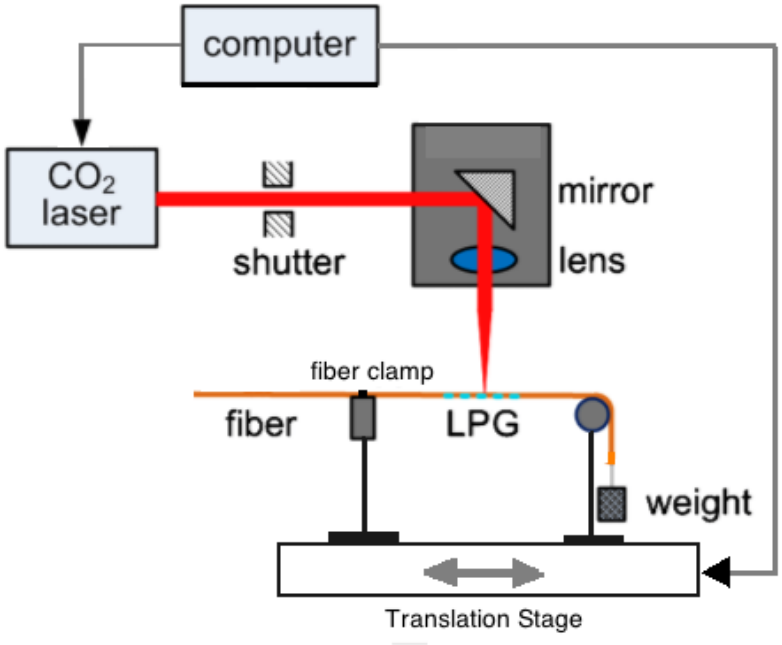

Figure 3.2: The design scheme of the LPG fabrication system used for producing LPG fiber sensor for experiments in this study. The Matlab program executed from the computer as the controlling unit will determine the laser beam's power, irradiation duration, pulse repetition and translation stage's movement following exact time frame to inscribe LPG of designated quality and characteristics.

to retain the ionization state. However, the outgoing beam's power level in such standby stage is negligible, meaning it is safe to keep shutter open while the operational signal is absent between each point-by-point irradiation step.

Depending on the fabrication requirement, the pulse frequency can also be set to 10 kHz or 20 kHz. Researchers have reported successful grating imprinting under both 5 kHz and 10 kHz, though in this study we have chosen to use 5 kHz as the default signal frequency setting, unless stated otherwise. The laser power is controlled through a process called pulse width modulation, or PWM. During this process, the percentage of a period the signal remains at

high voltage in a duty cycle will be translated into the percentage of output power through the laser's RF amplifier. For instance, in a 5 kHz signal frequency setting, each duty cycle is 200 μs in time length. Then a pulse signal consisting of 100 μs of high voltage and 100 μs of low voltage is corresponding to a 50% duty cycle, which in turn stimulates a 50% of maximum laser power to the outgoing beam. It shall be noted that in order to maintain pulse laser output, the maximum possible duty cycle is set for 95% by the laser controller system.

The output laser beam is a typical Gaussian beam, and is reflected by a ZnS mirror and focused by a cylindrical lens (focal length = 50 mm). The optical system will direct and focus the laser beam to the surface of the underlying SMF, where the elliptical spot has the size of 3 mm $\times$ 150 μm and is perpendicular to the longitude direction of the fiber. The affected fiber surface will be about 150 μm along the fiber axis over the incident side of the fiber, which will be equivalent to the surface area of $2.94 \times 10^{-4} cm^2$. Supposing the incident beam power is 4W, the power density on top of the incident side of the fiber will be $1.36 \times 10^4 W/cm^2$. Consequently, a 30 ms irradiation of the mentioned laser beam will eject a $408 J/cm^2$ energy flux on the fiber surface.

The translation stage is set over a stable optical table, whose motion direction is parallel to the fiber axis and is perpendicular to the elliptical spot of the focused beam. The on-axis accuracy of the translation stage is 100 nm, which compared with the ordinary grating period of 200 μm this instrumental accuracy is acceptable. Two poles with a fiber clamp and a free roller, respectively, are installed on the translation stage. The fiber clamp is used

to fix one end of the fiber, while the other end will be placed on the free roller and attached to a weight in some experiments, or fixed without external tension to the pole, depending on the chosen experimental parameters. The height of the poles are carefully adjusted such that the fiber will lie horizontally. This is critical to avoid making chirped or tilted gratings. The buffer jacket of the fiber needs to be stripped off, while adjusting the position of the optical mirrors as well as the translation stage to ensure the exposed fiber area will remain in the center of the ellipse spot.

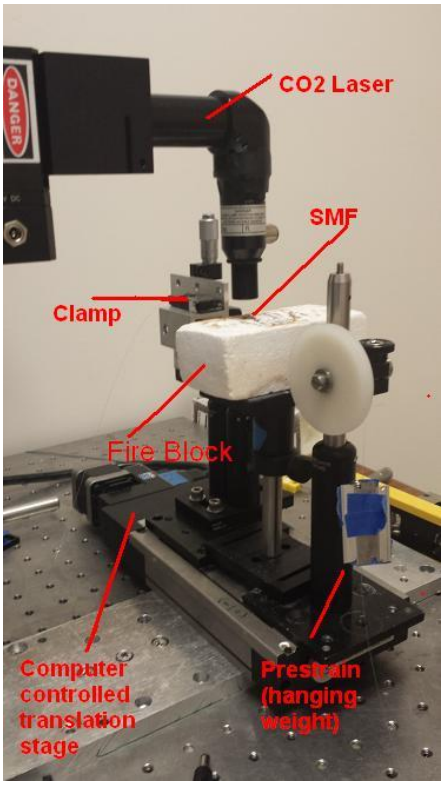

Figure 3.3: The design scheme of the LPG fabrication system used for producing LPG fiber sensors for experiments in this study.

Fig. 3.3 shows how the fabrication system is assembled in the laboratory. The optical components are incorporated and sealed into the L-shaped laser head. The fire block is

placed underneath the fiber and is responsible to collect dumped beam. A low-power, spot-showing laser is incorporated inside the beam guidance tube to show the location of the beam spot, which will help determine the relative locations between the laser and stage such that the fiber will lie right across the spot. The whole stage system region, including part of the L-shape laser head, will be shielded properly against laser splashing during fabrication operation.

The use of prestrain has been proven to be helpful in improving an LPG's fabrication efficiency and enhancing the contrast (determined by the attenuation intensity at the resonant wavelength). [24, 73, 81] The applied external tensile strain will work simultaneously with the laser irradiation during the grating writing process, where the extra tensile strain tends to further release the built-in viscoelasticity and modulate the refractive index in the fiber. As a result, less laser power will be needed to obtain a desired RI modulation of fiber gratings with the presence of prestrain.

On the other hand, this study has also found that a large prestrain could induce counter effects as well. In particular, under an asymmetrical irradiation as used in this study, a large attached weight (> 50 g) tends to create microbend at the grating positions, which may introduce nonaxially symmetric cladding modes and increase the risk of producing fiber cracks. Some of the LPGs fabricated with a large attached weight would also significantly increase the insertion loss and lead to fluctuates in the transmission spectrum, since some of the gratings may be stretched so much that the physical densification and/or deformation would weaken the transmission of the guided mode and make the fiber more vulnerable to

the small fluctuations of inner tension or environmental temperature.

3.3 Controlling program and functions of its interface

All fabrication parameters will be entered into the Matlab program that is specifically developed to coordinate the operation of the laser and the stage. This Matlab program is largely modified and improved to suit the purpose of this thesis from the previous version written by Mr. Bo Liu, which is kindly authorised for use by Mr. Liu. The interface of the Matlab program is shown in Fig. 3.4. The inputs are divided into a few groups depending on their functionalities and to avoid false parameter entrance.

The 'laser settings' contain all parameters that will control the power of the laser beam and its duration. 'Initial power' and 'ending power' correspond to the power level at the beginning and ending of writing a spot on the fiber, respectively. By default the initial power equals the ending power, however one can decide to use a varying laser power during the grating period for achieving certain grating effects or controlling the fiber's physical deformation. The 'rising time' and 'falling time' will control how long it will take to rise from zero output power to the full initial power level or fall from ending power to zero. The 'on time' will be controlling the time period between first reaching the initial power and right before the decline from the ending power. 'Time step' refers to the time period before making necessary output power adjustment. It should be noting that the minimum possible value for correct execution of this Matlab program requires a time step of 1 ms or more. If

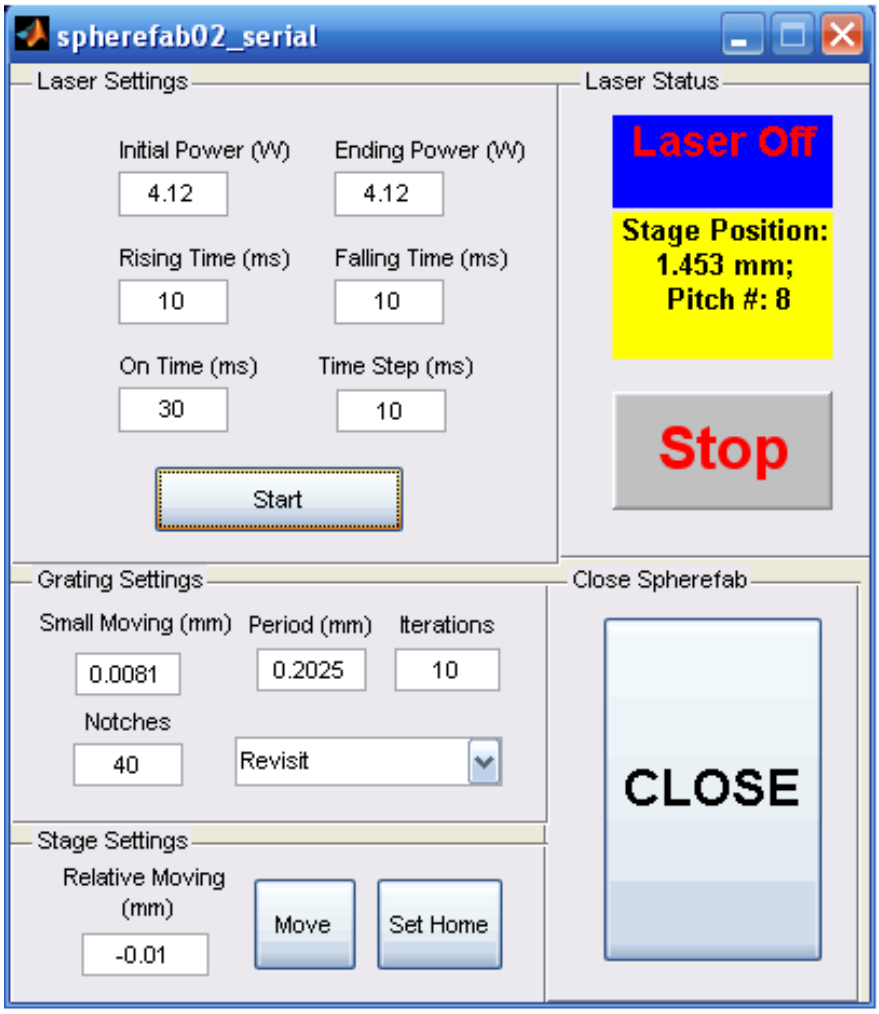

Figure 3.4: Program interface of the Matlab program developed for controlling all fabrication parameters of laser and stage operations. One can set the laser pulse power, the irradiation period at each writing cycle, the grating period, how the scanning process is to perform, moving the stage to default positions, or stop a LPG writing process for emergency reasons, etc.

the time step is entered larger than either of the 'rising time', 'falling time' or 'on time', the time step will be automatically set to the minimum value of the three. All units of the laser power data are in Watts (W), and all time data are in milliseconds (ms). Fig. 3.5 shows how these laser parameters determine the output power level of the CO_2 laser. It should be

noted that the 'rising time' and 'falling time' can be both set to 0, if necessary.

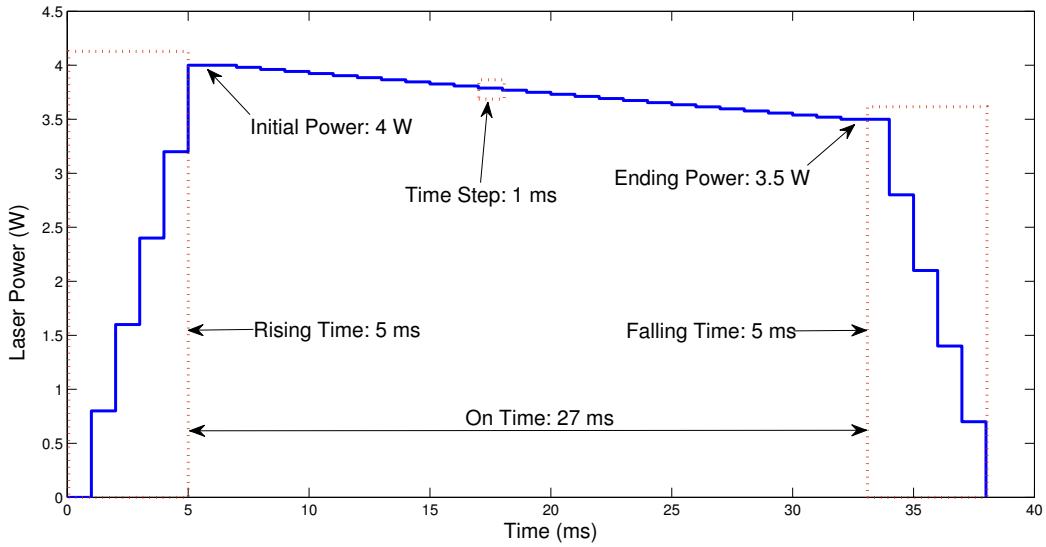

Figure 3.5: Chart of the relationship between parameters set in 'laser settings' and the output laser power in each grating cycle. In the case shown in this figure, the initial power is 4 W, the ending power is 3.5 W. Rising time and falling time are both 5 ms, the on time is 27 ms, and time step is 1 ms.

In the 'grating settings' one can enter controlling parameters regarding the movement of the translation stage. The 'Small Moving' indicates a small movement of the stage after each laser irradiation, for the purpose of offsetting the fiber tapering and stretching, or producing a so-called 'longer grating' where the grating region subjected to laser irradiation is purposely extended. 'Period' refers to LPG's grating period and it's in the unit of millimeters (mm). The stage accuracy is 100 nm, or 0.0001 mm, therefore the gratings period can be set to the level of 10^{-4} mm. Usually the grating period is a positive value, however, it could also take a negative value if the gratings are desired to be written at the reversed direction (the flexible fiber end is set as the positive and default direction). 'Iteration' denotes how many times

does the user wish to repeat the grating process. This repeating of grating writing can be processed in two different modes: the 'Revisit' mode and the 'Multiple Shot' mode, which can be chosen from the drag down menu right under the 'Period' and 'Iteration' block. In the 'revisit' mode, the laser will perform point-by-point inscription of gratings fully from the beginning point till the end point, then the laser will stay on standby while the translation stage brings the fiber back to the beginning point where the whole point-by-point imprinting process will repeat again. This cycle will repeat N times where N is entered under 'iteration'. For the 'Multiple Shot' mode, the translation stage will pause at the grating location and allow the laser to repeat the irradiation step N times before moving the fiber to its next grating position. In this process the stage will move the fiber from the beginning of the grating to the end of the grating only once. The 'notches' will determine the number of gratings to be written to the fiber. The system will stop and bring the stage to its initial position after the complete amount of iteration visits as well as grating notches have been accomplished.

The 'stage settings' is a separate unit for controlling the translation stage's controller and stage system. The move button will read the entry to the 'Relative Moving' and move the stage accordingly. It is worth noting that the stage will move from the position when the 'Move' button is pressed. Entry of a positive or negative value will direct the stage in either of its moving directions. The 'Set Home' button will set the current stage position as the home position, or in other words, this position will be set as the origin of the stage axis (the 0.000 mm location). This home position is important, since it will be the location

every grating writing process begins with and is reset to after all work is done.

Also, on the right half of the program there are status monitor and emergency buttons. The 'Laser Status' screen will reflect whether or not the laser is in operation: 'laser off' when laser is not in writing a grating and 'laser on' when laser's output beam is irradiating the fiber. The monitor screen also shows the current stage position (in millimeters) and the current notch number (which equals one plus the number of notches that have already been written). The 'Stop' button is for emergency use, which will abort all undergoing processes, kill off commanding signals to the power laser irradiation and bring the stage back to its initial home position. In addition, the 'close' button will perform every work done with the 'Stop' button and terminate the Matlab interface program as well. The 'start' button will read all the parameters displayed at each data entrance block, process and generate commands to start the computer-coordinated LPG fabrication.

3.4 Fabrication procedures

The fabrication of an LPG can be fully controlled by the computer program, hence the manual preparation work is minimal. The steps below list a complete procedure for LPG fabrication from the beginning:

Connect and power up the system:

1. Connect laser's power wires with the power source and power up the laser source. Connect laser's commanding port with the laser controller and turn on the laser controller

(UC-2000 in this study). It is important to check the settings of the laser controller: whether the controller is set to the 'remote mode', whether the signal frequency is set to the right value (5 kHz, 10 kHz or 20 kHz), *etc.*. Every person present in the laser room shall be wearing protection goggles at this step.

Note: disconnecting and reconnecting the serial-to-usb cable to the computer will have probability to generate a different port number in the device manager of the computer's OS, this port number should either be changed back to the previous one, or one needs to modify the relative port settings in the Matlab program. Otherwise the program won't be able to either recognize the laser controller or send commands through the correct port.

2. Turn on the laser switch and wait for 10 minutes to allow laser to warm up to the fully lasing conditions. There is a mandatory pause of 5 seconds between turning on the power switch and output of laser beam set by the manufacturer, if the laser has already been warmed up previously.

3. Connect the translation stage controller (ESP-300 in this study) with the stage and power up the controller. The controller will take around 15 seconds to preconfigure itself before taking any further operation requests. Check whether the stage is connected to the right port of the controller (port 1 by default), otherwise all the stage controlling commands of the Matlab program will require modification to reflect the change of the port.

4. Check the connections between laser/stage controller and the computer. When properly connected, configured and powered up, the computer's 'device manager' program should be able to reflect an NI's GPIB connector (for stage controller) and a serial connector (for laser controller) among other expandable devices.

5. Move the stage to its negative mechanical limit, either manually, through the native ESP-300 controller program, or through the Matlab program's 'Stage settings'. When the process is done, reset the present location as the home position, either manually on the controller's physical interface, through the native controller program, or through the Matlab program.

Fabrication of fiber gratings:

1. Take an SMF of 0.8 meter to 1 meter in length, strip off the buffer jacket at the middle section of this fiber for 120% length of the total gratings length (number of gratings $\times$ grating period). Use alcohol soaked optical paper to clear the stripped fiber section of any dust or fragments.

2. Tether one end of the fiber to the fiber clamp, wrap the other end over the free roller and fix a predetermined weight over this end of the fiber for a pre-strain. If no pre-strain is needed in the fabrication process, make sure to stretch the fiber straight between the clamp and roller and tether the free end of the fiber to the pole of the roller.

3. Enter all fabrication parameters and choose fabrication mode in the Matlab interface. It would be helpful to press 'enter' button on the keyboard to make sure the program

have taken the new data enter. Adjust the relative locations of the laser or translation stage such that the ellipse laser spot will be perpendicular to fiber's longitude direction and have the fiber go across the spot right through the center. The spot should sit at the beginning of the gratings, which is also the roller-side end of the stripped clear section.

4. Check if the fire block is placed underneath the fiber and the laser spot. Make sure the fire block is long enough to cover the entire gratings length.

5. Open the laser shutter, set up laser-splash protections and click the 'start' button in the Matlab interface to start the automatic fabrication process.

6. After the entire irradiation and iterations are finished, turn off the laser shutter immediately and remove necessary splash protections if it would hinder the removal of the fiber.

7. If more LPGs are to be fabricated, repeat step 1 through 6 with entry of new fabrication parameters.

8. When all fabrication work is done, turn off the laser switch, close the Matlab program and power down the laser source. If the system won't be used again in the next few days, it would also be helpful to disconnect signal cables from the instrument. Make sure the laser shutter is kept off, as it's purely manual.

   Note: Make sure the laser source is powered down before taking off eye protection goggles. It is also important to turn off the Matlab program first before shutting

down the controllers, since doing in the wrong order will create execution error to the program and cause the program to collapse. It can only be restarted if this has happened.

As has been discussed in previous chapter, the LPG will be fabricated in a point-by-point manner. There are a few ways to execute this fabrication strategy, including using a 2D scanner or rotation mirror, or moving the fiber and controlling time series of laser irradiation, *etc.*. Due to limited availability and accuracy of instruments, this study will stick with the fabrication strategy that the moving stage will move the fiber to the grating position, pause for laser irradiation, then move the fiber to the next grating position. In order to protect the laser from over heating, after laser irradiation the stage will pause for an extra period.

Certain situations may occur during the fabrication process that require immediate attention. For instance, after 3 to 4 hours of laser usage, the laser may become less stable in output power. A common situation might be a sudden burst of higher power level laser pulses that will cut through the grating and break the fiber. If such an emergency situation takes place, it is advised to press the 'stop' button in the Matlab interface at once and turn off the laser shutter. Once the laser shutter is turned off, the laser output will be terminated simultaneously and thereby clear the risk of further damaging the system operator or instrument.

The CO_2 laser's over heating can be also caused after writing a large number of gratings continuously (large grating number or large iteration number). This could be a serious issue

as the fluctuation of output laser power will be reflected as an uneven RI modulation to each grating. As has been shown previously, a 0.2% variation of the average RI modulation could lead to a considerable shift of the attenuation peak. The output power fluctuation will significantly enhance the unpredictability and reduce the LPG fabrication quality. A possible solution is to shut down the whole laser system and improve heat circulation of the laboratory space. During the studies in this thesis, the laser system was completely shut off for 1 hour after 2 to 3 hours operation.

Chapter 4

Fabrication and Testing of the LPG Sensor

4.1 Implementation of point-by-point irradiation scheme

Despite the simplicity of the point-by-point irradiation scheme, there are quite a few variations in how to implement this scheme.

The simplest implementation, or the 'single-run', is to irradiate every grating position once by the CO_2 laser. 'Single run' is the fastest fabrication scheme among all since every grating will only go through the laser irradiation cycle once. In order to obtain the required RI modulation, the laser power or attached weight is set higher than in other schemes. However, due to fluctuation of the output laser power, especially after the laser has been kept in working condition for hours, the RI modulation could see significant variations at

certain location, which could affect the coupling efficiency between the designated modes.

In order to offset the instability issue of the output laser power, a few rescanning methods are devised. As has been introduced in the Matlab program section in the previous chapter, there are currently two different 'scanning modes' already incorporated in the program: the 'revisit' mode and the 'multiple shot' mode. Under the revisit mode, each grating position will be irradiated only once during each iteration cycle, while iteration cycles start from the beginning of the LPG and scan along the longitude of the fiber repeatedly. On the contrary, the 'multiple shot' mode will only visit each grating position once during the process, while at each grating position the laser will repeat its programmed irradiation workload several times with a short pause to allow the fiber grating to cool down. The difference between the two modes may seem minimal, however from actual fabrication experience it is fair to say that the 'revisit' mode tends to produce slightly longer and shallower physical deformation dips at each grating, while the 'multiple shot' mode tends to produce slightly narrower and deeper physical deformation dips. It is easy to see that when the number of iteration cycles are set to 1, both modes are in fact equivalent to the 'single-run' implementation.

Fig. 4.1 shows a microscope image of an LPG imprinted on a SMF-28e (Corning) fiber after point-by-point exposure to the CO_2 laser. It is apparent that the LPG has been strongly tapered in this case, such that the fiber is stretched during the fabrication process which results in a longer grating period and narrower fiber diameter. In particular, the designated grating period in this case was 245 μm, while the microscope measurement of the fabricated LPG showed a grating period of 258.5 μm; also, the assumed to be 'unaffected, between

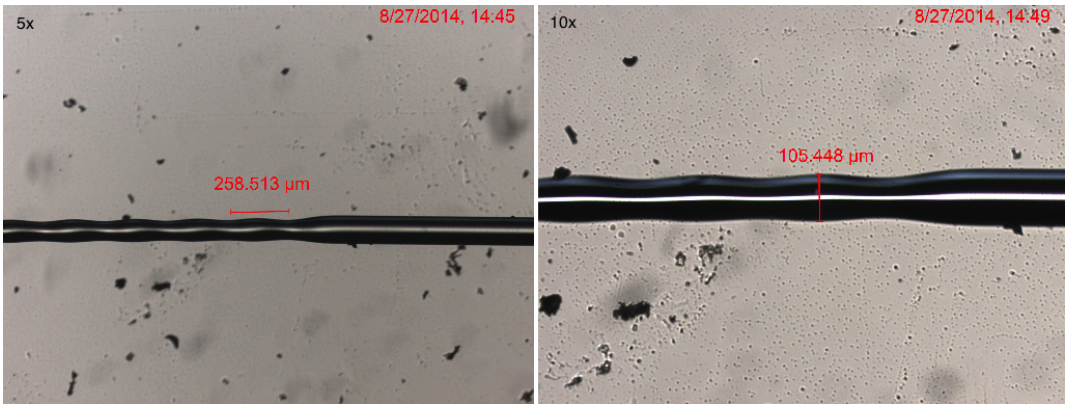

Figure 4.1: Microscope image of the fiber grating under high irradiation power. The fiber gratings have been strongly tapered due to extraordinary saturation of irradiation power absorption. The grating period was set to 245 μm, however the microscope measurement indicates the actual gratings period is 258.5 μm. In addition, the diameter of the untapered SMF is 125 μm, while after grating inscription, the widest diameter of the LPG region is only 105.45 μm.

grating' area has also been tapered with a reduced diameter of 105.45 μm from the standard diameter of 125 μm for this type of SMF. Fiber tapering is an unavoidable side-effect of exposure to the CO_2 laser, however, if the fiber tapering is strong, it could introduce high insertion loss and increase the chance of cracking or damaging the fiber. Strong fiber tapering usually occurs due to overwhelmingly strong laser power, large prestrain weight, or small grating period especially when it's smaller than the waist of the elliptical spot (150 μm). Using a small hanging weight and avoiding a high fabrication laser power can effectively reduce the fiber tapering issue. If the LPG has a grating period smaller than the waist of the ellipse spot, it would be wise to further reduce the laser power such that only the center of the ellipse spot would possess enough laser power to induce RI modulation to the fiber.

On the other hand, a weak laser irradiation would not be able to induce a large enough RI modulation to the fiber. Consequently the transmission spectrum could show no sign

of the resonant attenuation peak. Theoretical study shows that the coupling coefficient is proportional to the RI modulation, hence in order to observe the transmission loss spike or a significant shift of such spike for small RI modulation the LPG has to be excessively long. This issue can be easily avoided by setting the output laser power at a moderate level. Practically speaking, for the J48-2 laser used in this study, a power level between 3.2 W and 4.6 W, an energy density of 3 to 5 J/mm^2 on the exposed fiber surface and a prestrain weight under 10 grams are recommended. Within such fabrication parameters range, the gratings usually have an affected area of 50 μm along the axis direction of the fiber and minimum physical deformation at the laser-exposed gratings.

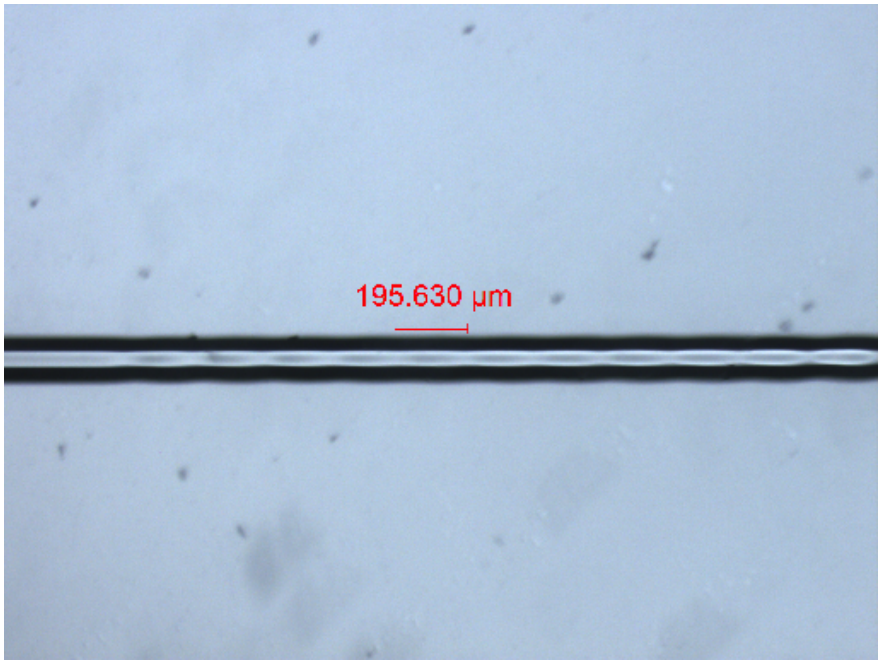

Figure 4.2: Microscope image of the fiber gratings of 195.6 μm, which is close to the designated gratings period of 195.0 μm as a moderate laser power is used during the fabrication process. The fiber tapering is minimum in this case, while the fringe pattern from the LPG area suggests the refractive index modulation of the gratings.

Fig. 4.2 shows an LPG fabricated at moderate parameters with a minimum fiber ta-

pering. The designated gratings period is 195 μm, while the actual gratings period after laser irradiation equals 195.63 μm, meaning the stretching and tapering are well controlled. Nevertheless, the fringe pattern suggests the fiber grating has been imprinted to the fiber core, where RI modulations are made and the background light are refracted differently at such locations from the unmodulated fiber core regions.

4.2 Exploration for ideal fabrication parameters

For the studies of this thesis, all LPGs were fabricated on Corning SMF-28 fiber family (SMF-28R or SMF-28e), otherwise the fiber type will be specified. After fabrication, the LPGs will be taken for measurement of the transmission spectrum between alternative ambient media to validate and examine its capacity for sensing ambient RI variation. We choose air ($n_{air} = 1.0$) and PBS solution ($n_{PBS} = 1.334$ at $\lambda = 589$ nm) [82] for standard ambient media and for a normal test, the transmission spectrum will be measured and compared when the LPG is placed in air and immersed in PBS solution, respectively. PBS solution (pH = 7) is used as one of the standard RI environments because the biosensor system we have developed using the LPG fiber sensor is restored and operated by immersing in PBS solution.

Before measurement, fiber ends will be first mounted with optical adaptors and then connected to a white light source and an optical spectrum analyzer, respectively. The LPG section of the fiber will be held straight and fixed to two separated fiber holders, which

makes the LPG ready for spectrum measurement in air. When measuring the transmission spectrum in PBS, a solution chamber filled with PBS will be lifted up to the LPG such that the measurement of the spectrum is conducted when the LPG is completely immersed in PBS. Since the LPG can also sense the change of stress, it is important to adjust the fiber between holders as the buoyancy may exert extra stress to the LPG and cause a false response.

Though the PMC presents an accurate relationship between the location of resonant wavelength and LPG's grating period, it is still difficult to fabricate the LPG as desired. The first reason is that this study lack accurate refractive index and dispersion data for accurate evaluation of the PMCs for the underlying SMF. Therefore the simulation would not perfectly matches the transmission spectrum of the LPGs.

The second reason is that it is almost impossible to determine the relationship between average RI modulation of the LPG's grating with the fabrication condition due to fluctuations of the laser's output power. This study has observed several examples in which two LPGs fabricated under identical fabrication parameters, such as optical energy density and laser exposure length, grating period, hanging weight, fiber type *etc.*, tend to exhibit different characteristics in their transmission spectrum. This means that it is still inaccurate and impractical to match the simulated spectrum with the experimental observation in order to find out the average RI modulation.

However, through comparing the simulation results of the PMC and published data under comparable fabrication methods, one can narrow down the search range for ideal

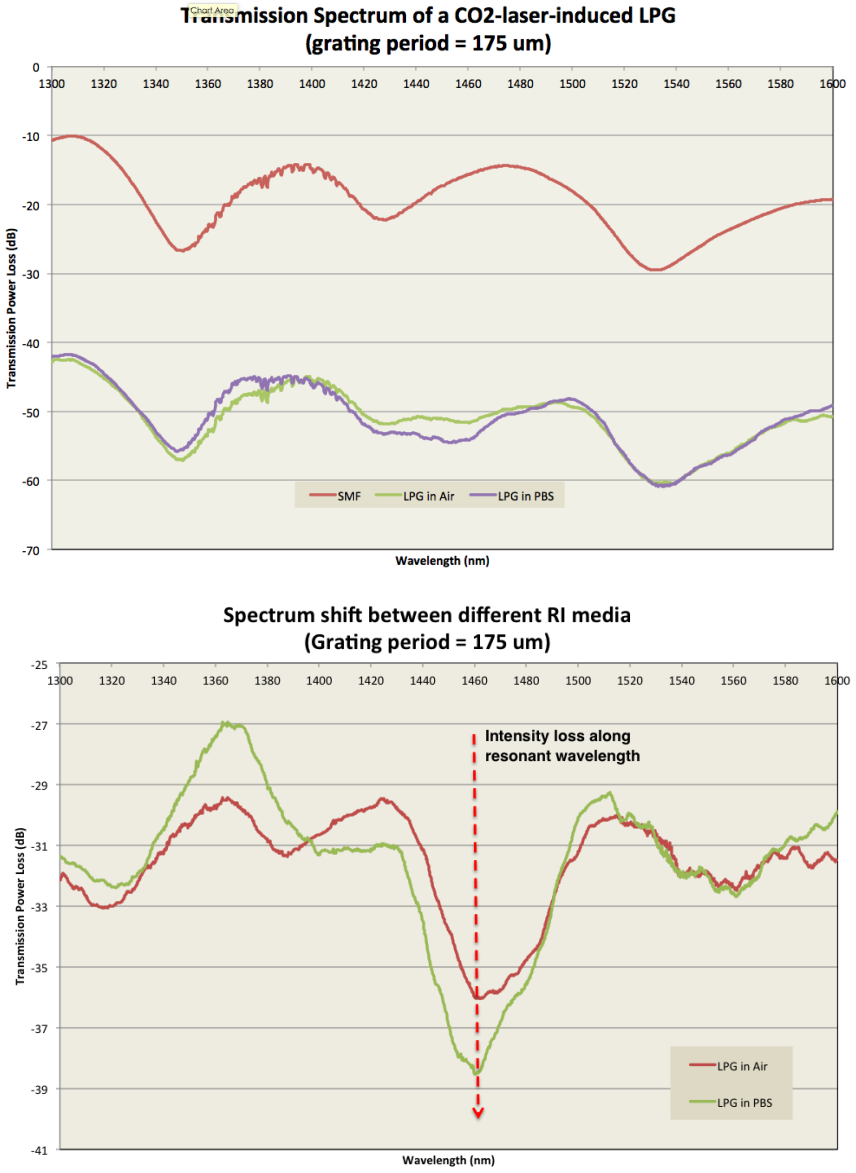

Figure 4.3: Transmission spectrum and peak shifting spectrum of LPG with grating period of 175 μm and exposed to 15 'multiple shot' cycles. The resonant attenuation peak remained at the 1459.6 nm when immersed in PBS pH = 7.0, however, the intensity of the peak increased. Top chart: transmission spectrum and comparison between bare SMF before inscription of LPG, SMF with LPG imprinted, the same LPG when immersed in PBS pH = 7.0, the same LPG when put back in air again, respectively. Bottom chart: the differential spectrum between LPG's transmission spectrum and SMF's transmission spectrum. Since this LPG is operating at the 'before-TAP' region, the change of ambient RI (from air to PBS solution) led to the increment of the peak intensity, instead of the peak shifting in wavelength.

parameter sets. Practically speaking, grating periods between 150 μm and 250 μm are usually expected to include at least one TAP close to the 1550 nm wavelength range. A grating period larger than 250 μm could still see a resonant peak around 1550 nm, however, the peak would shift to longer wavelength as the result of immersing the LPG in a medium of higher refractive index, since the PMCs of such mode couplings are monotonically increasing. On the contrary, if the grating period is smaller than 150 μm, the resonant peak around 1550 nm tends to shift to shorter wavelength as the result of higher ambient refractive index, due to the fact that the PMCs of such cases are monotonically decreasing.

Table 4.1: Fabrication parameters of LPG as shown in Fig. 4.3 and Fig. 4.4

Parameters	**Fiber-1**	**Fiber-2**
Iteration mode	*Multiple shot*	*Multiple shot*
Iteration cycles	15	10
Laser power (*initial/ending*)	4.75 W / 4.75 W	4.75 W / 4.75 W
Full power period	30 ms	30 ms
Rising/Falling time	10 ms / 10 ms	10 ms / 10 ms
Time step	10 ms	10 ms
Grating period	175 μm	150 μm
Number of gratings	20	45
Hanging weight	3 grams	3 grams

Fig. 4.3 depicts the transmission spectrum and the differential spectrum of an LPG

that has exhibited peak shifting due to the change of ambient media. The LPG is fabricated by CO_2 laser point-by-point irradiation and the fiber is Corning SMF-28R. The fabrication parameters are listed in Tab.4.1. In addition to the listed parameters and fabrication method, the fiber was shifted an extra 5 μm between each 'multiple-shot' cycle in order to imprint a long grating. In the long grating case, each grating is separated for a grating period, however, the grating region itself can be at a length of more than half the grating period. For LPG fabricated under parameters of Tab. 4.1, the grating period is 175 μm and the scanned-through region expanded at least $5 \times 15 = 75\mu$m, if not counting the tapered edges at both ends of the grating region that were only exposed to one cycle of irradiation. This is equivalent to a 2.33:1 period-to-grating-length-ratio.

This LPG's resonant attenuation peak shifts along the peak's intensity instead of along the resonant wavelength, which renders the most direct proof that the LPG's operating at the 'before-TAP' region, where the coupling resonance between core and cladding modes keeps gaining strength due to the change of ambient RI. The resonant peak appears at 1459.6 nm with the transmission loss of -35.96 dB (compared to bare SMF), while immersed in PBS solution of pH = 7.0 the transmission loss at this wavelength attenuated further to -38.46 dB, or 2.51 dB of peak intensity reduction.

Whereas the intensity shifting of this LPG, there is another notable change of the transmission power around 1360 nm. This can be explained for the reason that despite the interaction of the TAP, the CO_2 laser induced LPG could also possess and exhibit coupling to other cladding modes that are not operated in the TAP region. Shifting of PMCs at the

change of immersing medium would shift the power conversion rate of these coupled modes at corresponding resonant wavelengths as well, which was seen in Fig. 4.3 around 1360 nm when the discussed LPG was immersed in PBS.

Another example fabricated under the same 'multiple-shot' cycles is presented in Fig. 4.4. In this case all fabrication parameters were adopted similar to those shown in Tab. 4.1, the grating period was 150 μm, the iteration cycles was 10 times and the number of gratings was 45. For this LPG the period-to-grating-length-ratio equals 3:1.

Since the grating period of this LPG (150 μm) was shorter than the previously discussed case (the LPG with 175μm) and such grating period is on the lower boundary for TAP LPG, it is not be surprising to see its peak shifting along wavelength rather than along intensity peak, as shown in Fig. 4.4. In air, this resonant peak was located at 1393 nm with a resonant attenuation of 39 dB at the peak, when immersed in PBS solution, the resonant peak shifted to a shorter wavelength due to a monotonically decreasing PMC. The resonant peak when immersed in PBS was 1389.6 nm with the peak attenuation of 34.72 nm, which is a 3.4 nm shift in wavelength and 4.28 dB decrease in attenuation peak.

It is interesting to see that along the with shift in resonant wavelength, the transmission intensity of the loss peak also shifted due to change of ambient RI. This can be explained that despite the establishment of mode coupling at the resonant wavelength, the coupling coefficient will still play an essential role in determining the depth of the power loss peak as described in Eq. 2.14. Recalling Eq. 2.8 and Eq. 2.22, the coupling coefficient κ_g varies at the change of the environmental RI, which leads to the variation of the power conversion

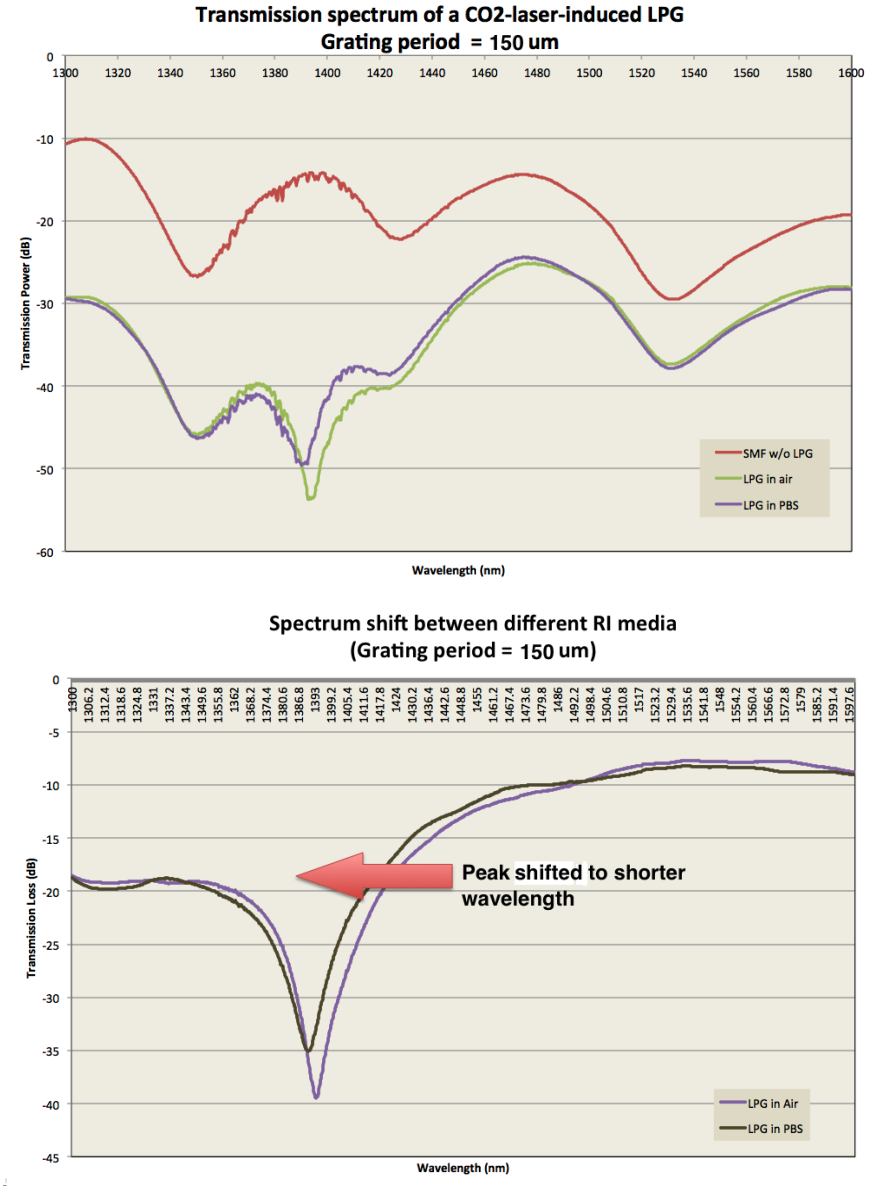

Figure 4.4: Transmission spectrum and peak shifting spectrum of LPG with grating period of 150 μm and 10 'multiple shot' cycles. The resonant attenuation peak was shifting to shorter wavelength as immersed in PBS pH = 7.0. Top chart: transmission spectrum and comparison between bare SMF before inscription of LPG, SMF with LPG imprinted, and the same LPG when immersed in PBS pH = 7.0, respectively. Bottom chart: the differential spectrum between LPG's transmission spectrum and SMF's transmission spectrum. When immersed in PBS solution that has a higher RI than air, the resonant peak shift to the shorter wavelength. This means that at this grating period, the PMC is monotonically decreasing at the examined wavelength bandwidth.

phase $\kappa_g L$ and eventually controls the attenuation peak intensity. Therefore, one can also observe a intensity change of attenuation peak from the wavelength shifting LPGs.

Exploration of the ideal LPG fabrication condition can start with a setting of parameters that has successfully produced LPGs responding to the change of ambient RI, then changing one parameter at a time while keeping the remaining parameters fixed for pursuing maximum sensitivity. Using this method can generate interesting results, which will be discussed in detail in the following section.

4.3 Study of LPG fabrication parameters

The most essential parameter for guiding an LPG's fabrication is the grating period, as it determines the location of the resonant attenuation peaks, the modes that the LPG couples with and the maximum sensitivity of each resonant peak. Analysis of the PMC also reveals the fact that with the increment of the cladding mode, the slope of the curves Λ/λ_{res} is decreasing at the identical resonant wavelength. From the perspective of the transmission spectrum, this means that with smaller grating period, the resonant peaks corresponding to coupling with a specific cladding mode will shift to shorter wavelength, while new resonant peak corresponding to higher order mode coupling shall appear at longer wavelength. That is to say, by varying the grating period and the order of the cladding mode to couple to, the resonant peaks will be observed at distinct locations.

Fig. 4.5 shows 4 LPGs fabricated at different grating periods while all other fabrica-

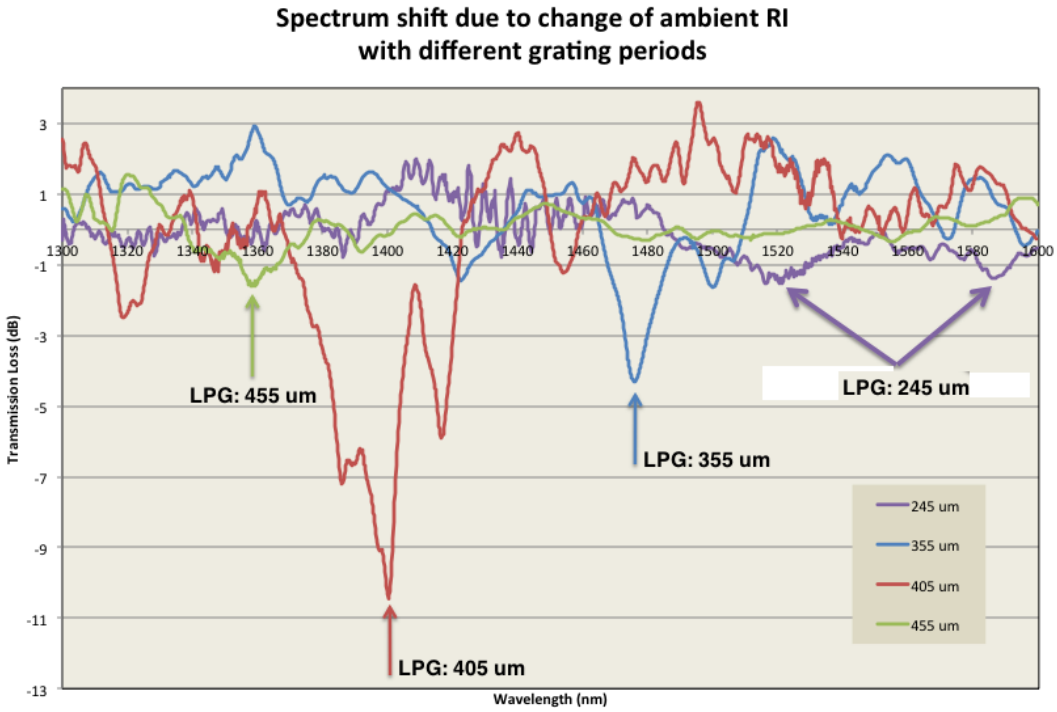

Figure 4.5: Differential spectra of four LPGs with different grating periods. The differential is evaluated for the decibel difference of transmission spectrum between LPG in air and in PBS solution. Apparently with shorter grating period the main resonant wavelength appears at longer wavelength, towards the telecommunication wavelength of 1550 nm. While at a much smaller grating period of 245 μm, the LPG started to operate at a 'post-TAP' area where dual-peaks were observed.

tion conditions remained identical, with the fabrication parameters listed in Tab. 4.2. The spectra shown in this figure correspond to the spectrum shifting differentials rather than the transmission spectrum as seen in previous LPG examples. The shifting differentials represent the decibel difference between the transmission spectrum when the LPG is in air and when the LPG is immersed in PBS solution, which are evaluated automatically by the optical spectrum analyser (OSA). Apparently, with a smaller grating period the main resonant peak appears at longer wavelength towards the telecommunication wavelength goal of 1550 nm. While at a much smaller grating period of 245 μm, the LPG appeared to operate at a

Table 4.2: Fabrication parameters of 4 LPGs shown in Fig. 4.5

Parameters	**Fiber-3**	**Fiber-4**	**Fiber-5**	**Fiber-6**
Iteration mode	*Single run*	*Single run*	*Single run*	*Single run*
Laser power (W)	4.12∼4.08	4.12∼4.08	4.12∼4.08	4.12∼4.08
Full power period (ms)	27	27	27	27
Rising/Falling time (ms)	5/5	5/5	5/5	5/5
Time step (ms)	1	1	1	1
Grating period (μm)	**245**	**355**	**405**	**455**
Number of gratings	24	24	45	40
Hanging weight (g)	3	3	3	3

'post-TAP' region and the change of ambient media led to a dual-peak separated by around 45 nm.

The differential spectra for the two RI media instead of referencing to the bare SMF was done two reasons: first, due to the variation of the insertion loss of each LPG the transmission spectra of LPG in air/PBS may locate at different offset levels and not be straightforward for comparison. However the spectrum differentials between the LPG in air and in PBS will compensate for the insertion loss and consequently emphasise the LPG characteristics as well as the shift of the underlying attenuation peaks. The second reason is similar, since the purpose of developing LPG is for sensing ambient RI variation, it is natural to show how the LPGs respond to the change of the external media's RI. Even though for

'wavelength-shifting' LPGs whose resonant wavelength varies at the change of ambient media, the differential spectrum still make good sense as all such peaks shift together.

Another interesting phenomenon worthy noting in Fig. 4.5 is that though each of the LPGs have shown resonant attenuation peak at corresponding wavelength, the magnitude of the main peaks were distinguishable. Although all three LPGs were fabricated under uniform conditions except the grating period, each LPG coupled the core mode to a different cladding mode. According to the power conversion equation in Eq. 2.14, the closer the value of $\kappa_g L$ is to $\pi/2 + m\pi$, the deeper the main attenuation peak will be. In addition, as the different grating periods coupled to different cladding modes, the coupling coefficient will be different as well. Therefore, it is plausible for observing resonant peaks with various power loss magnitude. In addition, in order to fabricate 'wavelength-shifting' LPGs for decent sensitivity (equivalent to largest possible power loss level), one can vary the number of gratings to search for proper grating length L until condition $\kappa_g L = \pi/2 + m\pi$ is met.

Since using point-by-point laser irradiation for LPG fabrication can be difficult to create identical gratings and RI modulations among individual attempts, post-fabrication treatment can be implemented to prepare an LPG for better sensitivity.

One such treatment is etching the fiber's cladding in the LPG region. In this treatment, the LPG portion of the fiber is immersed in a groove on a specially made acid holder, which is filled with 50 w% hydrofluoric acid (HF). Due to HF's volatility to emit corrosive fumes, the whole etching procedure must be conducted in a properly equipped fume hood and with full precautions as well as complete protection. HF is especially effective in corroding glasses

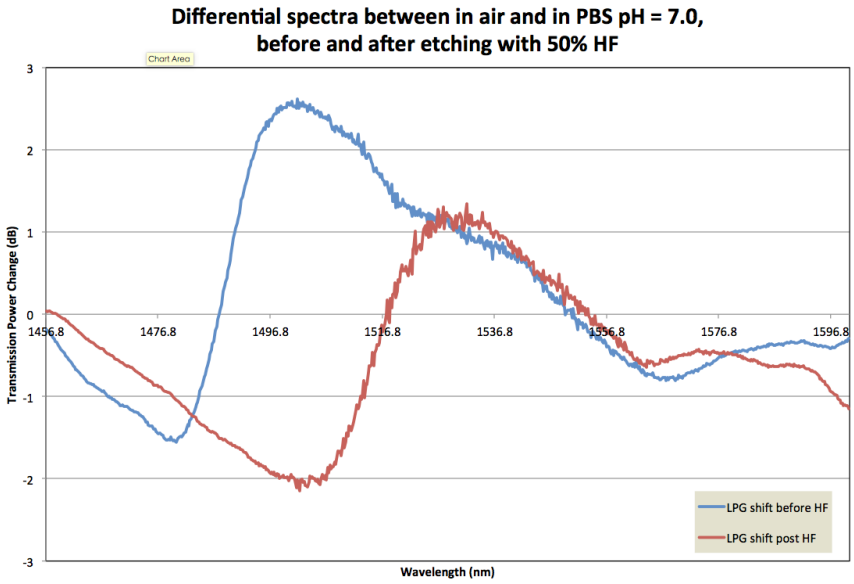

Figure 4.6: An example of etching LPG for enhancement of its sensitivity to ambient RI variation. Before treatment of 50% hydrofluoric acid (HF), the attenuation peak due to change of environmental media was -1.5 dB. After 5 minutes of HF treatment, the resonant peak further attenuated to -2.1 dB, with an additional 0.6 dB of power loss.

for its high reactivity. Therefore, applying HF to the fiber surface is able to efficiently remove the glass material from the cladding homogeneously. As has been predicted from theoretical analysis, reduction of the cladding radius will transform the spatial characteristics of the cladding mode, which would consequently shift the LPG's PMCs as well as induce a resonant peak at shifted wavelength.

Fig. 4.6 displays a case where an LPG had shown more transmitted power attenuation at the resonant wavelength due to etching. Before HF treatment, the attenuation peak locates at 1476.8 nm with a -1.5 dB of power loss. After treating the LPG region of the fiber with 50 w% HF for 5 minutes, the resonant peak was attenuated and shifted. The new attenuation peak locates at 1501 nm with a -2.1 dB of power loss.

This can be understood intuitively that the spatially redistributed cladding mode would affect the integral for calculating the coupling coefficient and alternate the power conversion phase value of $\kappa_g L$. Cladding's radius reduction can be estimated by the weight concentration of the HF acid and the length of the etching process. It is also important to avoid excessive etching since removal of cladding glass material could reduce the durability of the LPG sensor and make it fragile for reuse. In this discussed example, the LPG was broke not long after 28 minutes of fiber etching, due to the fact that the over-etched fiber can no longer resist the tension caused by buoyancy of the solution and broke.

In addition, fiber etching can be viewed as the reverse process of the deposition of organic thin films, which would effectively extend the cladding of the fiber and increase the effective RI of the cladding. Therefore, one can expect the spectrum of a post-etching LPG to resume its prior spectrum after deposition of ISAMs that compensate the loss of cladding material due to HF erosion.

The HF modification can be useful especially for tuning LPG towards working 'areas' as a post-imprinting treatment, where the PMCs can be shifted from the 'post-TAP' area to the 'before-TAP' area for TAP-LPGs, or shift the resonant wavelength of 'wavelength-shifting' LPGs close to the monitoring wavelength.

Manufacturers design and produce their single mode fiber with distinct dispersion characteristics from others by using patent-protected dopant compositions for the fiber core and slight variation of the core's geometry. Several commercial available SMF have been tested as the LPG fiber, and it has been found that the Corning SMF-28R and SMF-28e fiber are

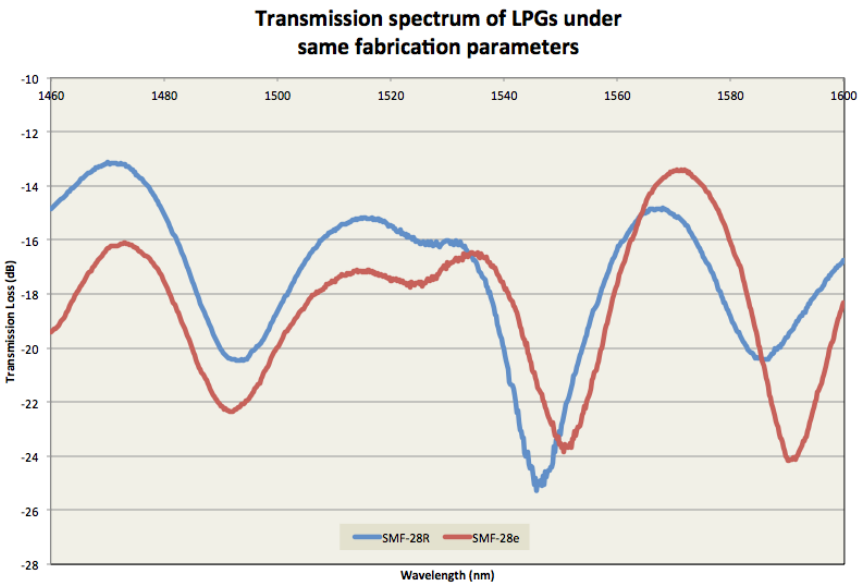

Figure 4.7: The transmission spectrum of LPGs fabricated under identical parameters, but with different single mode fiber type. Transmission spectrum of LPGs written on SMF-28R and SMF-28e shared close spectrum characteristics between 1460 nm to 1600 nm, though difference of resonant wavelengths and attenuation peaks can still be observed.

most suitable for fabricating LPGs and they are also commercially available.

Nevertheless, as has been discussed in previous chapters, the composition of the fiber's core will affect the dispersion behaviour across the bandwidth, which will lead to variation in the PMCs. Fig. 4.7 depicts the transmission spectrum of LPGs fabricated under identical fabrication parameters but with two different fiber types. The spectra between 1460 nm and 1600 nm wavelength have shown similarity in spectrum characteristics. However, the difference of resonant wavelengths and attenuation peaks can still be observed.. Change of the fiber type requires modifications to the existing parameters.

4.4 Testing CO_2-laser-induced LPGs with ISAMs

We have developed a MRSA biosensor system that detect the bioconjugation of MRSA analyte with the fiber sensor. The bioconjugation will immobilize the MRSA cell on sensor's exterior film serving as the sensing transducer and consequently increases the average thickness the film. Therefore, the effectiveness of the CO_2 laser induced LPG is determined by its sensitivity to the thickness variation of the deposited thin film on the cladding.

In order to examine the LPG's sensitivity to the thin film's thickness, it is necessary to establish a testing method where the thickness of the deposition film can be controlled and manipulated at the nanometer scale. Among several possible candidates, the ionic-self-assembled-multilayer (ISAM) technique stands out and was chosen for validating LPG's sensitivity after fabrication.

ISAM is a type of layer-by-layer thin film deposition technique that is well known for its thermal stability and mechanical durability, precise thickness control, rapid deposition and versatile biochemistry reactivity capabilities. The ISAM thin films are deposited in sandwich order, such that a pair of polyelectrolytes with opposite charges in solution are applied to the substrate alternately.

The polymers exhibiting positive charges in solution are called polycations, while the polymers exhibiting negative charges are called polyanions. The applied polyelectrolyte will be absorbed to the underlying layer of the thin film or substrate through electrostatic attraction and form a thin and extended layer. For this study the ISAMs were deposited on

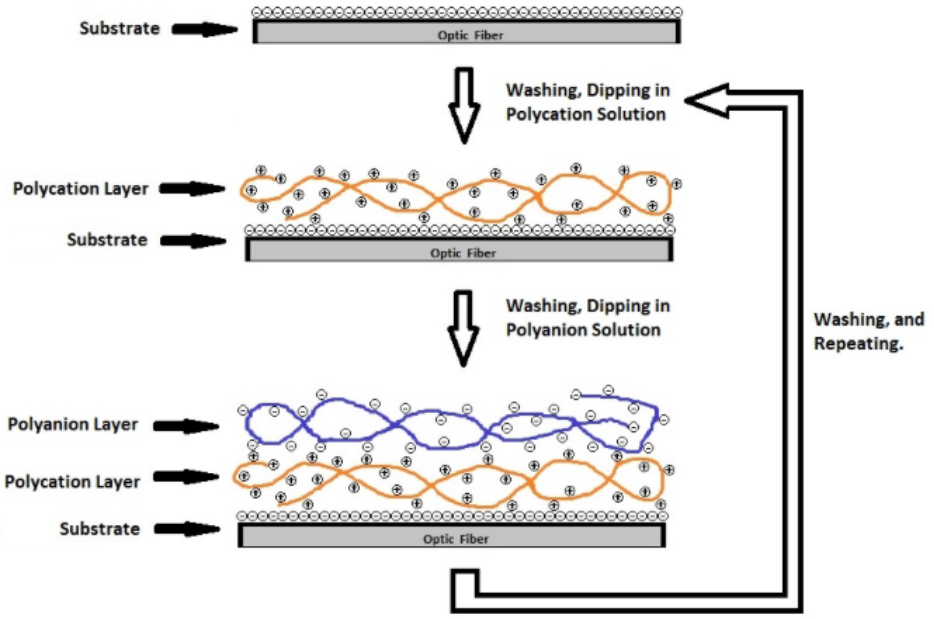

Figure 4.8: Deposition procedure for building one bilayer of ISAMs on top of a substrate that is negatively charged on the surface. Polycation solution will be applied to the substrate first, whose long-molecule-chains will be absorbed to the substrate surface due to electrostatic attraction and express positive net charge on the film surface. Then apply polyanion solution to the polycation coated substrate which will result in the deposition of a polyanion monolayer on top of the ISAMs film, which is then expressing negative net charge on thin film surface. Together this makes one bilayer of the ISAMs, repeating the process will produce multiple bilayers of film for a designated thickness. The film coats the entire fiber surface uniformly although this is not shown in the figure for clarity.

the cladding surface of the LPG fiber, hence the substrate (pure silica) is negatively charged when immersed in aqueous solution. As a result, the first ISAM monolayer needs to be the polyacation (PAH in this study). The deposition process is illustrated in Fig. 4.8.

In addition, the alternating deposition of polycation and polynion will reverse the sign of the net charge expressed by the ISAM thin film and repel additional deposition of the polymer with the same sign of charge as the ISAM thin film, which determines the specific thickness limit of each polymer layer. The thickness of the ISAM film can be precisely controlled

by a few factors: the number of bilayers (*i.e.* a pair of monolayers of polymer long-chain-molecules expressing opposite charges), the pH values and molecular concentration of the polymer solutions.

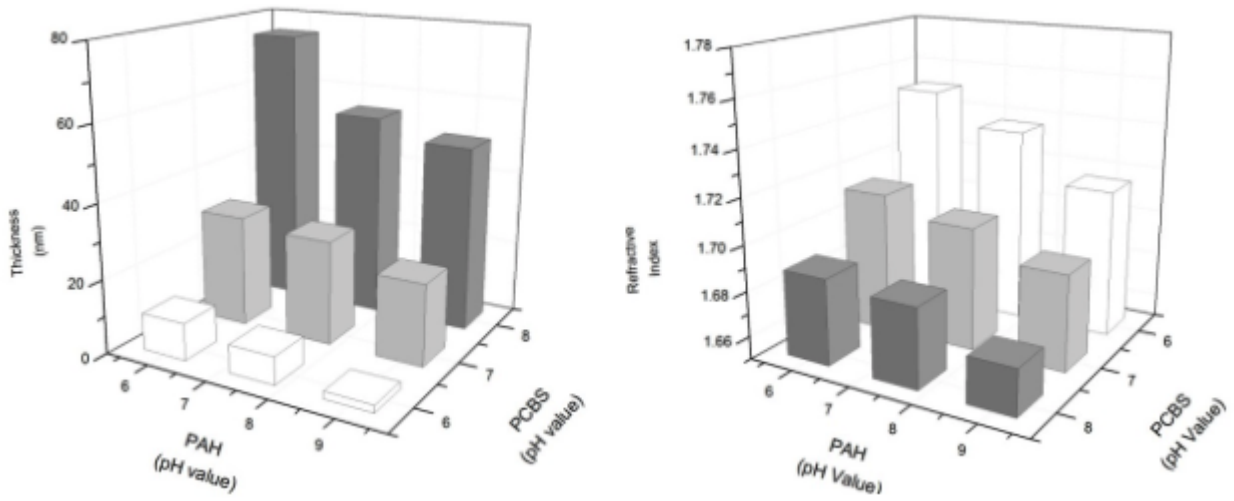

Figure 4.9: Thickness and refractive index dependence of 20 bilayers of ISAMs thin film. The thickness of the ISAMs film grows monotonically with the increment of PCBS's pH value and decrement of PAH's pH value. While the average refractive index of the film are monotonically decreasing as the increment of either PAH's pH value or PCBS's pH value.

Shiratori *et al.* [83] reported that polycation and polynion with pH values of 7.0 can produce the thinnest monolayer thickness. Experimental work by Heflin *et al.* [1] reported that PAH (polycation) and PCBS (polynion) at pH 7.0 was able to form 20 bilayers of ISAM at a total film thickness of 25 nm, or 1.25 nm/bilayer on average. The average refractive index of this ISAM thin film was around 1.71 and significantly higher than the RI of ordinary fiber cladding of 1.46. Therefore, the deposition of ISAM can be viewed as the expansion of LPG's cladding radius and modulating the effective RI of the cladding. Moreover, PAH and PCBS were used to construct ISAM in the present study. From Fig. 4.9, the thickness of

the ISAM bilayer grows monotonically with the decrease of PCBS's pH value and increase of PAH's pH value, while the average refractive index of the film are monotonically decreasing with the increase of either PAH's pH value or PCBS's pH value. Fig. 4.10 displays the distribution of an LPG's refractive index from the perspective of fiber radius. The figure was taken and modified from Dr. Wang's dissertation. [52] The thin film is marked as 'ambient' in the figure.

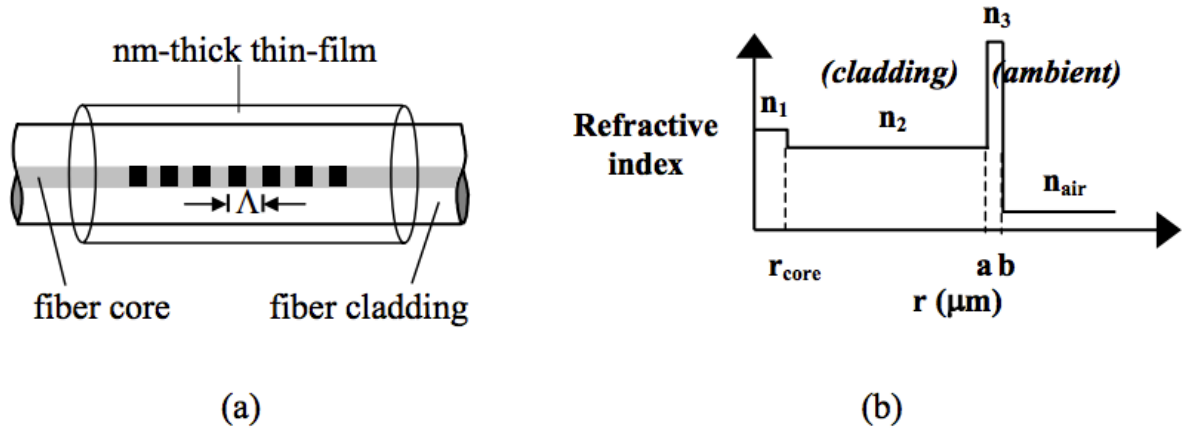

Figure 4.10: Radial distribution of a LPG after deposition of ISAM thin film. The film is a relatively small fiber radius increment, however, since the RI of the thin film is much higher than that of the fiber cladding, the cladding adsorption of the thin film can be viewed as the expansion of the cladding radius and raising of the average cladding RI. In chart (a), Λ represents the grating period of the LPG. In chart (b), a refers to the cladding radius while b - a refers to the thickness of the ISAM thin film.

Using deposition of ISAM thin films for the LPG validation test can be justified with the knowledge that ISAMs play an important role in construction of the MRSA biosensor system, where it serves as the substrate and provides the necessary chemical groups for cross-linking reactions with selective receptors, such as antibodies, DNA primers and so on. LPGs that are responsive and sensitive to the thickness increase of ISAM have been proven

to be an ideal candidate for our proposed biosensor system.

The deposition procedure starts with rinsing the bare LPG thoroughly with DI water for 1 minute and cleaning with alcohol soaked optical paper. Then the LPG is immersed in PAH solution (10 mM, pH = 7.0) for two minutes. Rinsing the fiber again, the LPG is then immersed in PCBS solution (10 mM, pH = 7.0) for another two minutes. The fiber is rinsed again after pulling it out of the PCBS solution. This will build one bilayer of ISAM. The LPG is alternately immersed in PAH and PCBS until designated number of ISAMs bilayers is built.

Fig. 4.11 depicts the evolution of transmission spectrum after each of seven bilayers of ISAMs were deposited on a CO_2-laser-induced LPG. The LPG used in this experiment is fabricated under the exact parameters listed as 'Fiber-3' in Tab. 4.2, which had a grating period of 405 μm and resonant wavelength centred at 1400 nm. In order to compare the effect of ISAM deposition, the transmission spectrum was measured after the LPG was thoroughly rinsed by DI water and immersed in PBS solution between deposition of each bilayers. From the spectrum evolution chart we can conclude that with deposition of each ISAM bilayer, the resonant peak shifted slightly to higher wavelength, while a gain of the attenuation loss of the peak was observed at the resonant wavelength as well. After deposition of a total of seven ISAM bilayers, the resonant peak shifted from 1400 nm to 1402 nm, while the intensity peak shifted from -10 dB to -25 dB.

This spectrum evolution can be explained from the perspective of the LPG's PMCs. With assistance of the simulation, it is found that at grating period of 405 μm, the PMC

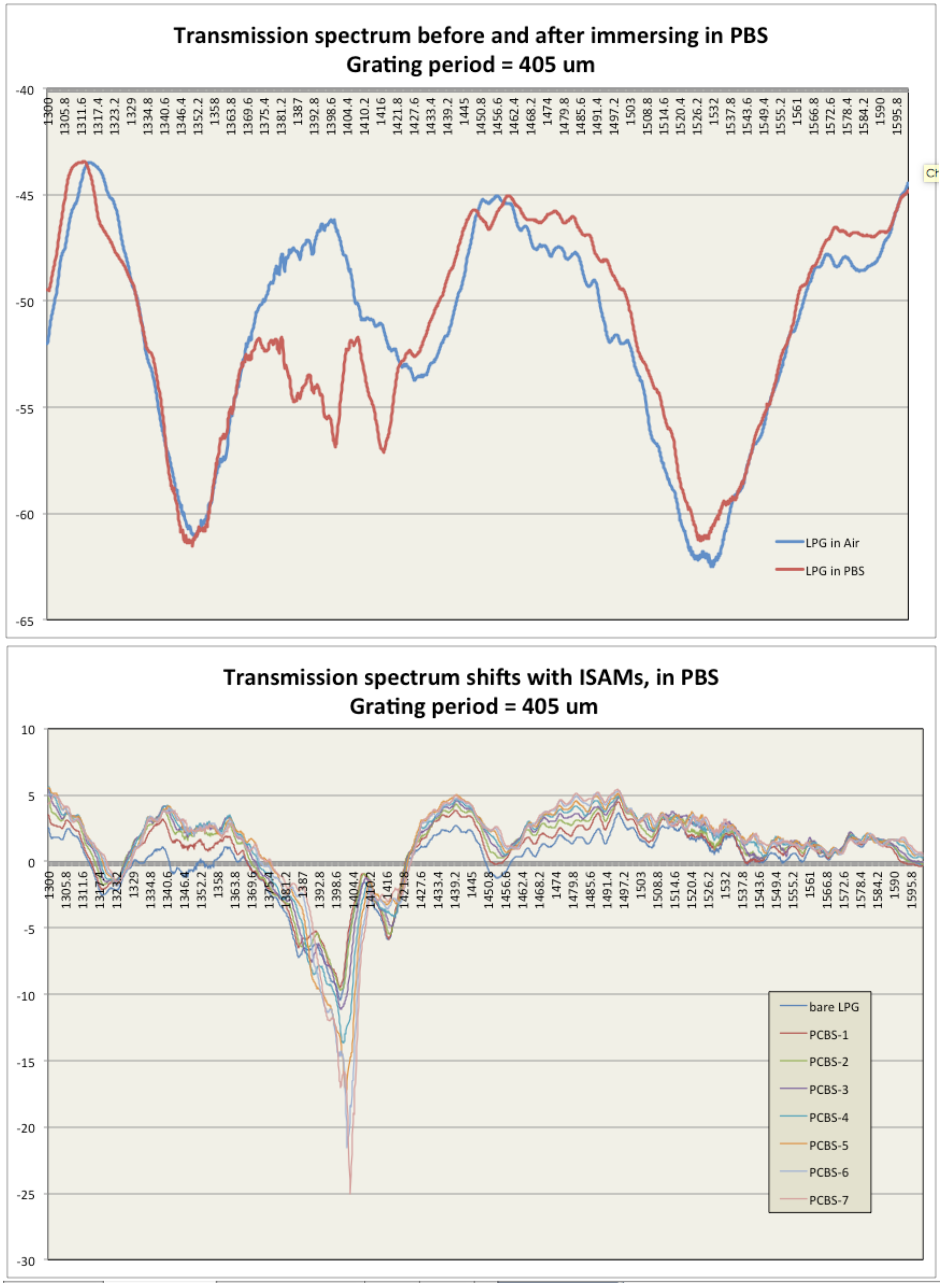

Figure 4.11: Spectrum evolution of LPG after deposition of each of seven bilayers of ISAMs on the fiber. The grating period of the LPG was 405 μm and the resonant wavelength was centred at 1400 nm. With deposition of seven ISAMs, the main attenuation peak of the transmission spectrum (measured in PBS solution) shifted slowly to higher wavelength, while the attenuation intensity significantly increased.

of the coupled modes are monotonically increasing for the studied LPG. Since deposition of ISAM can be viewed as expansion of cladding radius and increment of average cladding RI, the PMC shifted to lower grating period as a whole.

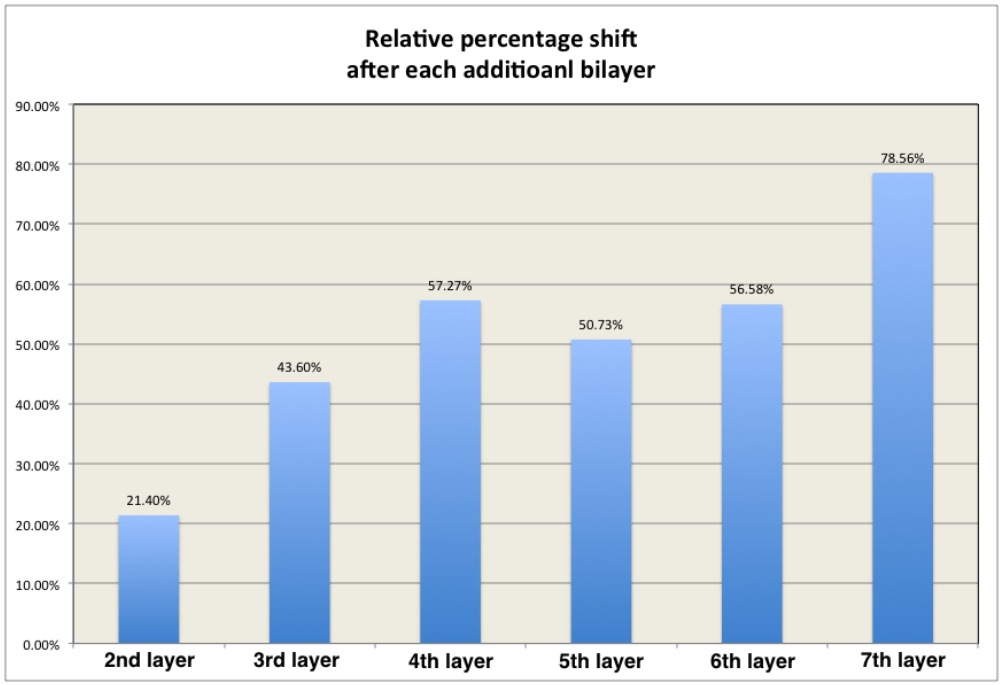

Figure 4.12: Relative percentage change after deposition of each additional ISAMs bilayer. The monitored wavelength was set at 1402 nm, which was happen to be the resonant wavelength of the LPG with seven bilayers of ISAMs. With deposition of each additional ISAMs, the percentage change of power loss compared to previous measurement was shown in the chart. The sensitivity grew along the resonant wavelength approaching the monitored wavelength.

However, in another occasion when power conversion phase $\kappa_g L$ is already at the maximum value of $\frac{\pi}{2} + m\pi, m = 0, 1, 2, ...$, deposition of ISAMs would alter the value of κ_g and lead to a decreasing power conversion ratio, or a reduced attenuation intensity loss at the main resonant peak. The LPG studied in Fig. 4.4 is an example of such a situation.

The LPG studied in Fig. 4.11 demonstrates a very interesting characteristic, that such

'wavelength-shifting' LPG has exhibited a larger shift in intensity than in wavelength. This characteristic makes such LPG a possible candidate for an intensity-based fiber sensor system as well. Generally, intensity-based LPG fiber sensors are made of TAP-LPGs due to the fact that the resonant peak remains at the same resonant wavelength and the intensity shifts are significant under deposition of ISAM.

This study showed that the wavelength-shifting LPGs could also operate as intensity-based fiber sensor as well, since under constant shifting the attenuation peak would swipe across the monitored single wavelength and create a consistent transmission power reduction when the attenuation peak enters the monitored wavelength, as well as a consistent power increase as the resonant wavelength passes across the monitored wavelength. Giving the fact that the coupling coefficient κ_g is usually in the magnitude of $10^{-}2$ cm^{-1}, [84] the power phase term is smaller than $\frac{\pi}{2}$ since the length of the LPG in order of a few centermeters. Therefore, LPG with longer grating region shall display improved sensitivity.

Fig. 4.12 depicts the relative percentage change of the attenuation peak at a fixed wavelength of 1402 nm, which is the resonant wavelength after deposition of all seven ISAM bilayers. Each data point shown in the chart represents the percentage of transmission power loss at the monitored wavelength of 1402 nm with respect to the prior measurement. From the chart it is evident that as the attenuation peak starts to swipe across the monitored wavelength, the power attenuation increased with higher percentage. Given the fact that each ISAM bilayer added a uniform thickness to the LPG, the sensitivity grows along with the shifting of the resonant peak towards the monitored wavelength as the result of the

evolving $\kappa_g L$ value. The maximum sensitivity was reached at the deposition of the 7th bilayer, which rendered a 78.56% of power attenuation at the monitored wavelength which is the resonant wavelength of the LPG at the time.

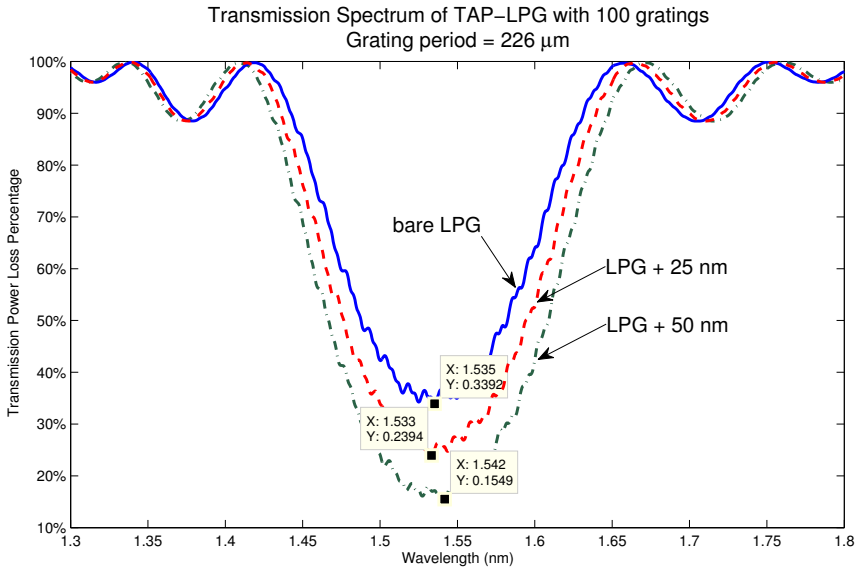

Figure 4.13: Simulation of the transmission spectrum of a LPG with deposition of thin films that effectively increase the cladding radius. The attenuation peak of LPG without any thin film deposition is at 1535 nm; with addition of average radius increment of 25 nm, the resonant wavelength of the peak shifts slightly to 1533 nm; then, for average radius increment of 50 nm, the resonant wavelength shifts to 1542 nm. As the PMCs of this LPG is approaching TAP along the increment of thin film thickness, the power loss grows from 66.08% to 85.51%.

It is worth noting that even for TAP-LPGs, the attenuation peak may also be slightly shifted from the initial wavelength, even though the assumption is made that the attenuation peak shifts only along a fixed resonance wavelength. This can be verified from the simulation results of the TAP on the PMC of a LPG with a slight increment of the cladding radius. The results are presented in Fig. 4.13.

The parameters of the simulated LPGs are: grating period of 226 μm with 100 gratings;

core and cladding initial radius are 4.2 μm and 62.5 μm, respectively; average RI modulation δn of 0.0014. It is evident that with increment of effective cladding radius of 50 nm, the TAP shifted slightly from 1541 nm to 1537 nm. With deposition of thin film that effectively increases the average thickness of the cladding, the LPG is approaching the TAP with more power loss at the dip of the attenuation peak – from 66.08% with no film deposition to 85.51% of transmission power loss with deposition of 50 nm of thin film. However, the dip of the attenuation peak, or the resonant wavelength, also shifts slightly during the process of intensity-shifting. The initial resonant peak locates at 1535 nm, then with deposition of 25 nm of thin film, the lowest point of the attenuation peak was found at 1533 nm, then an additional of 25 nm of thin film deposition pushes the resonant wavelength to 1542 nm, or a 7 nm shift from the initial position.

Therefore for LPG demonstrated in Fig. 4.11, though a slight wavelength shifting has been observed (under 2 nm), it is still possible the LPG was operating close to the TAP condition which showed a significant change in intensity increment with deposition of ISAMs thin film.

Chapter 5

Conclusions and Future Work

5.1 Conclusions

In conclusion, this thesis has explored the theories behind phase matching principles that support the selective transmission loss spikes at a resonant wavelength. With guidance of the phase matching curves simulated based on the phase matching conditions, as well as the understanding of the CO_2 laser induced refractive index modulation to the single mode fiber, this thesis has identified fabrication procedures and point-by-point laser irradiation methods. The discussions of relevant theories and principles can be found in chapter 2, while further discussions of the laser-stage system as well as the fabrication procedures can be found in chapter 3.

Using the assembled fabrication system according to the design and the Matlab program that was developed specifically for system control and coordination of instrument operation,

the thesis has presented successful examples of LPGs, which are discussed in chapter 4. Discussions regarding the behaviour and spectrum characteristics of various LPG types can also be found in the same chapter. In particular, this thesis found that LPGs can be categorized to two major types in regard to the spectrum shift: the 'wavelength-shifting' LPGs, whose resonant wavelength would shift in wavelength (either to larger wavelength or smaller wavelength, depending on the order of the coupled cladding mode) due to variation of the sensing element; and the 'intensity-shifting' LPGs, or TAP-LPGs, whose attenuation peak would shift in intensity at a fixed wavelength.

Tab. 5.1 and Tab. 5.2 summarize some of the fabrication parameter settings that have been proven practical and with decent spectrum quality for fabricating 'wavelength-shifting' LPGs and 'intensity-shifting' LPGs, respectively.

For 'Fiber-2', as shown in Fig. 4.4, the grating period was so short that the PMC exhibited a monotonically decreasing style, where the change of ambient media with different RI (air to PBS solution) resulted in a wavelength shifting to lower wavelength. While for 'Fiber-3' through 'Fiber-5', as seen in Fig. 4.5, the grating periods were longer, whose PMCs would exhibit a monotonically increasing style and lead to a wavelength shifting to higher wavelength due to increased RI of ambient media. Along with the wavelength shifting of the resonant attenuation peaks, variations of the intensity loss at the peaks have also been observed. This side-effect can be understood for the fact that the peak power conversion between the core and cladding mode controlled by a power conversion phase term $\kappa_g L$, where κ_g is denoted as the modes coupling coefficient and L is the length of the LPG. Therefore,

Table 5.1: 4 parameter setting examples for fabricating 'wavelength-shifting' LPGs

Parameters	**Fiber-2**	**Fiber-3**	**Fiber-4**	**Fiber-5**
Resonant wavelength (nm)	1393	1475	1400	1360
Iteration mode	*Multiple shots(10x)*	*Single run*	*Single run*	*Single run*
Laser power (W)	4.75∼4.75	4.12∼4.08	4.12∼4.08	4.12∼4.08
Full power period (ms)	30	27	27	27
Rising/Falling time (ms)	10/10	5/5	5/5	5/5
Time step (ms)	10	1	1	1
Grating period (μm)	**150**	**355**	**405**	**455**
Number of gratings	45	24	45	40
Hanging weight (g)	3	3	3	3

** Examples correspond to the LPGs discussed in Chapter 4 under same name tag.*

variation of the coupling coefficient as the result of change of ambient media will make a significant impact to the power conversion ratio and consequently alter the absolute intensity loss at the resonant wavelength.

For 'Fiber-1' (as seen in Fig. 4.3) and 'Fiber-6' (as seen in Fig. 4.5), the LPGs were operated in the 'intensity-shifting' mode, where the strength of the attenuation peaks can be shifted at a fixed wavelength. However, the two were tuned at different operational zones in regard to the relationship between grating period and location of the TAP. 'Fiber-5' was specifically tuned to be at the 'before-TAP' region, where the imprinted grating period was

Table 5.2: 2 parameter setting examples for fabricating 'intensity-shifting' LPGs

Parameters	**Fiber-1**	**Fiber-6**
Resonant wavelength (nm)	1459.6	1520 and 1585 (dual-peaks)
Iteration mode	*Multiple shots(15x)*	*Single run*
Laser power (W)	4.75∼4.75	4.12∼4.08
Full power period (ms)	30	27
Rising/Falling time (ms)	10/10	5/5
Time step (ms)	10	1
Grating period (μm)	**175**	**245**
Number of gratings	20	24
Hanging weight (g)	3	3

** Examples correspond to the LPGs discussed in Chapter 4 under same name tag.*

slightly longer than the location of the TAP such that change of ambient RI will augment the coupling between core and cladding modes and result in a deepened resonant peak. In contrast, 'Fiber-6' was tuned to be at the 'post-TAP' region, where the imprinted grating period was slightly smaller than the location of the TAP such that split peaks were observed on the transmission spectrum.

In addition, to prove the CO_2 laser induced LPGs are fit as fiber sensor element of the biosensor system, experiments to deposit ISAM thin films on the LPGs have been conducted to validate LPG's ability to sense thickness variation of the absorbed film. ISAM thin

films has been proven to be durable, thickness-controllable and as the basis of the biosensor system, sensing its thickness variation would provide direct proof for the LPG's qualification as the foundation of the biosensor system. With deposition of seven bilayers of ISAMs, a 'wavelength-shifting' LPG (Fiber-3 in Tab. 5.1) displayed a wavelength shifting of around 2 nm, while the intensity loss at the resonant peak grew from -10 dB to -25 dB – a 15 dB variation. If selecting 1402 nm as the monitoring wavelength for the intensity-based fiber sensor system, the last bilayer of ISAMs eliminated 78.5% of the transmitted power compared to the transmission spectrum right before the deposition of that bilayer.

5.2 Future work

Despite successful demonstrations of the CO_2 laser induced and fabricated LPGs that have shown potential to serve as the sensing component for biosensor systems, there are a few topics one can explore to further increase the sensitivity and reproducibility of the LPGs.

One of the ongoing works is to explore around the fabrication parameter settings listed in Tab. 5.2 and Tab. 5.1 and try to map out the ideal fabrication parameters for LPG's with resonant wavelength between 1500 nm and 1550 nm, which are the telecommunication wavelength and the monitoring wavelength of the biosensor system.

Also, the CO_2 laser induced TAP-LPGs have not been found to be reliable and stable under the current studies, it would be interesting to locate the fabrication conditions that will produce quality TAP-LPGs to compare with the 'wavelength-shifting' LPGs.

Reports have stating that better transmission spectrum can be obtained with usage of Boron-Germanium co-doped SMF for LPG fabrication. [63, 64] Exploring SMF with different dopant types could possibly yield valuable results.

It is also the ultimate goal to build biosensor system that is entirely based on the CO_2 laser induced LPGs. The assembly of the biosensor system has been previously discussed in detail by Zuo *et al.*. [38] The same procedures and sensor design can be directly applied to the CO_2 laser induced LPGs.

Bibliography

[1] Z. Wang, J. Heflin, R. Stolen, and S. Ramachandran, "Analysis of optical response of long period fiber gratings to nm-thick thin-film coating," *Optics Express*, vol. 13, no. 8, pp. 2808–2813, 2005.

[2] X. Shu, L. Zhang, and I. Bennion, "Sensitivity characteristics of long-period fiber gratings," *Journal of Lightwave Technology*, vol. 20, no. 2, p. 255, 2002.

[3] V. Grubsky and J. Feinberg, "Long-period fiber gratings with variable coupling for real-time sensing applications," *Optical Letters*, vol. 25, p. 203205, 2000.

[4] M. G. Young, U. Koren, B. I. Miller, M. A. Newkirk, M. Chien, M. Zirngibl, and G. Raybon, "A 16*1 wavelength division multiplexer with integrated distributed bragg reflector lasers and electroabsorption modulators," *IEEE Photonics Technology Letters*, vol. 5, no. 8, pp. 908–910, 1993.

[5] B. O. Guan, H. Y. Tam, S. T. Lau, and H. L. Chan, "Ultrasonic hydrophone based on distributed bragg reflector fiber laser," *IEEE Photonics Technology Letters*, vol. 17, no. 1, pp. 169–171, 2005.

[6] D. Chen, T. Yang, J. Wu, L. Shen, K. Liao, and H. S, "Band-rejection fiber filter and fiber sensor based on a bragg fiber of transversal resonant structure," *Opt Express.*, vol. 16, no. 21, pp. 16489–95, 2008.

[7] T. Wei, X. Lan, Y. Han, H.-L. Tsai, and H. Xiao, "Optical fiber sensors for high temperature harsh environment sensing," *IEEE*, pp. 978–1–4244–7935–1/11, 2011.

[8] M. Digonnet and H. J. Shaw, "Wavelength multiplexing in single-mode fiber couplers," *Applied optics*, vol. 22, no. 3, pp. 484–491, 1983.

[9] A. D. Kersey, T. A. Berkoff, and W. W. Morey, "Multiplexed fiber bragg grating strain-sensor system with a fiber fabryperot wavelength filter," *Optics letters*, vol. 18, no. 16, pp. 1370–1372, 1993.

[10] Y. Jeong, J. Sahu, D. Payne, and J. Nilsson, "Ytterbium-doped large-core fiber laser with 1kw continuous-wave output power," *Electronics Letters.*, vol. 40, p. 470472, 2004.

[11] G. Oulundsen, K. Farley, J. Abramczyk, and K. Wei, "Fiber for fiber lasers: Matching active and passive fibers improves fiber laser performance," *Laser Focus World*, vol. 48, no. 113, 2012.

[12] A. Othonos and K. Kalli, *Fiber Bragg Gratings: Fundamentals and Applications in Telecommunications and Sensing*. Artech House, 1999.

[13] P. Ferraro and G. D. Natale, "On the possible use of optical fiber bragg gratings as strain sensors for geodynamical monitoring," *Optics and Lasers in Engineering*, vol. 37, no. 2-3, p. 115130, 2002.

[14] W. J. Bock, J. Chen, P. Mikulic, and T. Eftimov, "A novel fiber-optic tapered long-period grating sensor for pressure monitoring," *IEEE Transactions on Instrumentation and Measurement*, vol. 56, no. 4, pp. 1176–1180, 2007.

[15] K. O. Hill, Y. Fujii, D. C. Johnson, and B. S. Kawasaki, "Photosensitivity in optical fiber waveguides: application to reflection fiber fabrication," *Appl. Phys. Lett.*, vol. 32, no. 10, p. 647, 1978.

[16] A. M. Vengsarkar, P. J. Lemaire, J. B. Judkins, V. Bhatia, T. Erdogan, and J. E. Sipe, "Long-period fiber gratings as band-rejection filters," *J. Lightwave Technol.*, vol. 14, p. 58, 1996.

[17] T. Erdogan, "Member-fiber grating spectra," *Journal of Lightwave Technology*, vol. 15, no. 8, p. 1277, 1997.

[18] C. E. Kerbage, B. J. Eggleton, P. S. Westbrook, and R. S. Windeler, "Experimental and scalar beam propagation analysis of an air-silica microstructure fiber," *Optics Express*, vol. 7, no. 3, p. 113, 2000.

[19] S. W. James and R. P. Tatam, "Optical fibre long-period grating sensors: characteristics and application," *Meas. Sci. Technol.*, vol. 14, p. R49R61, 2003.

[20] D. D. Davis, T. K. Gaylord, E. N. Glytsis, S. G. Kosinski, S. C. Mettler, and A. M. Vengsarkar, "Long-period fibre grating fabrication with focused co2 laser pulses," *Electron. Lett.*, vol. 34, p. 302, 1998.

[21] G. Kakarantzas, T. E. Dimmick, T. A. Birks, R. L. Roux, and P. S. J. Russell, "Miniature all-fiber devices based on co2 laser microstructuring of tapered fibers," *Opt. Lett.*, vol. 26, p. 1137, 2001.

[22] Y.-J. Rao, Y.-P. Wang, Z.-L. Ran, and T. Zhu, "Novel fiber-optic sensors based on long-period fiber gratings. written by high-frequency co 2 laser pulses," *J. Lightwave Technol.*, vol. 21, p. 1320, 2003.

[23] V. Grubsky and J. Feinberg, "Rewritable densification gratings in boron-doped fibers," *Optics Letters*, vol. 30, no. 11, pp. 1279–1281, 2005.

[24] Y.-P. Wang, D. N. Wang, W. Jin, Y.-J. Rao, and G.-D. Peng, "Asymmetric long period fiber gratings fabricated by use of co2 laser to carve periodic grooves on the optial fiber," *Appl. Phys. Lett.*, vol. 89, p. 151105, 2006.

[25] Y. Wang, W. Jin, J. Ju, H. Xuan, H. L. Ho, L. Xiao, and D. Wang, "Long period gratings in air-core photonic bandgap fibers," *Opt. Express*, vol. 16, p. 2784, 2008.

[26] H. Xuan, W. Jin, and M. Zhang, "Co2 laser induced long period gratings in optical microfibers," *Opt. Express*, vol. 17, no. 24, p. 21882, 2009.

[27] S. G. Kosinski and A. M. Vengsarkar, eds., *Splicer-based long-period fiber gratings*, (San Jose, CA), Optical Fiber Communication Conference, Feb. 22-27 1998.

[28] G. Rego, P. V. S. Marques, H. M. Salgado, and J. L. Santos, "Arc-induced long-period gratings," *Fiber and Integrated Optics*, vol. 24, no. 2, pp. 245–259, 2005.

[29] G. Rego, R. Falate, O. Ivanov, and J. L. Santos, "Simultaneous temperature and strain measurements performed by a step-changed arc-induced long-period fiber grating," *Applied Optics*, vol. 46, no. 9, pp. 1392–1396, 2007.

[30] Y. Kondo, K. Nouchi, T. Mitsuyu, M. Watanabe, P. G. Kazansky, and K. Hirao, "Fabrication of long-period fiber gratings by focused irradiation of infrared femtosecond laser pulses," *Opt. Lett.*, vol. 24, p. 646, 1999.

[31] A. Martinez, M. Dubov, I. Khrushchev, and I. Bennion, "Direct writing of fibre bragg gratings by femtosecond laser," *Electron. Lett.*, vol. 40, p. 1170, 2004.

[32] S. J. Mihailov, D. Grobnic, D. Huimin, C. W. Smelser, and B. Jes, "Femtosecond ir laser fabrication of bragg gratings in photonic crystal fibers and tapers," *IEEE Photonics Technol. Lett.*, vol. 18, p. 1837, 2006.

[33] S. Savin, M. J. F. Digonnet, G. S. Kino, and H. J. Shaw, "Tunable mechanically induced long-period fiber gratings," *Opt. Lett.*, vol. 25, p. 710, 2000.

[34] P. Steinvurzel, E. D. Moore, E. C. Magi, B. T. Kuhlmey, and B. J. Eggleton, "Long period grating resonances in photonic bandgap fiber," *Opt. Express.*, vol. 14, p. 3007, 2006.

[35] M. Fujimaki, Y. Ohki, J. L. Brebner, and S. Roorda, "Fabrication of long-period optical fiber gratings by use of ion implantation," *Opt. Lett.*, vol. 25, no. 2, p. 88, 2000.

[36] M. I. Braiwish, B. L. Bachim, and T. K. Gaylord, "Prototype co2 laser-induced long-period fiber grating variable optical attenuators and optical tunable filters," *Appl. Opt.*, vol. 43, p. 1789, 2004.

[37] Z. Wang, J. Heflin, K. V. Cott, R. H. Stolen, S. Ramachandran, and S. Ghalmi, "Biosensors employing ionic self-assembled multilayers adsorbed on long-period fiber gratings," *Sensors and Actuators B: Chemical*, 2009.

[38] Z. Zuo, *Development of a Nanoscale Optical Fiber Biosensor Assay.* PhD thesis.

[39] M. R. B. Andreeta, L. S. Cunha, L. F. Vales, L. C. Caraschi, and R. G. Jasinevicius, "Bidimensional codes recorded on an oxide glass surface using a continuous wave co2 laser," *Journal of Micromechanics and Microengineering*, vol. 21, no. 2, p. 025004, 2011.

[40] J. M. P. Coelho, M. Nespereira, C. Silva, D. Pereira, and J. Rebordo, *Current Developments in Optical Fiber Technology*, ch. Advances in Optical Fiber Laser Micromachining for Sensors Development. InTech, 2013.

[41] D. Nikogosyan, "Multi-photon high-excitation-energy approach to fiber grating inscription," *Measurement, Science and Technology.*, vol. 28, pp. R1–R29, 2007.

[42] *The Photonics Handbook*, ch. Polarization in Fiber Systems: Squeezing Out More Bandwidth, p. 1. Laurin Publishing, 2003.

[43] K. O. Hill, B. Malo, K. Vineberg, F. Bilodeau, D. Johnson, and I. Skinner, "Efficient mode-conversion in telecommunication fiber using externally written gratings," *Electron. Lett.*, vol. 26, pp. 1270–1272, 1990.

[44] F. Bilodeau, K. O. Hill, B. Malo, , and D. Johnson, "Efficient narrowband lp01 ¡–¿ lp02 mode conversion fabricated in photosensitive fiber: Spectral response," *Electron. Lett.*, vol. 27, pp. 682–684, 1991.

[45] R. Kashyap, *Fiber Bragg Gratings.* Optics and Photonics, Elsevier Science, 1999.

[46] A. Othonos, "Fiber bragg gratings," *Review of Scientific Instruments*, vol. 68, no. 12, pp. 4309–4341, 1997.

[47] Q. LIu, K. S. Chiang, and Y. Liu, "Characterization of single-mode fiber with fiber bragg gratings for the design of long-period gratings," *Journal of Lightwave Technology*, vol. 25, no. 8, p. 2129, 2007.

[48] T. W. MacDougall, S. Pilevar, C. W. Haggans, and M. A. Jackson, "Generalized expression for the growth of long period gratings," *IEEE Photonics Technology Letters*, vol. 10, no. 10, p. 1449, 1998.

[49] E. Lantz, D. Gindre, H. Maillotte, and J. Monneret, "Phase matching for parametric amplification in a single-mode birefringent fiber influence of the non-phase-matched waves," *J. Opt. Soc. AM. B*, vol. 14, no. 1, p. 116, 1997.

[50] T. Erdogan, "Fiber grating spectra," *Journal of Lightwave Technology*, vol. 15, pp. 1277–1294, 1997.

[51] *Selected Papers on Coupled-Mode THeory in Guided Wave Optics.* Bellingham, WA: SPIE OPtical Engineering Press, 1993.

[52] Z. Wang, *Ionic Self-Assembled Multilayers Adsorbed on Long Period Fiber Gratings for Use as Biosensors.* PhD thesis.

[53] X. Shu, T. Allsop, B. Gwandu, L. Zhang, and I. Bennion, "Room-tem- perature operation of widely tunable loss filter," *Electron. Lett.*, vol. 37, p. 216218, 2001.

[54] C. A. Angell, K. L. Ngai, G. B. McKenna, P. F. McMillan, and S. W. Martin, "Relaxation in glassforming liquids and amorphous solids," *App. Phys. Rev.*, vol. 88, no. 6, p. 31133157, 2000.

[55] P. G. Debenedetti and Stillinger, "Supercooled liquids and the glass transition," *Nature*, vol. 410, no. 6825, p. 259267, 2001.

[56] *Optical communication systems*, p. 209. ISBN: 0-13-638727-6, Hempstead, UK: Prentice-Hall, 2 ed., 1993.

[57] V. Neustruev, "Colour centres in germanosilicate glass and optical fibres.," *Journal of Physics: Condensed Matter*, vol. 6, no. 35, p. 69016936, 1994.

[58] V. Grubsky, D. Starodubov, and J. Feinberg, "Photochemical reaction of hydrogen with germanosilicate glass initiated by 3.4 5.4-ev ultraviolet light.," *Optics Letters*, vol. 24, no. 11, p. 729731, 1999.

[59] S. Mihailov, C. Smelser, P. Lu, R. Walker, D. Grobnic, H. Ding, G. Henderson, and U. J., "Fiber bragg gratings made with a phase mask and 800 nm femtosecond radiation.," *Optics Letters*, vol. 28, no. 12, p. 995997, 2003.

[60] B. H. Kim, Y. Park, T.-J. Ahn, D. Y. Kim, B. H. Lee, Y. Chung, U. C. Paek, and W.-T. Han, "Residual stress relaxation in the core of optical fiber by co2 laser irradiation," *Optics Letters*, vol. 26, no. 21, p. 1657, 2001.

[61] B. H. Kim, T. Ahn, D. Y. Kim, B. H. Lee, Y. Chung, U. C. Paek, and W. T. Han, "Effect of co2 laser irradiation on the refractive-index change in optical fibers," *Applied Optics*, vol. 41, no. 19, p. 3809, 2002.

[62] T. Zhu, Y.-J. Rao, and Q.-J. Mo., "Fiber bragg gratings made with a phase mask and 800 nm femtosecond radiation.," *IEEE Photonics Technol. Lett.*, vol. 17, no. 15, p. 2700, 2005.

[63] V. Grubsky and J. Feinberg, "Rewritable densification gratings in boron-doped fibers," *Opt. Lett.*, vol. 30, p. 1279, 2005.

[64] Y. Liu, H. W. Lee, K. S. Chiang, T. Zhu, and Y. J. Rao, "Glass structure changes in co_2-laser writing of long-period fiber gratings in boron-doped single-mode fibers," *J. Lightwave Technol.*, vol. 27, p. 857, 2009.

[65] K. Morishita and A. Kaino, "Adjusting resonance wavelengths of long-period fiber gratings by the glass-structure change.," *Appl. Opt.*, vol. 44, p. 5018, 2005.

[66] *Laser Fabrication and Machining of Materials*. New York: Springer, 2008.

[67] U. C. Paek and C. R. Kurkjian, "Calculation of cooling rate and induced stresses in drawing optical fiber," *J. Am. Ceram Soc.*, vol. 58, p. 330, 1975.

[68] G. Kakarantzas, T. E. Dimmick, T. A. Birks, R. L. Roux, and P. S. J. Russell, "Miniature all-fiber devices based on co2 laser microstructuring of tapered fibers," *Opt. Lett.*, vol. 26, p. 1137, 2001.

[69] G. D. VanWiggeren, T. K. Gaylord, D. D. Davis, M. I. Braiwish, E. N. Glytsis, and E. Anemogiannis, "Tuning, attenuating, and switching by controlled flexure of long-period fiber gratings," *Opt. Lett.*, vol. 26, no. 2, pp. 61–63, 2001.

[70] S. T. Oh, W. T. Han, U. C. Paek, and Y. Chung, "Azimuthally symmetric long-period fiber gratings fabricated with co2 laser," *Microwave Opt. Technol. Lett.*, vol. 41, p. 188, 2004.

[71] T. Zhu, Y.-J. Rao, and J.-L. Wang, "Azimuthally symmetric long-period fiber gratings fabricated with co2 laser," *Chin. Phys. Lett.*, vol. 24, p. 1971, 2007.

[72] Y. Li, T. Wei, J. A. Montoya, S. V. Saini, X. Lan, X. Tang, J. Dong, and H. Xiao, "Measurement of -laser-irradiation-induced refractive index modulation in single-mode fiber toward long-period fiber grating design and fabrication," *Appl. Opt.*, vol. 47, p. 5296, 2008.

[73] Y. Liu and K. S. Chiang, "Co2 laser writing of long-period fiber gratings in optical fibers under tension," *Opt. Lett.*, vol. 33, p. 1933, 2008.

[74] X. Zhong, Y. Wang, C. Liao, G. Yin, J. Zhou, G. Wang, B. Sun, and J. Tang, "Long period fiber gratings inscribed with an improved two-dimensional scanning technique," *Photonics Journal, IEEE*, vol. 6, no. 4, pp. 1–8, 2014.

[75] S. Chaubey, S. Kher, and S. M. Oak, "Radiation and taper tuning of long period grating for high sensitivity strain measurement," *Proc. IEEE 7th WFOPC*, pp. 1–4, 2011.

[76] S. Kher, S. Chaubey, R. Kashyap, and S. M. Oak, "Turnaround-point long period fiber gratings (tap-lpgs) as high radiation dose sensors," *IEEE Photon. Technol. Lett.*, vol. 24, no. 9, p. 742744, 2012.

[77] S. Kher, S. Chaubey, J. Kishore, and S. M. Oak, "Detection of fuel adulteration with high sensitivity using turnaround point long period fiber gratings in b/ge doped fibers," *IEEE SENSORS JOURNAL*, vol. 13, no. 11, p. 4482, 2013.

[78] F. Tian, J. Kanka, X. Li, and H. Du, "Exploration of higher-order mode coupling in long-period gratings for sensitive monitoring of polyelectrolyte self-assembly at nanoscale," vol. 9098, pp. 90980R–90980R–8, 2014.

[79] K. e. a. Jain, "Ultrafast deep-uv lithography with excimer lasers," *IEEE Electron Device Lett.*, vol. EDL-3, p. 53, 1982.

[80] Y. Wang, "Review of long period fiber gratings written by co2 laser.," *Journal of Applied Physics*, vol. 108, no. 8, p. 081101, 2010.

[81] H. W. Lee and K. S. Chiang, "Co2 laser writing of long-period fiber grating in photonic crystal fiber under tension," *Opt. Express*, vol. 17, p. 4533, 2009.

[82] R. L. Schoch, L. E. Kapinos, and R. Y. H. Lim, "Nuclear transport receptor binding avidity triggers a self-healing collapse transition in fg-nucleoporin molecular brushes," *PNAS*, vol. 109, no. 42, pp. 16911–16916, 2012.

[83] S. Shiratori and M. F. Rubner, "ph-dependent thickness behavior of sequentially adsorbed layers of weak polyelectrolytes," *Macromolecules*, vol. 33, no. 11, pp. 4213–4219, 2000.

[84] P. Giaccari, H. G. Limberger, and R. P. Salath, "Local coupling-coefficient characterization in fiber bragg gratings," *Optics Letters*, vol. 28, no. 8, pp. 598–600, 2003.

Appendix A

Matlab Source Code

A.1 Matlab code to calculate the phase-matching-curve

Note: *Matlab function pmc.m is dependent on the function calLP.m, therefore, the two functions must be placed under the same folder for proper execution.*

```
function [Lambda, neff_a, neff_b] = calLP(n1, n2, a, b, lambda, N)

% Author: Ziwei Zuo

% Date: Mar 9, 2015

% This function calculates @Lambda, which is the grating period of a LPG

% under giving parameters:

% @a = core radius;

% @b = cladding radius;

% @n1 = core RI;

% @n2 = cladding RI;
```

```
% @lambda = resonant wavelength;
% @N = number of considered cladding modes;
    eps = 1;
    acc = 10000;
    num = 1;
    uResA = 0;
    uResB = zeros([1 N]);
    neff_a = 0;
    neff_b = zeros([1 N]);
    n3 = 1.0;
    n2 = n2 + (n1 - n2)*a/b; % average RI for cladding mode.
    Lambda = zeros([1 N]);
    V_a = double(2*pi*a*sqrt(n1^2 - n2^2)/lambda);
    u_a = linspace(0, V_a, acc);
    w_a = double(sqrt(V_a^2 - u_a.^2));
    V_b = double(2*pi*b*sqrt(n2^2 - n3^2)/lambda);
    u_b = linspace(0, V_b, acc);
    w_b = double(sqrt(V_b^2 - u_b.^2));
    lp1a = double(besselj(0,u_a).*(w_a.*besselk(-1,w_a)));
    lp2a = double(besselk(0,w_a).*(u_a.*besselj(-1,u_a)));
    lp_a = lp1a + lp2a;
    % Finding core's effective RI
```

```
for i = 1:acc-2
    if sign(lp_a(i)) ~= sign(lp_a(i+1)) && abs(lp_a(i)-lp_a(i+1)) < eps
        uResA = u_a(i);
        break;
    end
end
lp1b = besselj(0,u_b).*(w_b.*besselk(-1,w_b));
lp2b = besselk(0,w_b).*(u_b.*besselj(-1,u_b));
lp_b = lp1b + lp2b;
% Finding cladding's effective RI
for i = 1:acc-2
    if sign(lp_b(i)) ~= sign(lp_b(i+1)) && abs(lp_b(i)-lp_b(i+1)) < eps
        if num > 1 && u_b(i) - uResB(num-1) > 0.1
            uResB(num) = u_b(i);
            num = num + 1;
        else
            uResB(1) = u_b(i);
            num = num + 1;
        end

        if num > N
            break;
```

```
            end
        end
    end
    neff_a = sqrt(n1^2 - (uResA/(2*pi*a/lambda)).^2);
    neff_b = sqrt(n2^2 - (uResB/(2*pi*b/lambda)).^2);
    Lambda = lambda./(neff_a - neff_b);
end

function tap = pmc(a,b,dp,M,dn)
% This program simulate the PMC plots.
% @a = core radius
% @b = cladding radius
% @dp = grating length, in percentage of the grating period. Value must be
    smaller than 100.
% @M = number of cladding modes to be considered
% @dn = average RI modulation to the gratings.
N = 250; % Wavelength range accuracy
l_ini = 1; % Initial wavelength of the considered wavelength range, in micro
    meters.
l_end = 2; % Ending wavelength
lambda = linspace(l_ini,l_end,N);
Lambda = zeros([N M]);
```

```
% if the grating affected region is longer than 75% of the grating period, takes
    75% instead.
if dp > 25
    dp = 25;
end
% Sellmeier's parameters for a SMF with 3.5 w% dopant in core, by default:
A21 = 0.6961663;
A22 = 0.4079426;
A23 = 0.8974794;
l21 = 0.068404;
l22 = 0.1162414;
l23 = 9.896161;
A11 = 0.7042038;
A12 = 0.4160032;
A13 = 0.9074049;
l11 = 0.0514415;
l12 = 0.1291600;
l13 = 9.896156;
% % Parameters for a SMF with 5.8 w% dopant in core:
% A21 = 0.6961663;
% A22 = 0.4079426;
% A23 = 0.8974794;
```

```
% l21 = 0.068404;

% l22 = 0.1162414;

% l23 = 9.896161;

% A11 = 0.7088876;

% A12 = 0.4206803;

% A13 = 0.8956551 ;

% l11 = 0.0609053 ;

% l12 = 0.1254514 ;

% l13 = 9.896162;

% Finding refractive indices for core and cladding under wavelength range.

n1 = double(sqrt(1 + A11*lambda.^2./(lambda.^2-l11^2) +

    A12*lambda.^2./(lambda.^2-l12^2) + A13*lambda.^2./(lambda.^2-l13^2)));

n2 = double(sqrt(1 + A21*lambda.^2./(lambda.^2-l21^2) +

    A22*lambda.^2./(lambda.^2-l22^2) + A23*lambda.^2./(lambda.^2-l23^2)));

n1 = n1 - dn*dp/100; % effective RI change to core after inscription of LPG.

n2 = (a*n1 + (b-a)*n2)./(b);

neff_a = zeros([N 1]);

neff_b = zeros([N M]);

% Calculate the grating periods for the designated LP modes

for i = 1:N

    [Lambda(i,:), neff_a(i), neff_b(i,:)] = calLP(n1(i),n2(i),a,b,lambda(i),M);

end
```

```
Periods = Lambda';
for j = 1:M
    temp = smooth(smooth(smooth(Periods(j,:))))';
    Periods(j,:) = temp;
end
Lambda = Periods';
% Finding the turnaround point from PMC:
[Max, I] = max(Lambda);
tap = [];
for p = 2:M
    if I(p) < N-3 && I(p) > 3
        tap = [tap;lambda(I(p)) Max(p)];
    end
end
figure();
hold on;
% Coupling from LP0,1 core mode to cladding modes starting from LP0,2
for s = 2:M
    plot(lambda, Periods(s,:), 'LineWidth', 1);
end
if ~isempty(tap)
    plot(tap(:,1),tap(:,2),'o','Color','r');
```

```
end

hold off;

end
```

A.2 Matlab code to plot the transmission spectrum

Note: *Matlab function spec.m is dependent on the function calLP.m, therefore, the two functions must be placed under the same folder for proper execution.*

```
function spectrum = spec(a,b,dp,M,dn,n,period)

% This program simulate the transmission spectrum.

% @a = Radius of SMF's core

% @b = Radius of SMF's cladding

% @dp = grating length in percentage of the grating period.

% @M = Number of cladding modes.

% @n = ambient circumstance RI.

% @period = grating period.

N = 250; % Wavelength range accuracy

l_ini = 1.0; % Initial wavelength of the considered wavelength range, in micro

    meters.

l_end = 2.0; % Ending wavelength

lambda = linspace(l_ini,l_end,N);

Lambda = zeros([N M]);

L = n * period; % n is the number of gratings, period is the grating length, in
```

```
    micrometers.
kg = 0.5*pi/L; % L is in micrometers
if dp > 25
    dp = 25;
end
% Parameters for a SMF with 3.5 w% dopant in core:
A21 = 0.6961663;
A22 = 0.4079426;
A23 = 0.8974794;
l21 = 0.068404;
l22 = 0.1162414;
l23 = 9.896161;
A11 = 0.7042038;
A12 = 0.4160032;
A13 = 0.9074049;
l11 = 0.0514415;
l12 = 0.1291600;
l13 = 9.896156;
% Finding refractive indices for core and cladding under wavelength range.
n1 = double(sqrt(1 + A11*lambda.^2./(lambda.^2-l11^2) +
    A12*lambda.^2./(lambda.^2-l12^2) + A13*lambda.^2./(lambda.^2-l13^2)));
n2 = double(sqrt(1 + A21*lambda.^2./(lambda.^2-l21^2) +
```

```
    A22*lambda.^2./(lambda.^2-l22^2) + A23*lambda.^2./(lambda.^2-l23^2)));
n1 = n1 - dn*dp/100; % effective RI change to core after inscription of LPG.
n2 = (a*n1 + (b-a)*n2)./(b);
neff_a = zeros([N 1]);
neff_b = zeros([N M]);
for i = 1:N
    [Lambda(i,:), neff_a(i), neff_b(i,:)] = calLP(n1(i),n2(i),a,b,lambda(i),M);
end
delta_r = abs(period*lambda(:)./(period*(neff_a - neff_b(:,M))-lambda(:))/pi);
delta = 1./delta_r;
p = 1 - sin(kg*L*sqrt(1+(delta/kg).^2)).^2./(1+(delta/kg).^2);
temp = smooth(p);
p = temp;
figure();
plot(lambda,p);
end
```

A.3 Matlab code to plot sensitivity map charts

Note: *Matlab function sensitivity.m is dependent with the function calLP.m, therefore, the two functions must be placed under the same folder for proper execution.*

```
function [s, w] = sensitivity(a,b,n_sur,M,dn)
N = 250;
```

```
l_ini = 1.0; % Initial wavelength of the considered wavelength range, in micro
    meters.
l_end = 2.0; % Ending wavelength
lambda = linspace(l_ini,l_end,N);
dl = (l_end - l_ini) / N;
Lambda = zeros([N M]);
% Sellmeier's Parameters:
A11 = 0.68698290;
A12 = 0.44479505;
A13 = 0.79073512;
l11 = 0.078087582;
l12 = 0.1155184;
l13 = 10.436628;
A21 = 0.6961663;
A22 = 0.4079426;
A23 = 0.8974794;
l21 = 0.0684043;
l22 = 0.1162414;
l23 = 9.896161;
% Finding refractive indices for core and cladding under wavelength range.
n1 = sqrt(1+ A11*lambda.^2./(lambda.^2-l11^2) + A12*lambda.^2./(lambda.^2-l12^2)
    + A13*lambda.^2./(lambda.^2-l13^2));
```

```
n2 = sqrt(1+ A21*lambda.^2./(lambda.^2-l21^2) + A22*lambda.^2./(lambda.^2-l22^2)
    + A23*lambda.^2./(lambda.^2-l23^2));
n1 = n1 - dn; % effective RI change to core after inscription of LPG.
neff_a = zeros([N M]);
neff_b = zeros([N M]);
% Calculate the grating periods for the designated LP modes
for i = 1:N
    [Lambda(i,:), neff_a(i,:), neff_b(i,:)] = calLP(n1(i),n2(i),a,b,lambda(i),M);
end
Periods = Lambda';
for j = M:M
    temp = smooth(smooth(smooth(Periods(j,:))))';
    Periods(j,:) = temp;
end
u_m = besszero(M,0);
dlambda = dl ./ (Periods(M,1:N-1)'-Periods(M,2:N)');
dtemp = [0; dlambda];
dlambda = dtemp;
gamma = dlambda ./ (neff_a(:,M)-neff_b(:,M));
Gamma =
    -((u_m)^2*lambda'.^3*n_sur)./(8*pi*b^3.*n2'.*(neff_a(:,M)-neff_b(:,M)).*(n2'.^2-n_sur^2).^1
sen = lambda'.*gamma.*Gamma;
```

```
temp = smooth(smooth(smooth(sen)));

sen = temp;

[s, id] = max(abs(sen));

w = lambda(id);

plot(lambda',abs(sen));

end
```

Note: *this Matlab code below will scan the possible values of average RI modulation for maximum sensitivity of the studied LPGs. It has to be put in the same folder with sensitivity.m to be functional.*

```
k = 20;

s = zeros([1 k]);

w = zeros([1 k]);

dn = linspace(0.0005, 0.002, k);

for i = 2:k

    [s(i), w(i)] = sensitivity(9.8/2,62.5,1.4,i,0.0011);

end

figure();

plot(w,s,'*');

figure();

plot(dn,s,'*');
```
